1971

A study of radiative heat transfer from a spherical layer

Hakimuddin Kalimuddin Khalil

Department:

A STUDY OF RADIATIVE HEAT TRANSFER FROM A SPHERICAL LAYER

by

HAKIMUDDIN KALIMUDDIN KHALIL, 1945-

A THESIS

Presented to the Faculty of the Graduate School of the

UNIVERSITY OF MISSOURI-ROLLA

In Partial Fulfillment of the Requirements for the Degree

MASTER OF SCIENCE IN MECHANICAL ENGINEERING

1971

Approved by

A. L. Crosbie (Advisor) B. F. Armaly

James W. Joiner

ABSTRACT

The problem of radiative heat transfer from a spherical layer of absorbing-emitting gas has been studied. First, the medium is assumed to be gray and then nongray. A thorough survey of literature from fields other than heat transfer, such as astrophysics and neutron transport has been made to stimulate further interest in this important area. To gain some insight into the effect of various parameters on the heat transfer, simple physical situations involving isothermal medium are considered. Comparison of the results obtained for the flux from the spherical and planar layers reveal that the curvature becomes increasingly important as the inner to outer optical radii ratio decreases. The study of a particular nonisothermal case shows that the temperature variations are important and cannot be neglected.

In the study of the nongray problem, a simplified rectangular model for the spectral absorption coefficient is first considered. The expressions developed for the simplified rectangular model turns out to be similar to the expressions for the gray analysis. With a small amount of additional computational time one can obtain the results for the simplified rectangular model. Carbon monoxide example is studied in order to illustrate how the rectangular model can be used to analyze radiative heat transfer in a nongray gas. The results of this example reveals that the influence of the 'windows' is quite profound, thus exposing the limitations of the gray analysis.

In order to determine the effect of line or band shape on the radiative transfer, five different models for the absorption

coefficient representing the rectangular, triangular, Doppler, exponential and Lorentz profiles are considered. The results obtained for the dimensionless flux reveal that the rectangular profile has the smallest numerical value of all the profiles. The effect of the "wings" of the Doppler, exponential and Lorentz profiles is evident only for large values of optical thickness.

The limiting cases of the functions on which the expressions for the local radiative flux (both from gray and nongray medium) depends are also studied. All the results (except for carbon monoxide example) reported graphically as well as in tabular form in this study are obtained using double precision.

ACKNOWLEDGEMENTS

The author wishes to express his gratitude to Dr. Alfred L. Crosbie for his valuable guidance and interest during the progress of the present study.

The author is grateful to Dr. Bassem F. Armaly for his critical review of the work.

Thanks are due to Mrs. Carol Rodman for typing the thesis.

TABLE OF CONTENTS

Table of Contents (continued) Page

Table of Contents (continued) Page

LIST OF FIGURES

List of Figures (continued) Page

List of Figures (continued) Page

LIST OF TABLES

List of Tables (continued) Page

List of Tables (continued) Page

NOMENCLATURE

Symbol	Significance
E	Function defined by equation (4.25)
$E_{b\nu}$	Planck's function defined by equation (4.69)
F	Incident flux that interact with the medium
F^*	Incident flux that do not interact with the medium
$\mathcal{G}$	Local radiative flux
$\mathcal{F}^*$	Dimensionless radiative flux
g_1	Function defined by equation (4.45)
g_2	Function defined by equation (4.46)
$\mathcal{g}_1$	Function defined by equation (5.42)
$\mathcal{g}_2$	Function defined by equation (5.43)
h	Planck's constant
h_1	Function defined by equation (3.3)
h_2	Function defined by equation (3.4)
$\mathcal{h}_1$	Function defined by equation (5.15)
$\mathcal{h}_2$	Function defined by equation (5.16)
H	Function defined by equation (3.5)
$\mathcal{H}$	Function defined by equation (5.17)
k	Boltzmann's constant
K	Function defined by equation (4.47)
$\mathcal{K}$	Function defined by equation (5.44)
L	Thickness of the planar layer
Q	Function defined by equation (4.51)
r	Radial distance of the spherical layer

Symbol	Significance
T	Absolute temperature
T^*	Reference temperature
	Greek Symbols
α	Dimensionless function, κ_ν/κ
γ	Quantity defined by equation (5.12)
Θ	Dimensionless function defined by equation (3.40)
κ	Volumetric absorption coefficient
κ_ω	Spectral absorption coefficient
κ_p	Planck mean absorption coefficient
ν	Frequency
$\overline{\nu}$	Dimensionless frequency, $h\nu/kT$
σ	Stefan-Boltzmann constant
τ	Optical radial distance (for the spherical layer); optical thickness (for the planar layer)
ϕ	Function defined by equation (4.48)
ψ	Function defined by equation (5.21)
ω	Wave number
	Subscripts
1	Conditions at inner boundary (for the spherical layer); conditions at left-hand boundary (for the planar layer)
2	Conditions at outer boundary (for the spherical layer); conditions at right-hand boundary (for the planar layer)
0	Isothermal quantity
p	Refers to planar layer
ν	Frequency dependent quantity

I. INTRODUCTION

The chief contributors to the mainstream of transfer research have been astrophysicists. During the past seventy years, they have given considerable attention to problems connected with radiation transfer in planetary atmospheres, the sun, nebulae, and galaxies. Research in the field of radiation heat transfer has increased due to recent developments in aerospace engineering. In particular, gaseous radiative heat transfer has received increased attention from engineers concerned with modern high-temperature power plants and reentry vehicles. Recent technological developments have emphasized the need for a better quantitative understanding of radiant heat transfer through absorbing, emitting and scattering media.

Mathematically, the introduction of radiation into heat transfer problems results in changing the energy equation from a differential equation to an integro-differential equation. Such an equation is quite difficult to solve and practically all engineering calculations are based on simplifying assumptions. Another factor which makes radiative heat transfer more complicated than conductive or even convective heat transfer, is connected with the fact that the radiative properties of the various substances encountered in engineering are more difficult to describe than, for instance, the thermal conductivity, knowledge of which is required for calculation of a heat-conduction process.

The transfer of radiative energy in plane-parallel atmospheres has been studied in great detail and reported in the astrophysical and heat transfer literature. In particular, the problem of radiative

transfer between two infinite parallel plates kept at two different but uniform temperatures and separated by an absorbing and emitting gas has received much attention. Studies of radiative transfer have been largely limited to the treatment of the planar problem because of its simple geometry. While various analytical techniques have been developed to study the planar problem, the extension of these techniques to non-planar media is not so clear. Radiation in non-planar media is of current interest, e.g. in plasmas, and shock layers surrounding reentry bodies.

The primary motivation for undertaking this work is to present a systematic study of radiative transfer in nonplanar media (spherical geometry) by considering first the medium to be gray and then nongray. Because of the time and effort involved in carrying out a detailed study, only certain aspects of the radiative transfer problem are considered. Moreover, to help future researchers in this area, a review of literature is presented in chapter two which throws light on the work done on the spherical geometry problem.

Chapter three deals with the gray analysis and is divided into six sections. The first section is devoted to the description of physical model and governing equations. The isothermal analysis is considered in the next three sections. To gain a better insight into the isothermal problem, simple physical situations are considered. A conduction temperature profile is assumed to carry out numerical calculations for the nonisothermal case which is studied in the fifth section.

Nongray analysis is considered in chapters four and five. The rectangular model (also known as box model) is considered in chapter

four, while the effect of band or line shape on radiative transfer is considered in chapter five. Chapters four and five are written on the same lines as chapter three except that in addition the case of radiative equilibrium is investigated. In order to make a comparative study, the planar layer is also considered in chapters three, four and five and the equations compared with those arising in the spherical layer problem.

It is hoped that this study will contribute to some extent toward better understanding of the effect of curvature on radiative heat transfer in an absorbing-emitting, gray and nongray medium.

II. REVIEW OF LITERATURE

Radiative transfer in a spherically symmetric medium has recently received considerable attention. Different techniques have been developed which provide both rigorous and approximate solutions to the spherical geometry problem. The aim of this chapter is to present a review of the literature on radiative transfer in spherical media.

The pertinent literature in the engineering field have been tabulated in chronological order in Table 2.1 for quick reference. Unless otherwise specified, the following assumptions are applicable to the radiative transfer problems discussed in Table 2.1:

(1) Steady state;

(2) Gray medium;

(3) Absorbing-emitting medium; no scattering;

(4) No convection or conduction;

(5) Index of refraction of unity.

The physical situations corresponding to geometries 1, 2, 3 and 4 in the table stand for the following radiative transfer problems:

Geometry 1 - The medium is confined in the space between two concentric black spheres.

Geometry 2 - The medium is a sphere of finite radius.

Geometry 3 - A small black sphere situated in an infinite medium.

Geometry 4 - A spherical region of constant heat generation imbedded in an infinite gray medium.

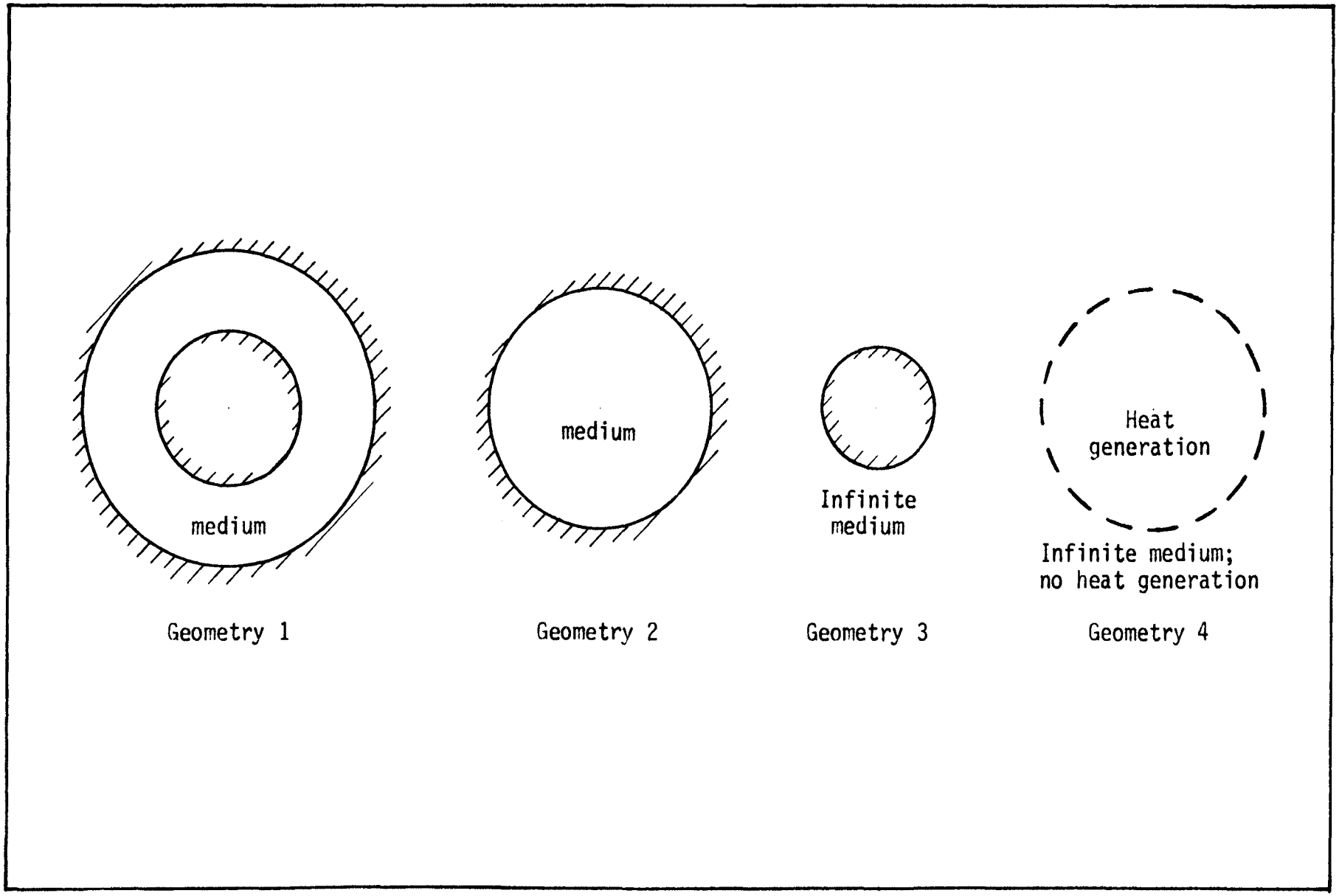

Figure 2.1 - Figures illustrating different geometries

Table 2.1

Review of literature table

Description of the Problem				
Year	Reference	Geometry	Physical situation	Method of solution
1951	Kuznetsov [1]*	2	Radiative equilibrium; Variable absorption coefficient	Formulates the integral equation
1961	Kennet and Strack [2]	1	Isothermal shock layer	Closed form expression for flux at the inner sphere
1961	Sparrow, Usiskin and Hubbard [3]	1	Uniform heat generation	Method of successive approximation
1962	Strack [4]	1	Nonisothermal shock layer	Numerical integration
1962	Koh [5]	1	Isothermal, nonisothermal shock layer	Numerical integration
1963	Kuznetsov [6]	2	Nongray medium; Gray walls; Heat generation	Formulates the integral equation
1963 1964	Cuperman, Engelmann and Oxenius [7,8]	2	Noncoherent scattering by a spectral line; Rectangular and Doppler profiles	Successive approximation; Eddington approximation; Modified Eddington approximation
1964	Giuffre and Engelmann [9]	2	Noncoherent scattering by a spectral line; Generalized Lorentz profile	Large optical thickness
1965	Heaslet and Warming [10]	2	Uniform heat generation; isotropic scattering	Invariance principles
1965	Koh [11]	2	Isothermal	Closed form expression
1965	Viskanta and Lall [12]	2	Transient cooling	Method of moments

Table 2.1 - (continued)

Review of literature table

Year	Reference	Geometry	Description of the Problem: Physical situation	Method of solution
1966	Heaslet and Warming [13]	2	Uniform heat generation; isotropic scattering; isotropic flux	Green's formula; Chandrasekhar-Ambartsumian functions
1966	Ryhming [14]	1	Radiative equilibrium	Method of undetermined parameters
1966	Viskanta and Lall [15]	2	Transient heating and cooling	Method of moments; Finite difference and least-squares
1967	Lall and Viskanta [16]	2	Transient cooling including convective effects	Finite difference and least-squares
1967	Viskanta and Crosbie [17]	1,2	Radiative equilibrium and uniform heat generation; gray walls	Method of successive approximation; Taylor expansion
1968	Chisnell [18]	1	Specified emissive power variation: constant; linear; quadratic	Exact; Differential approximation
1968	Chou and Tien [19]	1	Uniform heat generation	Modified moment method
1968	Emanuel [20]	1	Radiative equilibrium	Method of matched asymptotic expansions
1968	Hunt [21]	1	Uniform heat generation	Method of regional averaging
1968	Olfe [22]	1	Radiative equilibrium	Modified differential approximation
1968	Viskanta and Merriam [23]	1	Simultaneous conduction and radiation; absorbing, emitting and scattering medium with uniform heat generation; gray walls	Method of successive approximation

Table 2.1 - (continued)

Review of literature table

Description of the Problem				
Year	Reference	Geometry	Physical situation	Method of solution
1968	Voinov, Golovin and Petrov [24]	3	Radiative and conductive equilibrium; Radiative equilibrium; $\kappa r_0 \ll 1$; gray sphere	Linearization; Fourier and Laplace Transforms; Approximation solutions
1969	Voinov, Golovin and Petrov [25]	3	Unsteady radiative and conductive heat transfer; gray sphere; $\kappa r_0 \ll 1$	Linearization; Fourier and Laplace Transforms; Green's Functions
1969	Dennar and Sibulkin [26]	1	Uniform heat generation; gray walls	Differential approximation based upon half-range moments
1969	Emanuel [27]	3	Radiative equilibrium	Method of matched asymptotic expansions
1969	Lee and Olfe [28]	2,4	Heat generation	Iteration of the differential approximation
1969	Shahrokhi and Wolf [29,30]	1	Nonisothermal scattering medium	Finite difference iteration method
1969	Traugott [31]	1	Radiative equilibrium	Improved differential approximation
1970	Emanuel [32]	2	Super-radiant emission; Uniform temperature and composition	Closed form expression
1970	Gritton and Leonard [33]	2	Uniform heat generation	Singular integral equation theory
1970	Loyalka [34]	1	Radiative equilibrium	Variational method
1971	Finkleman [36]	1 2,4	(a) Radiative equilibrium (b) Heat generation	Generalized differential approximation

Table 2.1 - (continued)

Review of literature table

Description of the Problem				
Year	Reference	Geometry	Physical situation	Method of solution
1971	Chien [35]	1	Radiative equilibrium; Uniform heat generation; Linear temperature distribution	S_n method
1971	Saad [37]	1	Radiative equilibrium	Experimental and analytical; Matching jump boundary conditions with an assumed temperature profile

*Numbers in brackets designate references in Bibliography.

Going through the preceding table, one observes that geometries one and two are considered by most of the investigators who have pursued the study of radiative transfer in spherical geometry. Radiative transfer in a spherical layer (geometry one) and in the interior of a sphere (geometry two) is investigated in References [2-5, 14, 17-23, 26, 29-31, 34-37] and in References [1, 6-13, 15-17, 28, 32, 33, 36], respectively. The limiting case of a small sphere (geometry three) is considered in References [24, 25, 27], while the problem of a spherical region of constant heat generation imbedded in an infinite, gray medium (geometry four) is dealt with in References [28, 36].

Inspection of the column describing the physical situation in Table 2.1 reveals that the case of radiative equilibrium and that of heat generation is considered in References [1, 14, 17, 20, 22, 27, 31, 34-36] and in References [3, 6, 10, 13, 17, 19, 21, 26, 28, 33, 35-37], respectively. The isothermal shock layer is studied in References [2, 5, 11], while the nonisothermal shock layer is investigated in References [4, 5]. Unsteady heating and cooling is considered in References [12, 15, 16]. The problem of unsteady energy transfer is also considered in Reference [25]. References [23-25], unlike other references, consider conduction besides radiation. The problem of combined radiative and convective energy transfer between two concentric spheres is investigated experimentally in Reference [37]. Isotropic scattering is assumed in References [13, 23, 29, 30], while noncoherent scattering is assumed in References [7-9].

The solutions of integral equations which arise in the analysis of problems involving radiative transfer have been obtained by

numerical integration only in a limited number of cases. To circumvent some of the difficulties encountered, approximate methods have been devised to deal with this class of problems. References [7-9, 12, 15, 18-22, 24-27, 31, 34-37] deal with various approximate methods. Numerical calculations are carried out in References [3, 14-17, 23, 28-30], while sophisticated analytical solutions are reported in References [10, 13, 33].

A thorough survey of literature on radiative transfer in non-planar media (spherical geometry) was made. This survey included contributions from fields other than heat transfer, such as astrophysics and neutron transport. Although the survey is exhaustive, it may be incomplete.

Much of the theory of radiative transfer in the field of astrophysics is devoted to the study of transport processes in plane-parallel atmospheres. However, in many situations, curvature cannot be neglected. The general progress to date dealing with the spherical geometry problem in astrophysics is recorded in References [38-77].

Although the physical phenomenon of neutron transport is quite different from radiative transfer (photon transport), the governing equations are mathematically similar. References [78-108] deal with the spherical problem in the field of neutron transport.

Summarizing the review of literature on radiative transfer in a spherical media, one may thus conclude:

(1) Very few investigators deal with problems involving geometries three and four.

(2) Though there are various approximate methods to deal with radiative transfer problems in spherical geometry, exact

solutions are reported in only a few limited cases.

(3) The amount of work done considering the intervening medium to be nongray is very limited.

(4) There exists very little work dealing with problems that include other modes of heat transfer.

(5) Even though a mathematical analogy exists between thermal radiation, neutron transport and astrophysics in media with spherical symmetry, interchange of information between the various fields is almost nonexistent.

(6) The survey reveals that there is a lack of experimental work.

III. GRAY ANALYSIS

A. Physical Model and Governing Equations

1. Spherical Layer

The spherical system considered (similar to Geometry 1) is shown schematically in Figure 3.1. It illustrates a spherical gas layer of outer radius r_2 and inner radius r_1. The layer contains an absorbing and emitting gray gas with a volumetric absorption coefficient κ. The following assumptions are made:

(a) The energy transfer is steady and one-dimensional.

(b) The medium is non-scattering and is in local thermodynamic equilibrium.

(c) The index of refraction of the medium is considered to be unity.

(d) The volumetric absorption coefficient κ is independent of frequency, i.e. the medium is gray.

Although the gray medium approximation is rarely a physically realistic approximation, it serves at least as an initial stepping stone toward nongray analysis. These assumptions are introduced in order to simplify the mathematics without losing any essential physical features.

Under the above assumptions the local radiative flux can be expressed as [17]

$$\tau^2 \mathcal{G}(\tau) = 2F_1 h_1(\tau;\tau_1) - 2F_2 h_2(\tau;\tau_1,\tau_2) + 2\int_{\tau_1}^{\tau_2} H(\tau,t;\tau_1)\sigma T^4(t)dt \quad (3.1)$$

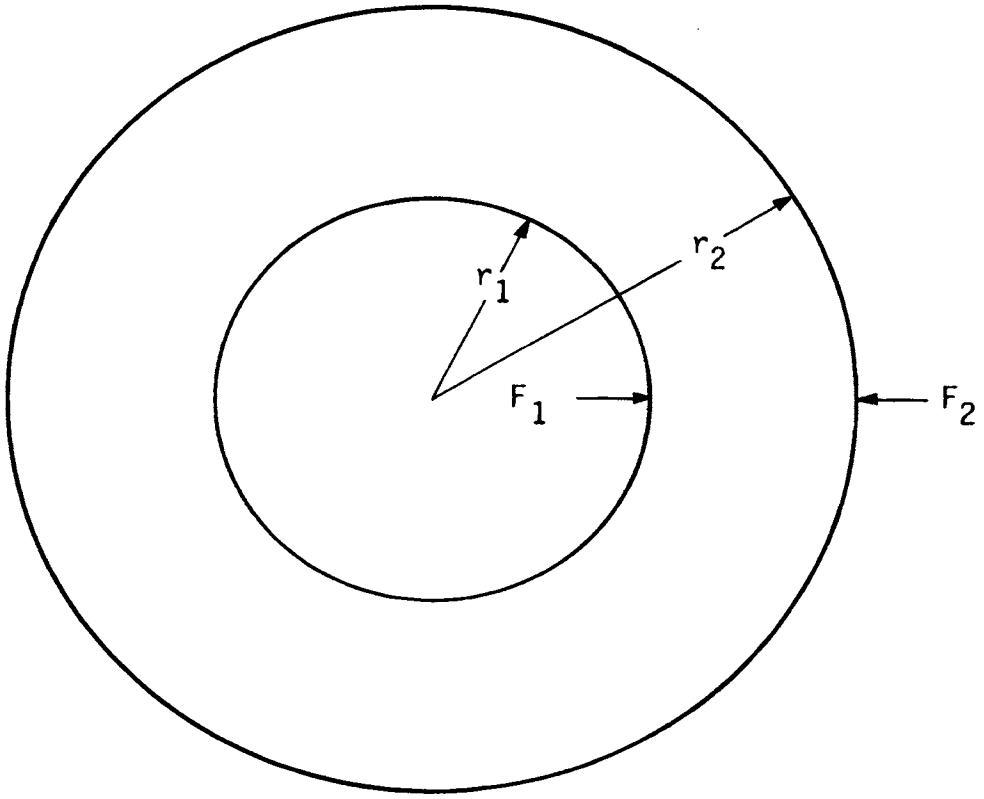

Figure 3.1 - Schematic diagram for a spherical geometry

where the optical radial distance τ is defined as

$$\tau = \int_0^r \kappa dr = \kappa r \qquad (3.2)$$

and the inner and outer optical radii as

$$\tau_1 = \kappa r_1 \qquad \text{and} \qquad \tau_2 = \kappa r_2$$

In equation (3.1) the quantity σT^4 is the black body emissive power, where σ is the Stefan-Boltzmann constant and T is the absolute temperature. The functions $h_1(\tau;\tau_1)$, $h_2(\tau;\tau_1,\tau_2)$ and $H(\tau,t;\tau_1)$ are defined

as

$$h_1(\tau;\tau_1) = \tau\tau_1 E_3(\tau-\tau_1) - (\tau-\tau_1)E_4(\tau-\tau_1) - E_5(\tau-\tau_1)$$
$$+ (\tau^2-\tau_1^2)^{\frac{1}{2}}E_4[(\tau^2-\tau_1^2)^{\frac{1}{2}}] + E_5[(\tau^2-\tau_1^2)^{\frac{1}{2}}] \qquad (3.3)$$

$$h_2(\tau;\tau_1,\tau_2) = \tau\tau_2 E_3(\tau_2-\tau) - (\tau_2-\tau)E_4(\tau_2-\tau) - E_5(\tau_2-\tau)$$
$$+ (\tau_2^2-\tau_1^2)^{\frac{1}{2}}(\tau^2-\tau_1^2)^{\frac{1}{2}}E_3[(\tau_2^2-\tau_1^2)^{\frac{1}{2}} + (\tau^2-\tau_1^2)^{\frac{1}{2}}]$$
$$+ [(\tau_2^2-\tau_1^2)^{\frac{1}{2}} + (\tau^2-\tau_1^2)^{\frac{1}{2}}]E_4[(\tau_2^2-\tau_1^2)^{\frac{1}{2}} + (\tau^2-\tau_1^2)^{\frac{1}{2}}]$$
$$+ E_5[(\tau_2^2-\tau_1^2)^{\frac{1}{2}} + (\tau^2-\tau_1^2)^{\frac{1}{2}}] \qquad (3.4)$$

$$H(\tau,t;\tau_1) = \{\tau \text{ sign } (\tau-t)E_2(|\tau-t|) + E_3(|\tau-t|)$$
$$- (\tau^2-\tau_1^2)^{\frac{1}{2}}E_2[(t^2-\tau_1^2)^{\frac{1}{2}} + (\tau^2-\tau_1^2)^{\frac{1}{2}}]$$
$$- E_3[(t^2-\tau_1^2)^{\frac{1}{2}} + (\tau^2-\tau_1^2)^{\frac{1}{2}}]\}\ t \qquad (3.5)$$

where the exponential integral function $E_n(\tau)$ is defined as

$$E_n(\tau) = \int_0^1 \mu^{n-2}\, e^{-\tau/\mu}\, d\mu = \int_1^\infty e^{-\tau x}\, x^{-n}\, dx \qquad (3.6)$$

The function $h_2(\tau;\tau_1,\tau_2)$ is the same as in Reference [17] except for the change in sign. The change in sign makes equation (3.1) more compatible with the expression for the local radiative flux in case of a planar layer.

In equation (3.1) and in Figure 3.1 F_1 and F_2 represent the radiative fluxes incident on the inside and outside of the layer respectively. If the gas layer is confined between two black surfaces, then $F_1 = \sigma T_1^4$ and $F_2 = \sigma T_2^4$ where T_1 and T_2 are the temperatures of

the inner and outer surfaces respectively. If the layer represents the shocked gas region in front of a blunt body, then the incident fluxes F_1 and F_2 will be essentially zero. This is due to the fact that the temperature in the shock layer will be high in comparison to the free stream temperature and the wall temperature.

Thus, given the geometry (r_1,r_2) the absorption coefficient (κ), the incident fluxes (F_1,F_2) and the temperature distribution (T), the radiative heat flux can be calculated from equation (3.1).

2. Planar Layer

In order to make a comparative study of the spherical geometry problem with that of the planar medium, the physical system shown schematically in Figure 3.2 is considered. The figure illustrates a plane gas layer of thickness L. The layer contains an absorbing and emitting gray gas with volumetric absorption coefficient κ. All the assumptions as enunciated before for the spherical geometry, hold for this geometry.

The expression for the local radiative flux is [109]

$$\mathcal{F}_p(\tau) = 2F_1E_3(\tau-\tau_1) - 2F_2E_3(\tau_2-\tau) + 2\int_{\tau_1}^{\tau_2} \text{sign}(\tau-t)E_2(|\tau-t|)\,\sigma T^4(t)dt \qquad (3.7)$$

where the optical depth τ is defined as

$$\tau = \int_0^x \kappa dx = \kappa x \qquad (3.8)$$

and the inner and outer optical thicknesses as

$$\tau_1 = \kappa x_1 \qquad \text{and} \qquad \tau_2 = \kappa x_2$$

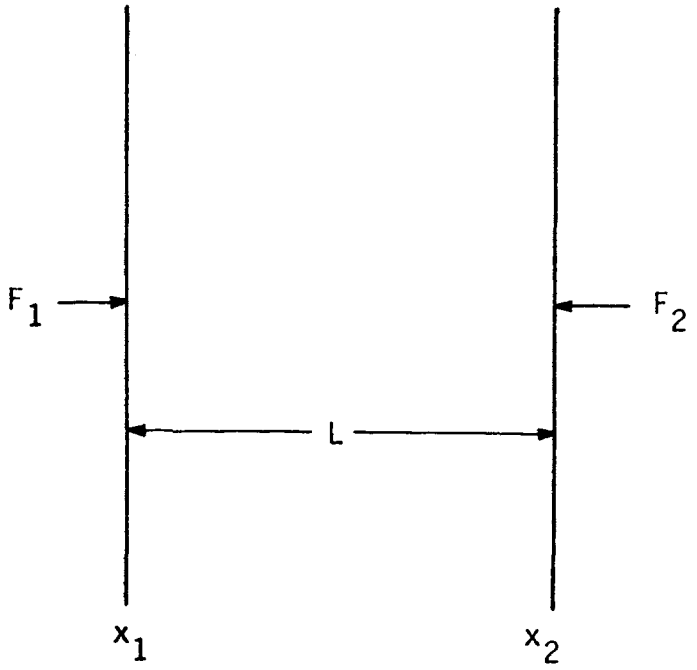

Figure 3.2 - Schematic diagram for a planar geometry

3. Isothermal Layer

The governing equations (3.1) and (3.7) for the local radiative flux can be simplified by considering the intervening gas to be isothermal. Moreover, this analysis facilitates the study of many interesting problems, e.g. thermal radiation from a shock layer.

For the isothermal case, i.e. $T(t) = T_0$, equation (3.1) reduces to

$$\tau^2 \mathcal{G}(\tau) = 2h_1(\tau;\tau_1)(F_1-\sigma T_0^4) - 2h_2(\tau;\tau_1,\tau_2)(F_2-\sigma T_0^4) \qquad (3.9)$$

To arrive at the above expression for the local radiative flux, the following relation is used

$$\int_{\tau_1}^{\tau_2} H(\tau,t;\tau_1)dt = - h_1(\tau;\tau_1) + h_2(\tau;\tau_1,\tau_2) \qquad (3.10)$$

Now, considering the case when there is no flux incident on the inner and outer layers, i.e. when $F_1 = F_2 = 0$, equation (3.9) further simplifies to

$$\tau^2 \mathcal{G}(\tau) = -2\sigma T_0^4 [h_1(\tau;\tau_1) - h_2(\tau;\tau_1,\tau_2)] \qquad (3.11)$$

With $T(t) = T_0$, the governing equation (3.7) for the local radiative flux in case of a planar medium reduces to

$$\mathcal{F}_p(\tau) = 2E_3(\tau-\tau_1)(F_1-\sigma T_0^4) - 2E_3(\tau_2-\tau)(F_2-\sigma T_0^4) \qquad (3.12)$$

When $F_1 = F_2 = 0$, equation (3.12) simplifies to

$$\mathcal{F}_p(\tau) = -2\sigma T_0^4 [E_3(\tau-\tau_1) - E_3(\tau_2-\tau)] \qquad (3.13)$$

Comparison of equations (3.11) and (3.13) reveals that the functions $h_1(\tau;\tau_1)/\tau^2$ and $h_2(\tau;\tau_1,\tau_2)/\tau^2$ are analogous to the functions $E_3(\tau-\tau_1)$ and $E_3(\tau_2-\tau)$ respectively.

Examination of equation (3.9) reveals that the local radiative flux depends on the functions $h_1(\tau;\tau_1)$ and $h_2(\tau;\tau_1,\tau_2)$. Therefore, to gain some insight into the local radiative flux, it seems appropriate to study the functions $h_1(\tau;\tau_1)$ and $h_2(\tau;\tau_1,\tau_2)$.

B. Isothermal Analysis: Function $h_1(\tau;\tau_1)$

In order to give the function $h_1(\tau;\tau_1)$ a physical interpretation, consider the case described in Figure 3.3. When the outer boundary is

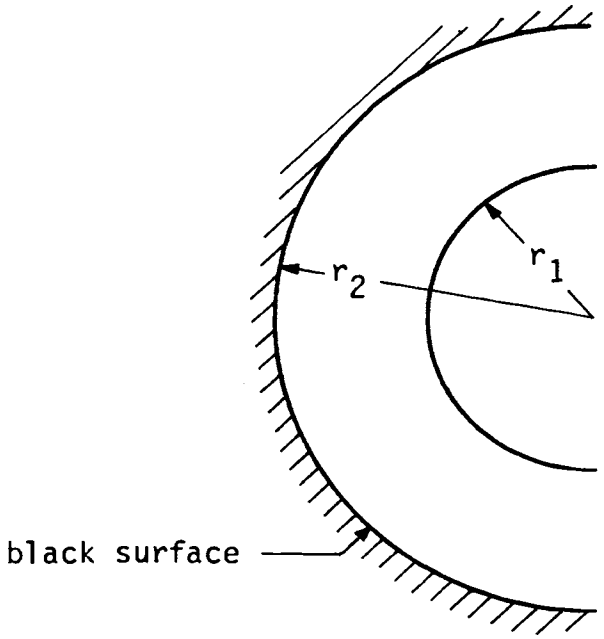

Figure 3.3 - Outer boundary isothermal with the intervening medium

a black surface at the temperature of the medium, i.e. $T_2=T_0$, then inspection of equation (3.9) reveals that $\mathcal{G}(\tau)$ is proportional to $h_1(\tau;\tau_1)/\tau^2$. From expression (3.3) one finds that the function $h_1(\tau;\tau_1)$ does not contain τ_2. Therefore, the variation in the outer radius of the spherical layer does not influence the function $h_1(\tau;\tau_1)$. The following cases of the function $h_1(\tau;\tau_1)$ are studied:

1. Exact Results

Numerical results are obtained using the exact expression (3.3) for the function $h_1(\tau;\tau_1)$. The results for four different cases, i.e. τ_1 = 0.01, 0.1, 1 and 5, are tabulated in Tables 3.1 and 3.2 and presented graphically in Figures 3.4 and 3.5. The influence of radius ratio τ_1/τ on $h_1(\tau;\tau_1)/\tau^2$ is shown in Figure 3.4, while the influence

of optical thickness $\tau-\tau_1$ on $h_1(\tau;\tau_1)/\tau^2$ is shown in Figure 3.5.

Figure 3.4 shows that all the four curves (displayed as unbroken lines) start at the same value when $\tau_1/\tau = 1$. For the first two cases ($\tau_1 = 0.01$ and 0.1) decrease in $h_1(\tau;\tau_1)/\tau^2$ is quite gradual as $\tau_1/\tau \to 0$, while for the next two cases ($\tau_1 = 1$ and 5) decrease in $h_1(\tau;\tau_1)/\tau^2$ is quite rapid as $\tau_1/\tau \to 0$. In all the four cases $h_1(\tau;\tau_1)/\tau^2$ approaches zero as τ_1/τ tends to zero. The curves, for each of the four cases, for the function $E_3(\tau-\tau_1)$ are shown by broken lines.

Figure 3.5 shows that all the four curves (displayed as unbroken lines) start at the same value when $\tau-\tau_1 = 0$. For the first two cases ($\tau_1 = 0.01$ and 0.1) decrease in $h_1(\tau;\tau_1)/\tau^2$ is quite rapid as $\tau-\tau_1 \to \infty$, while for the next two cases ($\tau_1 = 1$ and 5) decrease in $h_1(\tau;\tau_1)/\tau^2$ is quite gradual as $\tau-\tau_1 \to \infty$. In all the four cases $h_1(\tau;\tau_1)/\tau^2$ approaches zero as $\tau-\tau_1$ tends to infinity. The curve for the function $E_3(\tau-\tau_1)$ is shown by broken lines.

In examining the results presented in Figures 3.4 and 3.5, we note that the planar layer approximation appears to be useful only for values of $\tau \simeq \tau_1$ and for large values of τ_1. The calculations were performed by using the series representation for the function $E_2(\tau)$ as given by equation (A.8) and the recurrence relation as given by equation (A.2). These calculations were made by using double precision and the method breaks down for large τ.

Table 3.1

Values of the function $h_1(\tau;\tau_1)/\tau^2$ versus τ_1/τ

τ_1/τ	$h_1(\tau;\tau_1)/\tau^2$			
	τ_1=0.01	τ_1=0.10	τ_1=1.0	τ_1=5.0
0.01	1.8518D-5	2.4277D-9		
0.02	1.2212D-4	1.4416D-6		
0.03	3.2462D-4	1.7177D-5		
0.04	6.2727D-4	7.0284D-5		
0.05	1.0304D-3	1.8110D-4		
0.06	1.5341D-3	3.6405D-4	2.3748D-10	
0.07	2.1384D-3	6.2888D-4	3.1096D-09	
0.08	2.8435D-3	9.8223D-4	2.4273D-08	
0.09	3.6492D-3	1.4287D-3	1.2347D-07	
0.10	4.5556D-3	1.9716D-3	4.6408D-07	
0.15	1.0599D-2	6.1988D-3	2.9597D-05	
0.20	1.9162D-2	1.3035D-2	2.8173D-04	
0.25	3.0245D-2	2.2538D-2	1.2103D-03	
0.30	4.3849D-2	3.4737D-2	3.4343D-03	1.5280D-7
0.35	5.9977D-2	4.9651D-2	7.6152D-03	2.3392D-5
0.40	7.8628D-2	6.7298D-2	1.4389D-02	1.8978D-5
0.45	9.9804D-2	8.7693D-2	2.4343D-02	1.0050D-4
0.50	1.2351D-1	1.1085D-1	3.8017D-02	3.9404D-4
0.55	1.4974D-1	1.3679D-1	5.5910D-02	1.2400D-3
0.60	1.7850D-1	1.6552D-1	7.8500D-02	3.3073D-3
0.65	2.0979D-1	1.9707D-1	1.0626D-01	7.7668D-3
0.70	2.4361D-1	2.3146D-1	1.3966D-01	1.6511D-2
0.75	2.7997D-1	2.6872D-1	1.7924D-01	3.2443D-2
0.80	3.1887D-1	3.0888D-1	2.2557D-01	5.9901D-2
0.85	3.6031D-1	3.5198D-1	2.7938D-01	1.0535D-1
0.90	4.0430D-1	3.9810D-1	3.4163D-01	1.7875D-1
0.95	4.5086D-1	4.4733D-1	4.1388D-01	2.9696D-1
1.00	5.0000D-1	5.0000D-1	5.0000D-01	5.0000D-1

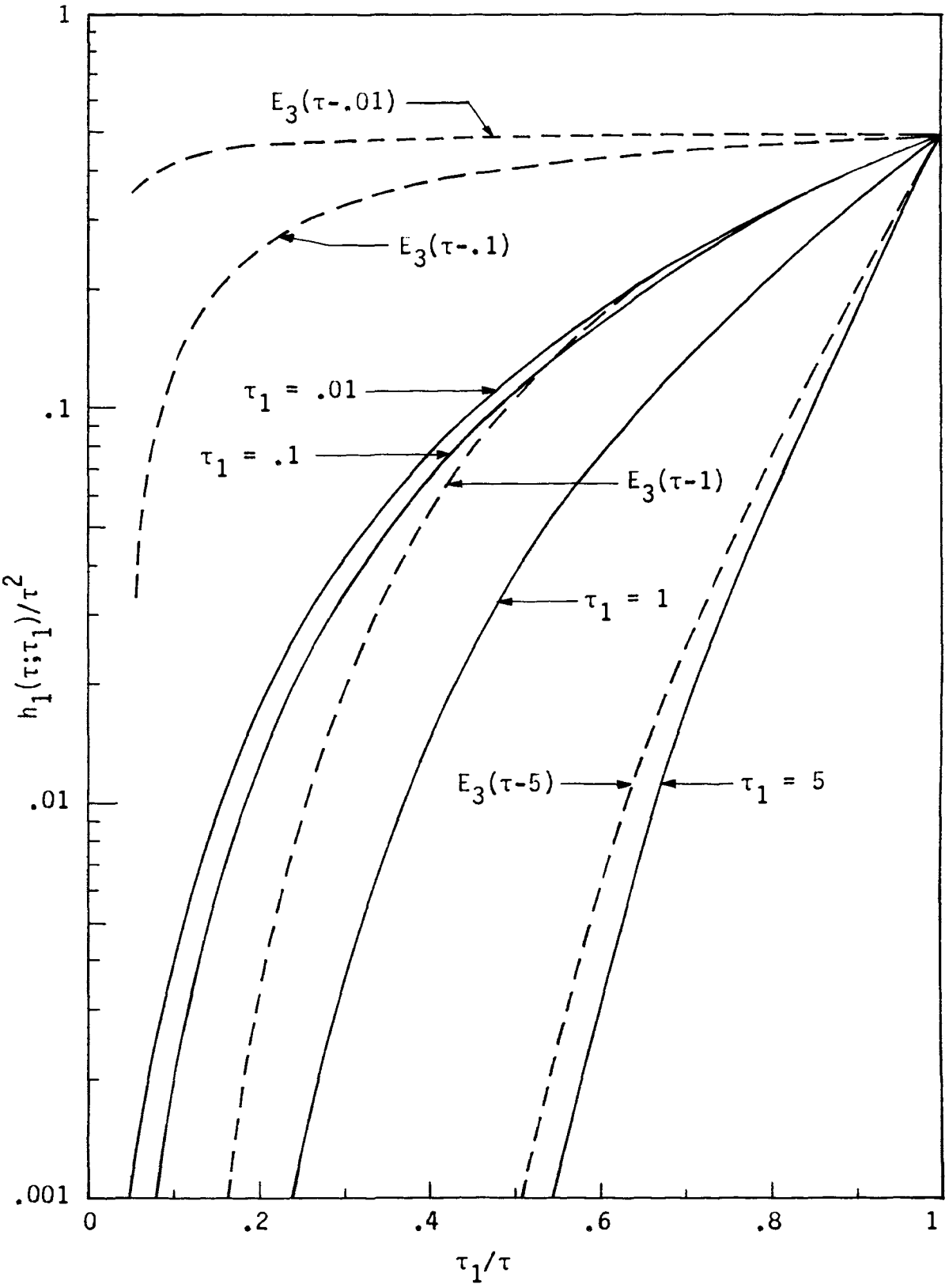

Figure 3.4 - Function $h_1(\tau;\tau_1)/\tau^2$ versus τ_1/τ

Table 3.2

Values of the function $h_1(\tau;\tau_1)/\tau^2$ versus $\tau-\tau_1$

$\tau-\tau_1$	$h_1(\tau;\tau_1)/\tau^2$			
	τ_1=0.01	τ_1=0.1	τ_1=1.0	τ_1=5.0
0	5.0000D-1	5.0000D-1	5.0000D-1	5.0000D-1
0.001	4.1258D-1	4.8925D-1	4.9803D-1	4.9882D-1
0.002	3.4621D-1	4.7889D-1	4.9610D-1	4.9765D-1
0.003	2.9463D-1	4.6886D-1	4.9419D-1	4.9649D-1
0.004	2.5374D-1	4.5916D-1	4.9230D-1	4.9534D-1
0.005	2.2078D-1	4.4976D-1	4.9043D-1	4.9420D-1
0.006	1.9382D-1	4.4065D-1	4.8857D-1	4.9307D-1
0.007	1.7150D-1	4.3181D-1	4.8673D-1	4.9194D-1
0.008	1.5281D-1	4.2323D-1	4.8491D-1	4.9082D-1
0.009	1.3700D-1	4.1490D-1	4.8309D-1	4.8971D-1
0.010	1.2351D-1	4.0681D-1	4.8130D-1	4.8860D-1
0.020	5.4320D-2	3.3728D-1	4.6397D-1	4.7784D-1
0.030	3.0245D-2	2.8382D-1	4.4767D-1	4.6754D-1
0.040	1.9162D-2	2.4182D-1	4.3225D-1	4.5763D-1
0.050	1.3173D-2	2.0822D-1	4.1762D-1	4.4807D-1
0.060	9.5813D-3	1.8094D-1	4.0368D-1	4.3883D-1
0.070	7.2624D-3	1.5851D-1	3.9040D-1	4.2988D-1
0.080	5.6809D-3	1.3984D-1	3.7771D-1	4.2120D-1
0.090	4.5556D-3	1.2415D-1	3.6558D-1	4.1278D-1
0.100	3.7274D-3	1.1085D-1	3.5397D-1	4.0460D-1
0.200	9.2529D-4	4.4377D-2	2.6056D-1	3.3366D-1
0.300	3.8419D-4	2.2538D-2	1.9622D-1	2.7784D-1
0.400	1.9873D-4	1.3035D-2	1.5032D-1	2.3290D-1
0.500	1.1621D-4	8.1839D-3	1.1674D-1	1.9624D-1
0.600	7.3503D-5	5.4372D-3	9.1703D-2	1.6603D-1
0.700	4.9093D-5	3.7651D-3	7.2738D-2	1.4096D-1
0.800	3.4130D-5	2.6908D-3	5.8179D-2	1.2003D-1
0.900	2.4467D-5	1.9716D-3	4.6877D-2	1.0247D-1
1.000	1.7972D-5	1.4740D-3	3.8017D-2	8.7681D-2
2.000	1.6694D-6	1.4863D-4	5.9640D-3	2.0171D-2
3.000	2.7385D-7	2.5081D-5	1.2103D-3	5.1396D-3
4.000	5.6762D-8	5.2739D-6	2.8173D-4	1.3930D-3
5.000	1.3378D-8	1.2538D-6	7.1436D-5	3.9404D-4

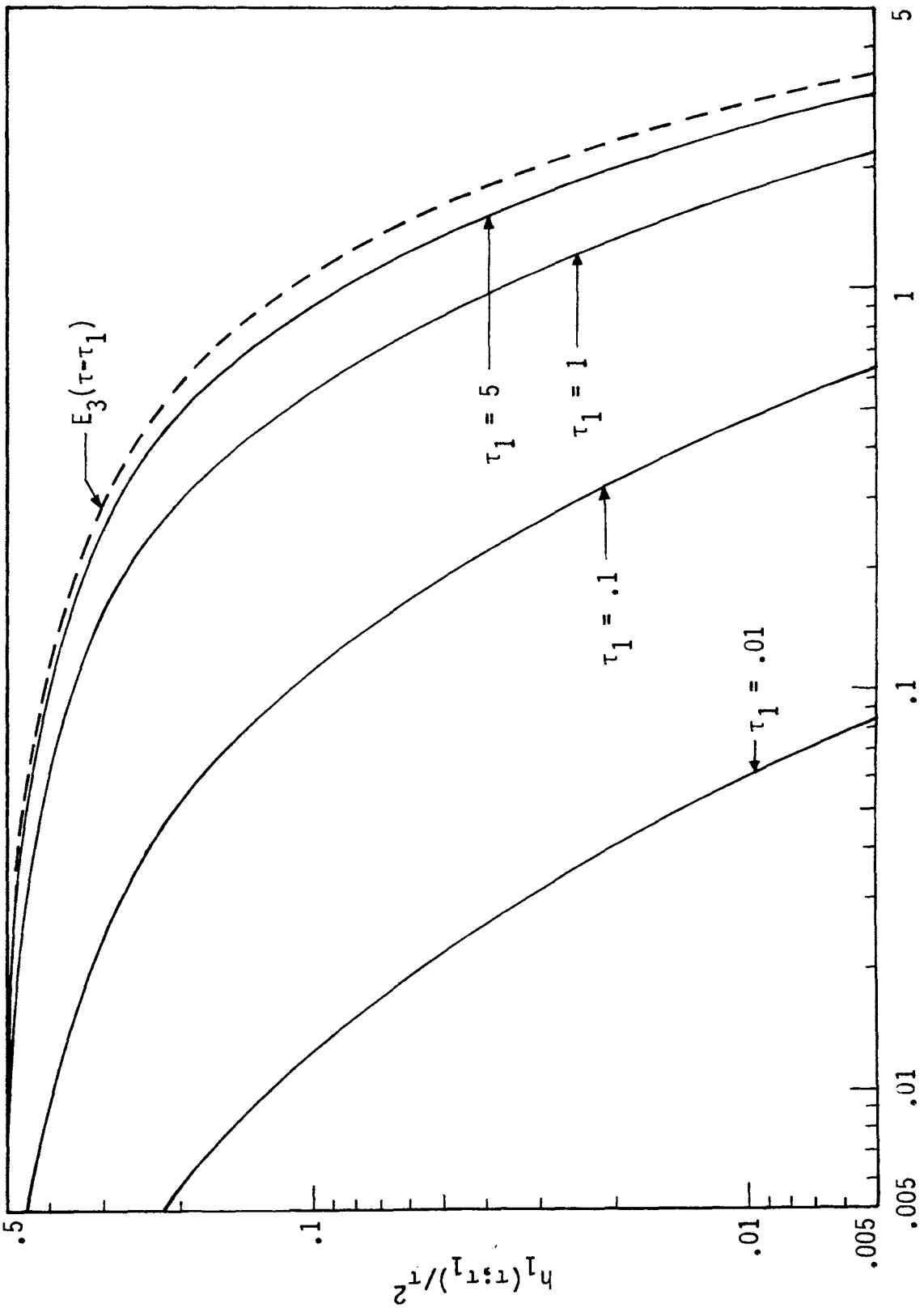

Figure 3.5 - Function $h_1(\tau;\tau_1)/\tau^2$ versus $\tau-\tau_1$

2. Special Limiting Results

a. Optically Thin

By utilizing the asymptotic expansions for functions $E_3(\tau)$, $E_4(\tau)$ and $E_5(\tau)$ as $\tau \to 0$ (see Appendix A), the function $h_1(\tau;\tau_1)$ in the optically thin approximation becomes

$$h_1(\tau;\tau_1) = \frac{\tau_1^2}{2} - \frac{(\tau^3-\tau_1^3)}{3} + \frac{(\tau^2-\tau_1^2)^{3/2}}{3} \qquad (3.14)$$

From equation (3.14) it is possible to deduce that

$$\lim_{\tau\to\tau_1} h_1(\tau;\tau_1) = \frac{\tau_1^2}{2} \qquad (3.15)$$

Substitution of $\tau = \tau_1$ in expression (3.3) leads to the same result as in (3.15), i.e. $h_1(\tau=\tau_1;\tau_1) = \tau_1^2/2$. It is found that for $\tau_1 = 0.01$ and for values of $\tau \geq 0.1$, the error in using equation (3.14) instead of equation (3.3) is less than 0.5%, while for $\tau_1 = 0.1$ and for values of $\tau \geq 0.4$, the error is less than 7%. Equation (3.14) is not at all useful for values of $\tau_1 \geq 1$.

b. Optically Thick

By utilizing the approximate expressions for large τ for functions $E_3(\tau)$, $E_4(\tau)$ and $E_5(\tau)$ as $\tau \to \infty$ (see Appendix A), the function $h_1(\tau;\tau_1)$ in the optically thick limit becomes

$$h_1(\tau;\tau_1) = \frac{\tau\tau_1 e^{-(\tau-\tau_1)}}{(\tau-\tau_1+3)} - \frac{(\tau-\tau_1)e^{-(\tau-\tau_1)}}{(\tau-\tau_1+4)} - \frac{e^{-(\tau-\tau_1)}}{(\tau-\tau_1+5)}$$

$$+ \frac{(\tau^2-\tau_1^2)^{\frac{1}{2}}e^{-(\tau^2-\tau_1^2)^{\frac{1}{2}}}}{[(\tau^2-\tau_1^2)^{\frac{1}{2}}+4]} + \frac{e^{-(\tau^2-\tau_1^2)^{\frac{1}{2}}}}{[(\tau^2-\tau_1^2)^{\frac{1}{2}}+5]} \qquad (3.16)$$

Numerical results obtained show that the approximate expression (3.16) cannot be used for small optical radii. But as τ_1 increases, the approximation shows good agreement. The results reveal that the approximation cannot be used when $\tau_1 = 0.01$. For the case when $\tau_1 = 0.1$, the error is less than 1% for values of $\tau_1/\tau \leq 0.2$. The error is within 1.5% when $\tau_1 = 1$ and the ratio $\tau_1/\tau \leq 0.1$, while the same is the case when $\tau_1 = 5$ and the ratio $\tau_1/\tau \leq 0.3$.

Table 3.3 present the values of the function $h_1(\tau;\tau_1)$ as obtained by using the exact expression (3.3) and the approximate expression (3.16) for the case when $\tau_1 = 5$. For the cases when $\tau_1 = 0.01$, 0.1 and 1, the error is much worse and thus the results are not presented.

Table 3.3

Comparison of the exact and optically thick values of the function $h_1(\tau;\tau_1)$ for $\tau_1 = 5$

τ	$h_1(\tau;\tau_1)$		Relative Error (%)
	Exact	Approximate	
	τ_1=5.0		
0.3	4.2445D-5	4.1927D-5	1.22
0.4	2.9654D-3	2.8957D-3	2.35
0.5	3.9404D-2	3.7826D-2	4.01
0.6	2.2967D-1	2.1511D-1	6.34
0.7	8.4239D-1	7.6138D-1	9.62
0.8	2.3399D+0	2.0067D+0	14.24
0.9	5.5170D+0	4.3546D+0	21.10
1.0	1.2500D+1	8.3333D+0	33.40

c. Small Sphere

Expansion of the function $h_1(\tau;\tau_1)$ in a Taylor's series about $\tau_1 = 0$ yields

$$h_1(\tau;\tau_1) = \frac{\tau_1^2}{2} e^{-\tau} + \frac{\tau_1^3}{3} e^{-\tau} \tag{3.17}$$

From equation (3.17), we find that

$$\lim_{\tau_1 \to 0} h_1(\tau;\tau_1) = 0 \tag{3.18}$$

On substituting $\tau_1 = 0$ in expression (3.3), one gets the same result as in (3.18), i.e. $h_1(\tau;\tau_1=0) = 0$. In order to determine the accuracy of equation (3.17) numerical results are obtained for three different cases, i.e. $\tau_1 = 0.01$, 0.1 and 1. The exact results tabulated in Table 3.4 are obtained by using expression (3.3), while the approximate results are obtained by using equation (3.17) with only the first term taken into account.

Inspection of Table 3.4 reveals that for $\tau_1 = 0.01$ and $\tau = 0.01$, the relative error is 1% and the error decreases as τ increases. For the second case, i.e. $\tau_1 = 0.1$, the maximum error (9.5%) occurs when $\tau = 0.1$, while for the case when $\tau_1 = 1$, the error is maximum (63%) when $\tau = 1$. In all the cases the error decreases as τ increases.

C. Isothermal Analysis; Function $h_2(\tau;\tau_1,\tau_2)$

Figure 3.6 represents the situation when the inner boundary is a black surface at the temperature of the medium, i.e. $T_1 = T_0$. For this case from equation (3.9) one finds that $\mathcal{G}(\tau)$ is proportional to $h_2(\tau;\tau_1,\tau_2)/\tau^2$. It is for this reason that a study of the function

Table 3.4

Comparison of the exact and small sphere values of the function $h_1(\tau;\tau_1)$ for τ_1 = 0.01, 0.1 and 1

τ	$h_1(\tau;\tau_1)$		Relative Error (%)
	Exact	Approximate	
	(i) τ_1=0.01		
0.01	5.0000D-5	4.9502D-5	1.00
0.02	4.9402D-5	4.9010D-5	0.79
0.03	4.8888D-5	4.8522D-5	0.75
0.04	4.8391D-5	4.8039D-5	0.73
0.05	4.7903D-5	4.7561D-5	0.71
0.06	4.7423D-5	4.7088D-5	0.71
0.07	4.6948D-5	4.6620D-5	0.70
0.08	4.6479D-5	4.6156D-5	0.70
0.09	4.6015D-5	4.5697D-5	0.69
0.10	4.5556D-5	4.5242D-5	0.69
	(ii) τ_1=0.10		
0.10	5.0000D-3	4.5242D-3	9.52
0.20	4.4340D-3	4.0937D-3	7.68
0.30	3.9939D-3	3.7041D-3	7.26
0.40	3.6061D-3	3.3516D-3	7.06
0.50	3.2588D-3	3.0327D-3	6.94
0.60	2.9462D-3	2.7441D-1	6.86
0.70	2.6642D-3	2.4829D-3	6.81
0.80	2.4096D-3	2.2466D-3	6.76
0.90	2.1796D-3	2.0328D-3	6.73
1.00	1.9716D-3	1.8394D-3	6.71
	(iii) τ_1=1.0		
1.0	5.0000D-1	1.8394D-1	63.21
2.0	1.5207D-1	6.7668D-2	55.50
3.0	5.3676D-2	2.4894D-2	53.62
4.0	1.9366D-2	9.1578D-3	52.71
5.0	7.0433D-3	3.3690D-3	52.17
6.0	2.5717D-3	1.2394D-3	51.81
7.0	9.4105D-4	4.5594D-4	51.55
8.0	3.4482D-4	1.6773D-4	51.36
9.0	1.2646D-4	6.1705D-5	51.21
10.0	4.6408D-5	2.2700D-5	51.09

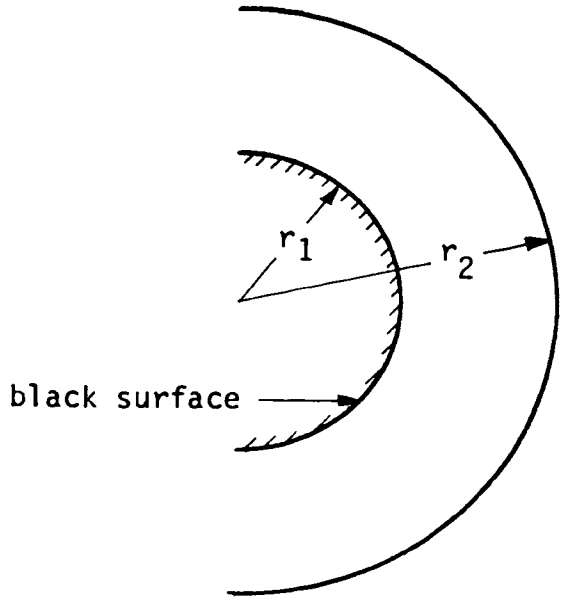

Figure 3.6 - Inner boundary isothermal with the intervening medium

$h_2(\tau;\tau_1,\tau_2)$ is undertaken in this section. The following cases of the function $h_2(\tau;\tau_1,\tau_2)$ are considered:

1. Exact Results

Results are obtained using the exact expression (3.4) for the function $h_2(\tau;\tau_1,\tau_2)$ for five different values of τ_2 and four different ratios of inner to outer optical radii. The results shown in Table 3.5 and presented graphically in Figures 3.7 through 3.10 reveal that for any fixed value of $\tau_2 \leq 1$, the influence of radius ratio τ_1/τ_2 on the function $h_2(\tau;\tau_1,\tau_2)/\tau^2$ is quite significant, while for any fixed value of $\tau_2 \leq 5$, the results for different radii ratios do not vary

much. In each of the Figures 3.7 through 3.10, the curve for the function $E_3(\tau_2-\tau)$ is shown in broken lines.

One may thus conclude that for large values of τ_2, the values of the function $h_2(\tau;\tau_1,\tau_2)/\tau^2$ will depend only on the ratio τ/τ_2, the effect of τ_1 being negligible. To put it differently, the results reveal that as τ_2 increases, the planar layer approximation becomes more accurate as seen from Figure 3.10.

2. Special Limiting Results

a. Optically Thin

With the aid of the asymptotic expansions for functions $E_3(\tau)$, $E_4(\tau)$ and $E_5(\tau)$ as $\tau \to 0$, it can be shown that the function $h_2(\tau;\tau_1,\tau_2)$ in the optically thin limit becomes

$$h_2(\tau;\tau_1,\tau_2) = \frac{\tau_1^2}{2} - \frac{(\tau_2^3-\tau^3)}{3} + \frac{(\tau_2^2-\tau_1^2)^{3/2}}{3} + \frac{(\tau^2-\tau_1^2)^{3/2}}{3} \quad (3.19)$$

From equation (3.19) one observes that

$$\lim_{\substack{\tau\to\tau_1 \\ \tau_2\to\tau_1}} h_2(\tau;\tau_1,\tau_2) = \frac{\tau_1^2}{2} \quad (3.20)$$

It is interesting to note that the limits of expressions for the functions $h_1(\tau;\tau_1)$ and $h_2(\tau;\tau_1,\tau_2)$ in the optically thin limit tend to the same value $\tau_1^2/2$.

b. Function $h_2(\tau;\tau_1,\tau_2)$ evaluated at $\tau = \tau_1$

In order to gain some idea about the variation of the flux at the inner boundary, this case is investigated. The following relation

Table 3.5

Values of the function $h_2(\tau;\tau_1,\tau_2)/\tau^2$ for various ratios of inner to outer optical radii

τ/τ_2	$h_2(\tau;\tau_1,\tau_2)/\tau^2$				
	τ_2=0.1	τ_2=0.5	τ_2=1.0	τ_2=5.0	τ_2=10.0
			(a) τ_1/τ_2=0		
0.10	6.0333D-3	2.0243D-2	2.4599D-2	2.3257D-3	3.4063D-5
0.20	1.2075D-2	4.0639D-2	4.9645D-2	5.1571D-3	9.5263D-5
0.30	1.8131D-2	6.1347D-2	7.5609D-2	9.1481D-3	2.3771D-4
0.40	2.4212D-2	8.2540D-2	1.0301D-1	1.5307D-2	6.0065D-4
0.50	3.0326D-2	1.0441D-1	1.3245D-1	2.5347D-2	1.5708D-3
0.60	3.6484D-2	1.2719D-1	1.6469D-1	4.2373D-2	4.2731D-3
0.70	4.2699D-2	1.5116D-1	2.0069D-1	7.2316D-2	1.2152D-2
0.80	4.8988D-2	1.7672D-1	2.4184D-1	1.2735D-1	3.6552D-2
0.90	5.5378D-2	2.0448D-1	2.9040D-1	2.3569D-1	1.1995D-1
0.95	5.8624D-2	2.1951D-1	3.1874D-1	3.3122D-1	2.3090D-1
1.00	6.1923D-2	2.3576D-1	3.5150D-1	4.9000D-1	4.9750D-1
			(b) τ_1/τ_2=0.1		
0.10	4.5556D-1	3.1396D-1	1.9716D-1	4.7896D-3	4.6408D-5
0.20	1.2311D-1	1.0978D-1	8.7887D-2	5.4924D-3	9.6164D-5
0.30	6.6968D-2	9.0510D-2	9.0917D-2	9.2364D-3	2.3785D-4
0.40	5.1404D-2	9.8126D-2	1.1078D-1	1.5336D-2	6.0068D-4
0.50	4.7553D-2	1.1389D-1	1.3695D-1	2.5359D-2	1.5708D-3
0.60	4.8327D-2	1.3345D-1	1.6751D-1	4.2378D-2	4.2731D-3
0.70	5.1313D-2	1.5553D-1	2.0256D-1	7.2318D-2	1.2152D-2
0.80	5.5518D-2	1.7990D-1	2.4314D-1	1.2735D-1	3.6552D-2
0.90	6.0485D-2	2.0687D-1	2.9133D-1	2.3569D-1	1.1995D-1
0.95	6.3185D-2	2.2161D-1	3.1954D-1	3.3122D-1	2.3090D-1
1.00	6.6018D-2	2.3760D-1	3.5218D-1	4.9001D-1	4.9750D-1
			(c) τ_1/τ_2=0.5		
0.50	4.7084D-1	3.7047D-1	2.7492D-1	2.6565D-2	1.5761D-3
0.60	3.3796D-1	2.9875D-1	2.4974D-1	4.2722D-2	4.2736D-3
0.70	2.6150D-1	2.6967D-1	2.5588D-1	7.2449D-2	1.2152D-2
0.80	2.1459D-1	2.6238D-1	2.7948D-1	1.2741D-1	3.6552D-2
0.90	1.8478D-1	2.6850D-1	3.1701D-1	2.3571D-1	1.1995D-1
0.95	1.7414D-1	2.7544D-1	3.4136D-1	3.3123D-1	2.3090D-1
1.00	1.6561D-1	2.8489D-1	3.7084D-1	4.9002D-1	4.9750D-1
			(d) τ_1/τ_2=0.9		
0.90	4.9232D-1	4.6293D-1	4.2894D-1	2.3870D-1	1.2005D-1
0.95	4.4752D-1	4.4140D-1	4.3171D-1	3.3248D-1	2.3092D-1
1.00	4.1035D-1	4.2857D-1	4.4570D-1	4.9069D-1	4.9750D-1

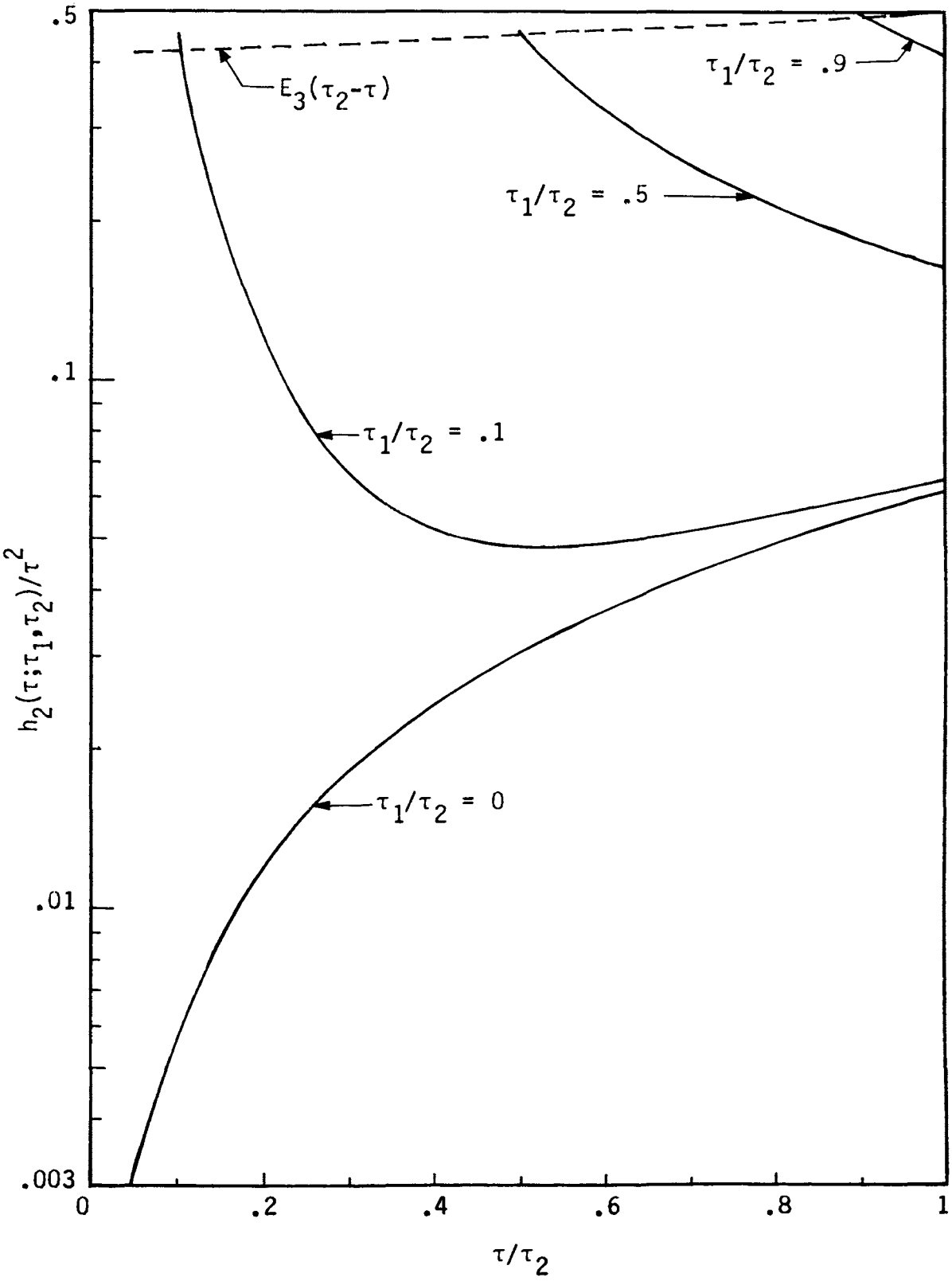

Figure 3.7 - Function $h_2(\tau;\tau_1,\tau_2)/\tau^2$ versus τ/τ_2 for $\tau_2 = 0.1$

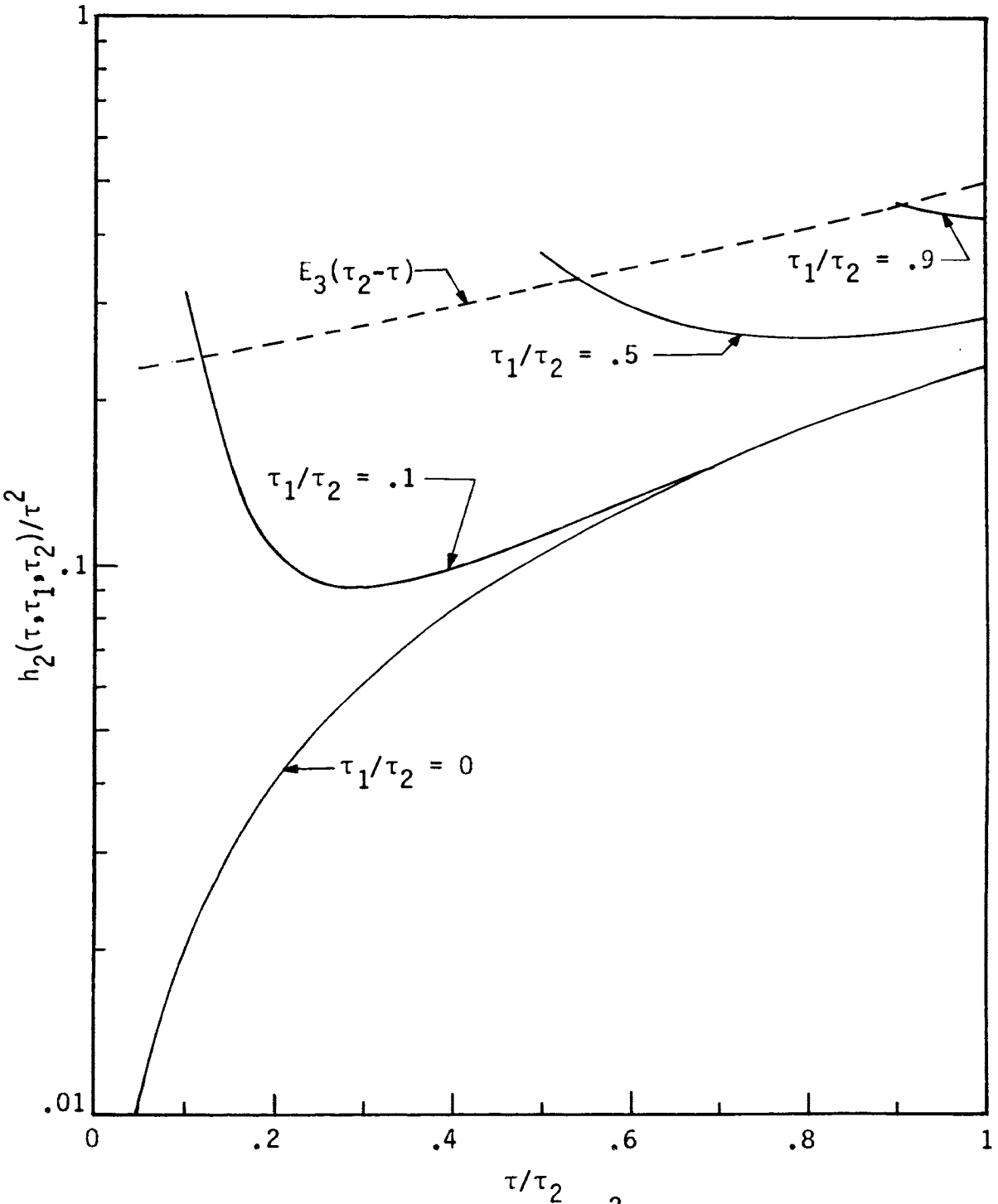

Figure 3.8 - Function $h_2(\tau;\tau_1,\tau_2)/\tau^2$ versus τ/τ_2 for $\tau_2 = 0.5$

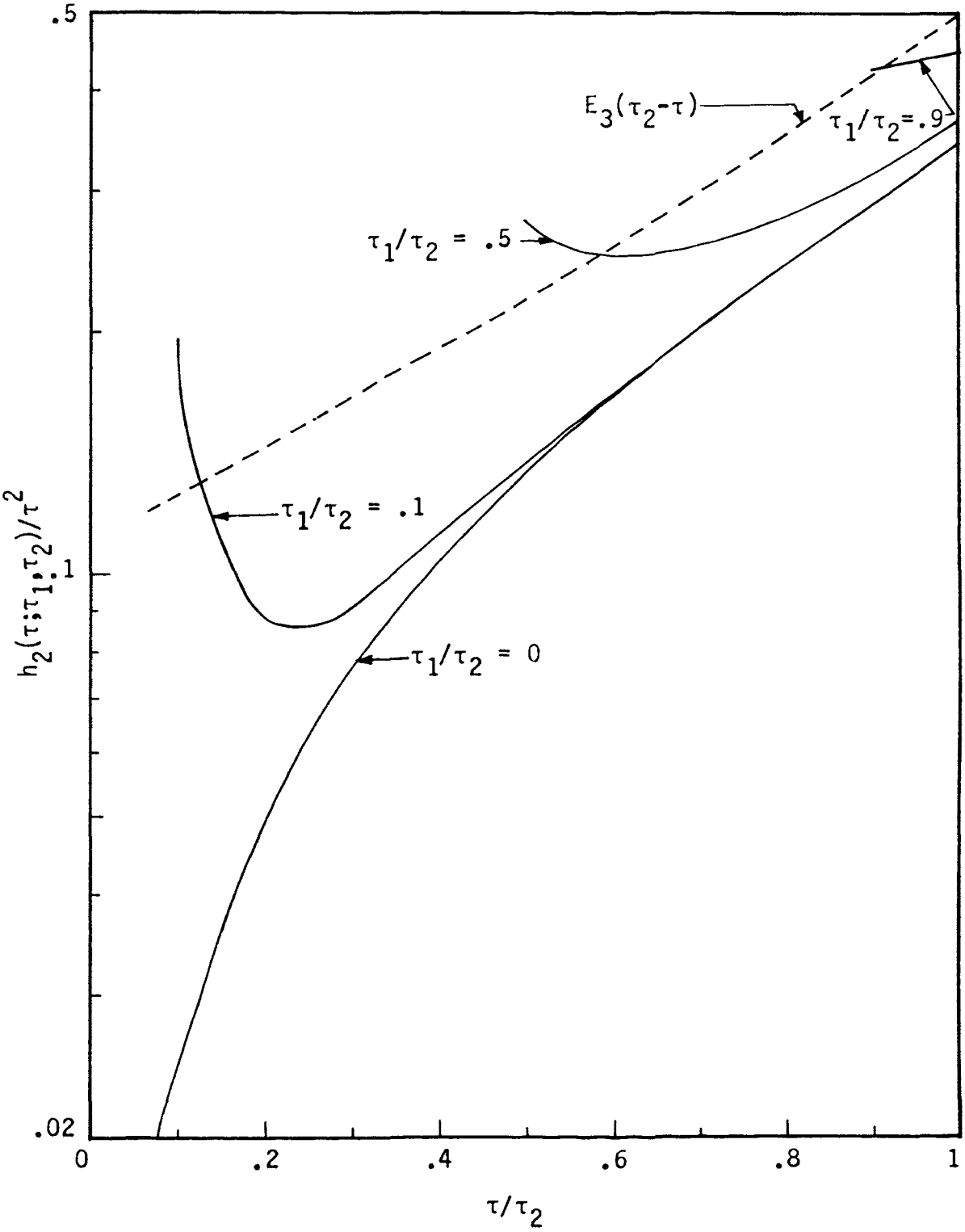

Figure 3.9 - Function $h_2(\tau;\tau_1,\tau_2)$ versus τ/τ_2 for $\tau_2 = 1$

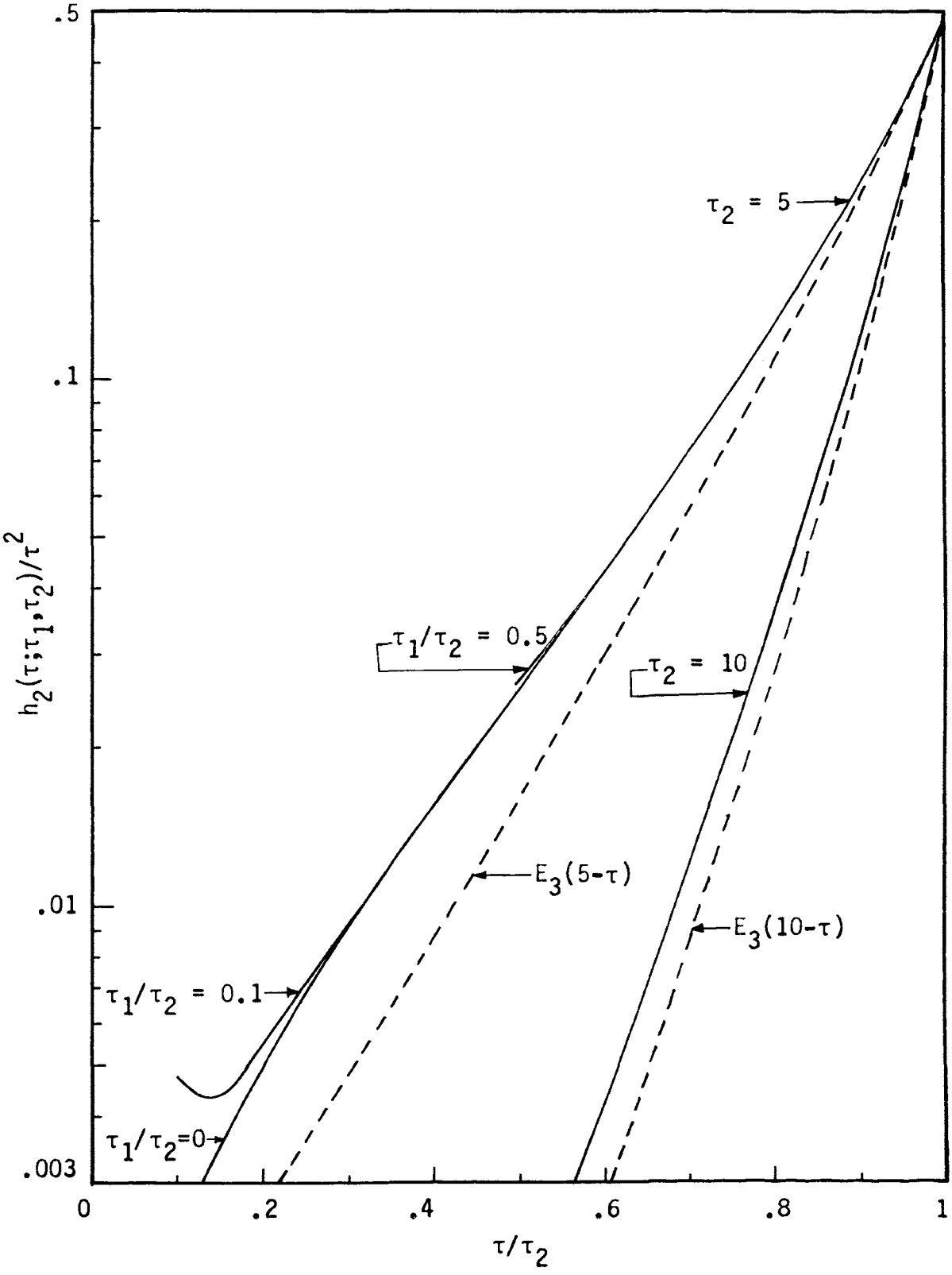

Figure 3.10 - Function $h_2(\tau;\tau_1,\tau_2)/\tau^2$ versus τ/τ_2 for $\tau_2 = 5$ and $\tau_2 = 10$

exist for the functions $h_1(\tau;\tau_1)$ and $h_2(\tau;\tau_1,\tau_2)$

$$h_2(\tau=\tau_1;\tau_1,\tau_2) = h_1(\tau=\tau_2;\tau_1) \tag{3.21}$$

Expansion of the function $h_2(\tau=\tau_1;\tau_1,\tau_2)$ in a Taylor's series about $\tau_1 = 0$ yields

$$h_2(\tau=\tau_1;\tau_1,\tau_2) = \frac{\tau_1^2}{2} e^{-\tau_2} + \frac{\tau_1^3}{3} e^{-\tau_2} \tag{3.22}$$

Comparison of expressions (3.17) and (3.22) reveal similarity.

c. Function $h_2(\tau;\tau_1,\tau_2)$ evaluated at $\tau = \tau_2$

For the case under consideration, the expression (3.4) for the function $h_2(\tau;\tau_1,\tau_2)$ reduces to

$$h_2(\tau=\tau_2;\tau_1,\tau_2) = (\tau_2^2-\tau_1^2)E_3[2(\tau_2^2-\tau_1^2)^{\frac{1}{2}}] + 2(\tau_2^2-\tau_1^2)^{\frac{1}{2}}E_4[2(\tau_2^2-\tau_1^2)^{\frac{1}{2}}] + E_5[2(\tau_2^2-\tau_1^2)^{\frac{1}{2}}] + \frac{\tau_2^2}{2} - \frac{1}{4} \tag{3.23}$$

From equation (3.23), we find that

$$\lim_{\tau_2\to\tau_1} h_2(\tau=\tau_2;\tau_1,\tau_2)/\tau_2^2 = \frac{1}{2} \tag{3.24}$$

$$\lim_{\tau_2\to\infty} h_2(\tau=\tau_2;\tau_1,\tau_2)/\tau_2^2 = \frac{1}{2} \tag{3.25}$$

Numerical results obtained for expression (3.23) are tabulated in Table 3.6. The limiting cases in expressions (3.24) and (3.25) were used to construct Figure 3.11. From Figure 3.11 one finds that for large values of τ_1 (in this case, $\tau_1 = 5$), there is not much difference in the results for various values of τ_1/τ_2.

Table 3.6

Values of the function $h_2(\tau=\tau_2;\tau_1,\tau_2)/\tau_2^2$

τ_1/τ_2	$h_2(\tau=\tau_2;\tau_1,\tau_2)/\tau_2^2$			
	τ_1=0.01	τ_1=0.10	τ_1=1.00	τ_1=5.00
0.001	0.497500			
0.002	0.490005			
0.003	0.477720	0.499873		
0.004	0.461617	0.499600		
0.005	0.443224	0.499375		
0.006	0.423914	0.499100		
0.007	0.404638	0.498775		
0.008	0.385970	0.498400		
0.009	0.368215	0.497975		
0.010	0.351508	0.497500		
0.020	0.235832	0.490005		
0.030	0.175545	0.477720	0.499817	
0.040	0.139669	0.461623	0.499600	
0.050	0.116139	0.443247	0.499375	
0.060	0.099666	0.423977	0.499100	
0.070	0.087609	0.404778	0.498775	
0.080	0.078509	0.386231	0.498400	
0.090	0.071495	0.368651	0.497975	
0.100	0.066018	0.352182	0.497500	
0.200	0.050231	0.243191	0.490006	0.499600
0.300	0.063838	0.198774	0.477786	0.499100
0.350	0.076597	0.190421	0.470296	0.498775
0.400	0.092613	0.188718	0.462284	0.498400
0.450	0.111646	0.192589	0.454127	0.497975
0.500	0.133549	0.201321	0.446233	0.497500
0.550	0.158231	0.214430	0.439023	0.496975
0.600	0.185632	0.231583	0.432930	0.496400
0.650	0.215712	0.252549	0.428400	0.495775
0.700	0.248442	0.277171	0.425910	0.495102
0.750	0.283805	0.305348	0.425987	0.494383
0.800	0.321790	0.337027	0.429252	0.493630
0.850	0.362391	0.372200	0.436493	0.492881
0.900	0.405611	0.410918	0.448827	0.492273
0.950	0.451463	0.453335	0.468158	0.492421
1.000	0.500000	0.500000	0.500000	0.500000

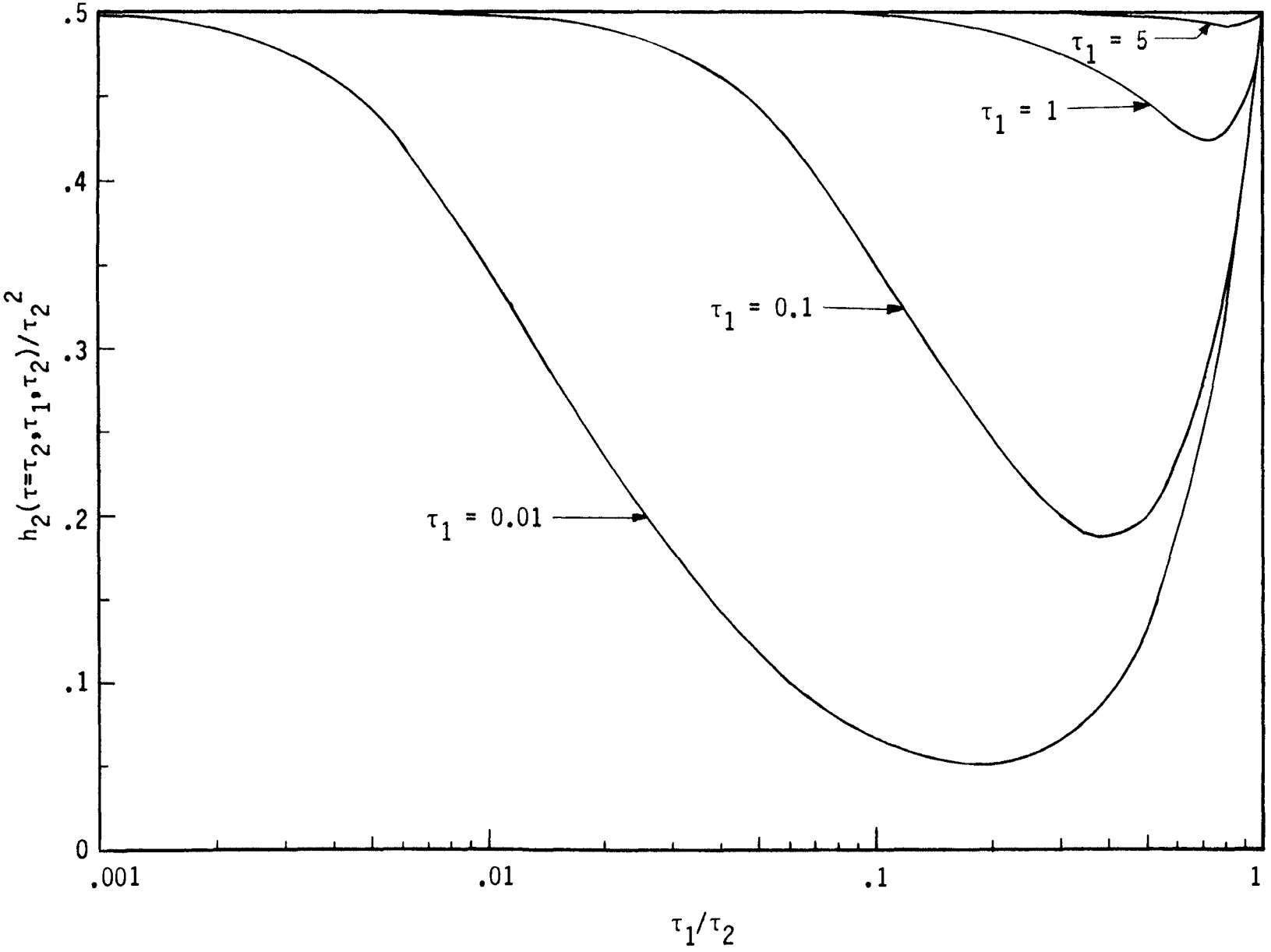

Figure 3.11 - Function $h_2(\tau=\tau_2;\tau_1,\tau_2)/\tau_2^2$ versus τ_1/τ_2

D. Isothermal Shock Layer

Consider the case of a hypersonic flow over a blunt body. Near the stagnation point, we may idealize the situation by a one-dimensional model as shown in Figure 3.12 [110]. In order to estimate the radiative energy, the following approximations are made:

(1) The detached shock is considered as a constant temperature gas layer of thickness L.

(2) The wall of the body is assumed to be black and its temperature is much smaller than the gas temperature.

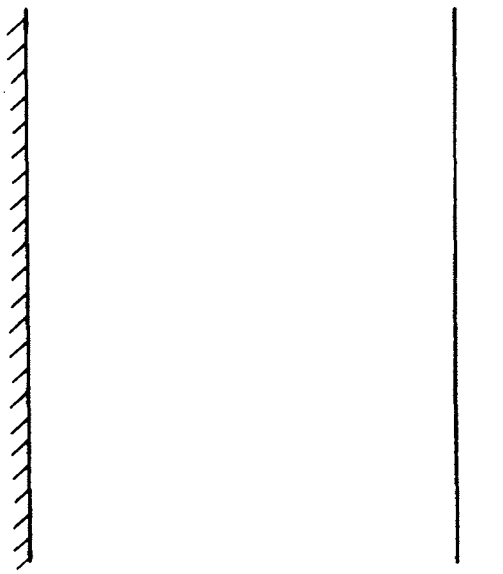

Figure 3.12 - Idealized model of the radiating region behind a hypersonic normal shock

For the case under consideration, equation (3.13) corresponds to the expression for the local radiative flux. The following two particular expressions are obtained from equation (3.13):

(1) The radiation flux from the shock layer to the body:

$$\mathcal{G}_p(\tau_1) = 2\sigma T_0^4 [E_3(\tau_2-\tau_1) - \tfrac{1}{2}] \tag{3.26}$$

(2) The radiation flux from the shock layer into the free stream:

$$\mathcal{G}_p(\tau_2) = 2\sigma T_0^4 [\tfrac{1}{2} - E_3(\tau_2-\tau_1)] \tag{3.27}$$

In the above analysis, the shocked gas region in front of a blunt body has been approximated by a plane layer. The validity of this approximation has not been established.

Consider the same situation by choosing a spherical nose shape and taking the shock shape to be concentric with the body as shown in Figure 3.13.

Equation (3.11) represents the expression for the local radiative flux in this case. By substituting first $\tau = \tau_1$ and then $\tau = \tau_2$ in

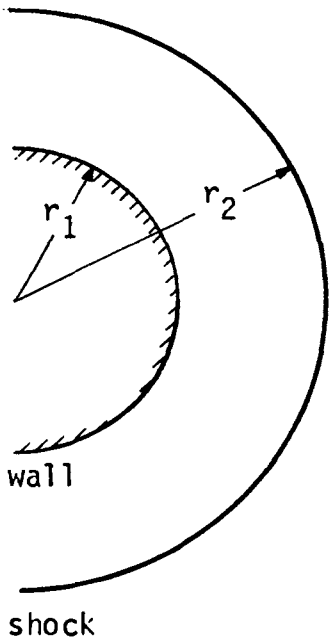

Figure 3.13 - Geometry when the shock shape is taken to be concentric with the body

equation (3.11), the following expressions for the radiation flux from the shock layer to the body and into the free stream respectively are obtained:

$$\tau_1^2\,\mathcal{G}(\tau_1) = -2\sigma T_0^4[h_1(\tau=\tau_1;\tau_1) - h_2(\tau=\tau_1;\tau_1,\tau_2)]$$

$$= 2\sigma T_0^4\{-\tau_1\tau_2 E_3(\tau_2-\tau_1) + (\tau_2-\tau_1)E_4(\tau_2-\tau_1) + E_5(\tau_2-\tau_1)$$

$$-(\tau_2^2-\tau_1^2)^{\frac{1}{2}}E_4[(\tau_2^2-\tau_1^2)^{\frac{1}{2}}] - E_5[(\tau_2^2-\tau_1^2)^{\frac{1}{2}}] + \tau_1^2/2\} \quad (3.28)$$

$$\tau_2^2\,\mathcal{G}(\tau_2) = -2\sigma T_0^4[h_1(\tau=\tau_2;\tau_1) - h_2(\tau=\tau_2;\tau_1,\tau_2)]$$

$$= 2\sigma T_0^4\{-\tau_1\tau_2 E_3(\tau_2-\tau_1) + (\tau_2-\tau_1)E_4(\tau_2-\tau_1) + E_5(\tau_2-\tau_1)$$

$$- (\tau_2^2-\tau_1^2)^{\frac{1}{2}}\,E_4[(\tau_2^2-\tau_1^2)^{\frac{1}{2}}] - E_5[(\tau_2^2-\tau_1^2)^{\frac{1}{2}}]$$

$$+ \tau_2^2/2 - \tfrac{1}{4} + (\tau_2^2-\tau_1^2)^{\frac{1}{2}}\,E_3[2(\tau_2^2-\tau_1^2)^{\frac{1}{2}}]$$

$$+ 2(\tau_2^2-\tau_1^2)^{\frac{1}{2}}\,E_4[2(\tau_2^2-\tau_1^2)^{\frac{1}{2}}] + E_5[2(\tau_2^2-\tau_1^2)^{\frac{1}{2}}]\} \quad (3.29)$$

Making use of the asymptotic expansions for the functions $E_3(\tau)$, $E_4(\tau)$ and $E_5(\tau)$ as $\tau \to 0$ (see Appendix A), one can show that for $(\tau_2-\tau_1)<<1$, the foregoing equations (3.26-3.29) reduces to:

$$\mathcal{G}_p(\tau_1) = -2\sigma T_0^4(\tau_2-\tau_1) \quad (3.30)$$

$$\mathcal{G}_p(\tau_2) = 2\sigma T_0^4(\tau_2-\tau_1) \quad (3.31)$$

$$\tau_1^2\,\mathcal{G}(\tau_1) = \tfrac{2}{3}\,\sigma T_0^4[-(\tau_2^3-\tau_1^3) + (\tau_2^2-\tau_1^2)^{3/2}] \quad (3.32)$$

$$\tau_2^2\,\mathcal{G}(\tau_2) = \tfrac{2}{3}\,\sigma T_0^4[(\tau_2^3-\tau_1^3) + (\tau_2^2-\tau_1^2)^{3/2}] \quad (3.33)$$

Numerical results obtained by using the approximate expressions (3.30-3.33) are tabulated in Table 3.7 alongside with the results

obtained by using the exact expressions (3.26 - 3.29). The optically thin results are greater than the exact results for the two cases, i.e. $\tau_2 - \tau_1 = 0.01$ and 0.1. When $\tau_2 - \tau_1 = 0.01$, the error for the dimensionless flux at the outer boundary, increases from 0.7% to 3% as τ_1/τ_2 increases from 0 to 0.99, while for $\tau_2 - \tau_1 = 0.1$, the error increases from 7% to 30%. For the dimensionless flux at the inner boundary, the variation is from 0.5% to 0.8% for the case when $\tau_2 - \tau_1 = 0.01$ and from 5% to 8% for the case when $\tau_2 - \tau_1 = 0.1$.

Numerical results obtained for the several ratios of τ_1/τ_2 for equations (3.26 - 3.29) are presented graphically in Figures 3.14 through 3.17 and in Tables 3.8 through 3.11. One finds that there is considerable difference between the results for the two geometries. The effect of curvature increases with decreasing τ_1/τ_2. Examination of Figures 3.14 and 3.15 reveals that the non-dimensionalized radiative fluxes at the inner and outer spherical boundaries approach the dimensionless radiative flux for the planar medium as $\tau_1/\tau_2 \to 1$ and $\tau_2 - \tau_1$ becomes large. Moreover, the optically thick limit is approached in all the cases as $\tau_2 - \tau_1 \to \infty$.

Figures 3.16 and 3.17 presents essentially the same thing but in a slightly different manner. Inspection of these figures show that as the thickness of the shell decreases, i.e. as $\tau_2 - \tau_1 \to 0$, one approaches closer to the planar medium. For a small spacing $\tau_2 - \tau_1 = 0.1$ and $\tau_1/\tau_2 = 0.99$, the difference between the dimensionless flux across a plane layer and the dimensionless flux at the outer boundary of the spherical shell is less than 5%, while for $\tau_2 - \tau_1 = 2$ and $\tau_1/\tau_2 = 0.99$ it is less than 1%. From Figure 3.16 one finds that

Table 3.7

Comparison of the exact and optically thin values of the dimensionless radiative flux at the inner and outer boundaries

τ_1/τ_2	$-\mathcal{G}(\tau_1)/\sigma T_0^4$		$\mathcal{G}(\tau_2)/\sigma T_0^4$	
	Exact	Approximate	Exact	Approximate
	(a) $\tau_2-\tau_1=0.01$			
0	9.9502D-3	1.0000D-2	1.3234D-2	1.3333D-2
0.01	9.9832D-3	9.9837D-3	1.3366D-2	1.3467D-2
0.10	1.0289D-2	1.0343D-2	1.4576D-2	1.4697D-2
0.20	1.0650D-2	1.0707D-2	1.5960D-2	1.6105D-2
0.30	1.1040D-2	1.1102D-2	1.7361D-2	1.7534D-2
0.40	1.1470D-2	1.1537D-2	1.8749D-2	1.8954D-2
0.50	1.1952D-2	1.2026D-2	2.0086D-2	2.0327D-2
0.60	1.2511D-2	1.2593D-2	2.1317D-2	2.1600D-2
0.70	1.3187D-2	1.3278D-2	2.2363D-2	2.2694D-2
0.80	1.4059D-2	1.4167D-2	2.3079D-2	2.3467D-2
0.90	1.5353D-2	1.5488D-2	2.3126D-2	2.3588D-2
0.95	1.6408D-2	1.6573D-2	2.2559D-2	2.3076D-2
0.99	1.8055D-2	1.8293D-2	2.1070D-2	2.1672D-2
Planar Layer	1.9447D-2	2.0000D-2	1.9447D-2	2.0000D-2
	(b) $\tau_2-\tau_1=0.10$			
0	9.5163D-2	1.0000D-1	1.2385D-1	1.3333D-1
0.01	9.5465D-2	1.0018D-1	1.2500D-1	1.3467D-1
0.10	9.8254D-2	1.0343D-1	1.3550D-1	1.4696D-1
0.20	1.0153D-1	1.0708D-1	1.4732D-1	1.6105D-1
0.30	1.0505D-1	1.1102D-1	1.5907D-1	1.7534D-1
0.40	1.0890D-1	1.1537D-1	1.7041D-1	1.8954D-1
0.50	1.1319D-1	1.2026D-1	1.8094D-1	2.0327D-1
0.60	1.1812D-1	1.2593D-1	1.9011D-1	2.1600D-1
0.70	1.2400D-1	1.3278D-1	1.9706D-1	2.2694D-1
0.80	1.3145D-1	1.4167D-1	2.0033D-1	2.3467D-1
0.90	1.4213D-1	1.5488D-1	1.9652D-1	2.3588D-1
0.95	1.5037D-1	1.6573D-1	1.8883D-1	2.3076D-1
0.99	1.6171D-1	1.8294D-1	1.7453D-1	2.1673D-1
Planar Layer	1.6742D-1	2.0000D-1	1.6742D-1	2.0000D-1

Table 3.8

Values of the dimensionless radiative flux at the inner boundary for different ratios of inner to outer optical radii

$\tau_2-\tau_1$	$-\mathcal{G}(\tau_1)/\sigma T_0^4$				
	$\tau_1/\tau_2=0$	$\tau_1/\tau_2=0.1$	$\tau_1/\tau_2=0.5$	$\tau_1/\tau_2=0.9$	Planar Layer
0.001	0.001000	0.001034	0.001202	0.001547	0.001992
0.002	0.001998	0.002066	0.002402	0.003092	0.003971
0.003	0.002996	0.003098	0.003601	0.004634	0.005939
0.004	0.003992	0.004128	0.004799	0.006174	0.007897
0.005	0.004988	0.005158	0.005994	0.007710	0.009844
0.006	0.005982	0.006186	0.007189	0.009244	0.011783
0.007	0.006976	0.007214	0.008382	0.010775	0.013712
0.008	0.007968	0.008240	0.009574	0.012304	0.015632
0.009	0.008960	0.009265	0.010764	0.013830	0.017543
0.010	0.009950	0.010289	0.011952	0.015353	0.019447
0.020	0.019801	0.020473	0.023759	0.030439	0.038063
0.030	0.029554	0.030551	0.035423	0.043792	0.056005
0.040	0.039211	0.040526	0.046944	0.059830	0.073352
0.050	0.048771	0.050398	0.058326	0.074146	0.090162
0.060	0.058235	0.060168	0.069569	0.088216	0.106478
0.070	0.067606	0.069838	0.080676	0.102045	0.122335
0.080	0.076884	0.079408	0.091648	0.115636	0.137761
0.090	0.086069	0.088880	0.102487	0.128996	0.152781
0.100	0.095163	0.098254	0.113194	0.142128	0.167417
0.200	0.181269	0.186849	0.213375	0.261869	0.296109
0.300	0.259182	0.266736	0.302064	0.363179	0.399916
0.400	0.329680	0.338770	0.380601	0.449234	0.485427
0.500	0.393469	0.403724	0.450167	0.522592	0.556791
0.600	0.451188	0.462294	0.511803	0.585334	0.616899
0.700	0.503415	0.515109	0.566427	0.639156	0.667878
0.800	0.550671	0.562733	0.614850	0.685455	0.711352
0.900	0.593430	0.605677	0.657786	0.725383	0.748594
1.000	0.632121	0.644402	0.695867	0.759896	0.780616
1.500	0.776870	0.787902	0.830835	0.875081	0.886521
2.000	0.864665	0.873474	0.905421	0.933477	0.939733
2.500	0.917915	0.924511	0.946871	0.963971	0.967409
3.000	0.950213	0.954954	0.970024	0.980236	0.982139
3.500	0.959481	0.973117	0.983019	0.989048	0.990109
4.000	0.981684	0.983954	0.990345	0.993882	0.994477
5.000	0.993262	0.994281	0.996848	0.998054	0.998244

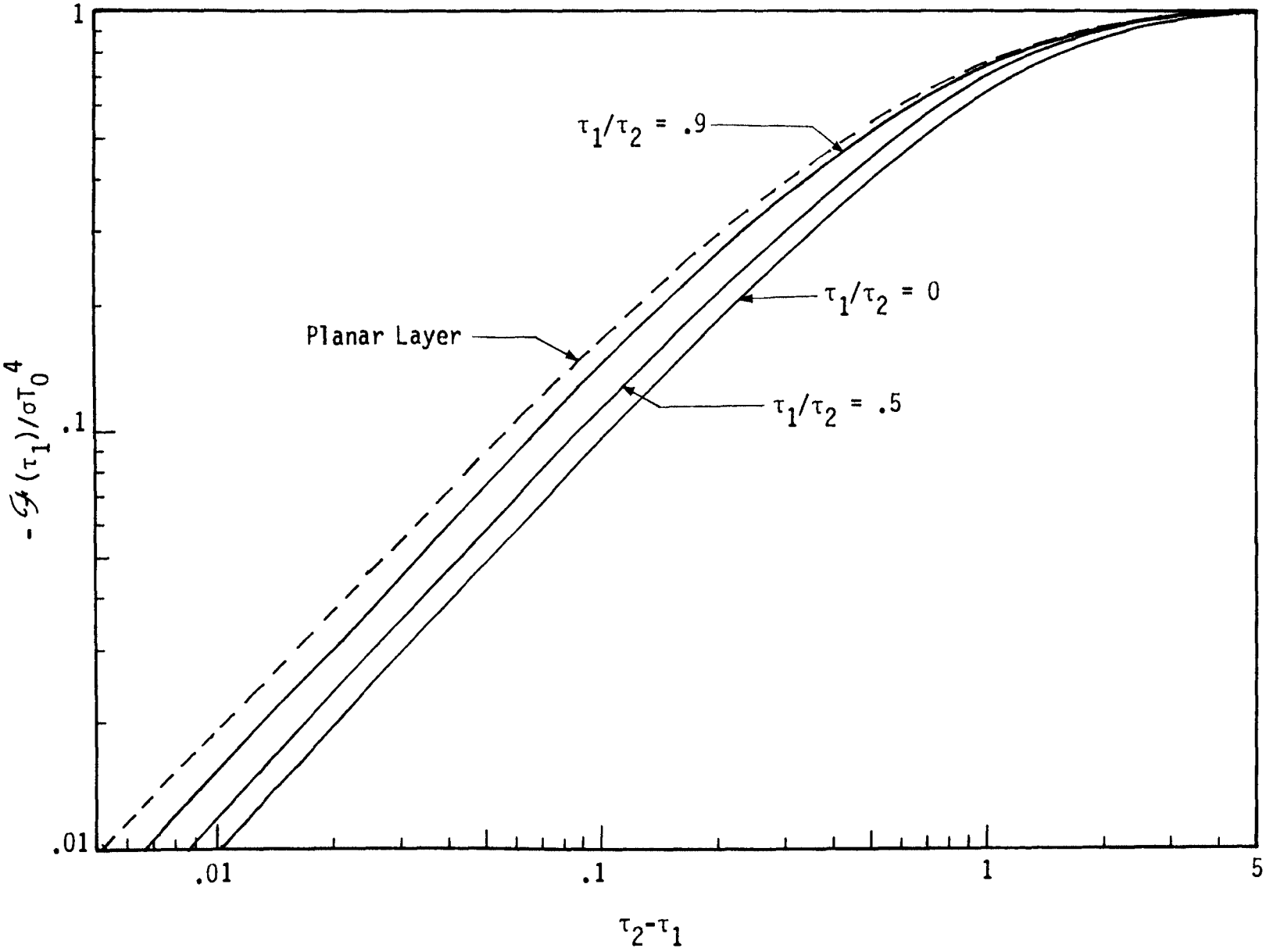

Figure 3.14 - Dimensionless radiative flux at the inner boundary versus difference of outer to inner optical radii

Table 3.9

Values of the dimensionless radiative flux at the outer boundary for different ratios of inner to outer optical radii

$\tau_2-\tau_1$	$\mathcal{F}(\tau_2)/\sigma T_0^4$				
	$\tau_1/\tau_2=0$	$\tau_1/\tau_2=0.1$	$\tau_1/\tau_2=0.5$	$\tau_1/\tau_2=0.9$	Planar Layer
0.001	0.001332	0.001468	0.002030	0.002354	0.001992
0.002	0.002663	0.002934	0.004056	0.004699	0.003971
0.003	0.003991	0.004398	0.006076	0.007034	0.005939
0.004	0.005317	0.005859	0.008092	0.009360	0.007897
0.005	0.006642	0.007318	0.010103	0.011677	0.009844
0.006	0.007964	0.008774	0.012109	0.013985	0.011783
0.007	0.009285	0.010228	0.014110	0.016284	0.013715
0.008	0.010603	0.011680	0.016107	0.018573	0.015632
0.009	0.011919	0.013129	0.018099	0.020854	0.017543
0.010	0.013234	0.014576	0.020086	0.023126	0.019447
0.020	0.026271	0.028913	0.039697	0.045361	0.038063
0.030	0.039114	0.043015	0.058847	0.066756	0.056005
0.040	0.051767	0.056887	0.077547	0.087357	0.073352
0.050	0.064232	0.070532	0.095810	0.107207	0.090162
0.060	0.076512	0.083955	0.113646	0.126346	0.106478
0.070	0.088611	0.097158	0.131066	0.146624	0.122335
0.080	0.100531	0.110147	0.148082	0.162642	0.137761
0.090	0.112275	0.122925	0.164703	0.179867	0.152781
0.100	0.123845	0.135496	0.180940	0.196519	0.167417
0.200	0.230601	0.250551	0.324240	0.337093	0.296109
0.300	0.322770	0.348439	0.438475	0.443311	0.399916
0.400	0.402475	0.431889	0.530150	0.526919	0.485427
0.500	0.471518	0.503178	0.604221	0.594671	0.556791
0.600	0.531427	0.564210	0.664473	0.650694	0.616899
0.700	0.583503	0.616575	0.713817	0.697675	0.667878
0.800	0.628852	0.661606	0.754496	0.737565	0.711352
0.900	0.668418	0.700420	0.788250	0.771409	0.748594
1.000	0.703003	0.733954	0.816433	0.800523	0.780616
1.500	0.822033	0.846064	0.904059	0.896593	0.886521
2.000	0.886447	0.904077	0.945348	0.944866	0.939733
3.000	0.945408	0.955002	0.978622	0.983435	0.982139
4.000	0.968844	0.974563	0.989774	0.994732	0.994477
5.000	0.980010	0.983746	0.994212	0.998224	0.998244

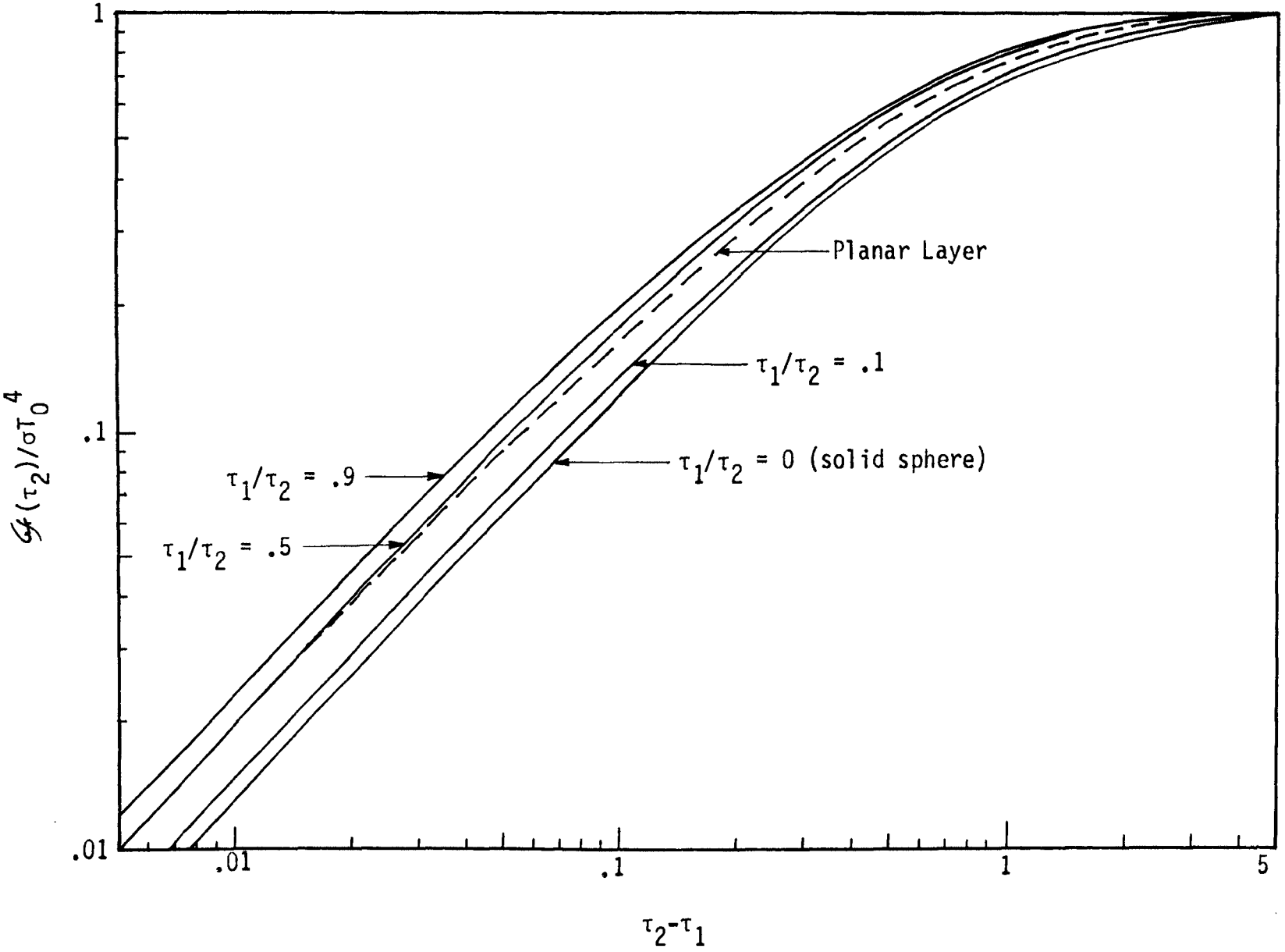

Figure 3.15 - Dimensionless radiative flux at the outer boundary versus difference of outer to inner optical radii

the dimensionless flux at the inner boundary for spherical geometry is always less than the dimensionless flux for planar layer with the same optical thickness $\tau_2 - \tau_1$. Figure 3.17 shows that for a particular value of $\tau_2 - \tau_1$, the dimensionless flux at the outer boundary for spherical geometry is less than that of the planar layer to begin with. But as τ_1/τ_2 increases, the dimensionless flux at the outer boundary also increases and finally exceeds the dimensionless flux of the planar layer at a certain value of τ_1/τ_2.

Direct substitution of $\tau_1 = 0$ in expression (3.28) leads to an indeterminate result. Therefore, to obtain numerical results for the dimensionless flux at the inner boundary for the ratio $\tau_1/\tau_2 = 0$, a different expression is developed as shown below.

Substitution of $\tau = \tau_1$ in expression (3.11) gives

$$\tau_1^2 \mathcal{G}(\tau_1) = -2\sigma T_0^4 [h_1(\tau=\tau_1;\tau_1) - h_2(\tau=\tau_1;\tau_1,\tau_2)] \tag{3.34}$$

Substituting $\tau = \tau_1$ in equation (3.17), we get

$$h_1(\tau=\tau_1;\tau_1) = \frac{\tau_1^2}{2} e^{-\tau_1} + \frac{\tau_1^3}{3} e^{-\tau_1} \tag{3.35}$$

Utilizing equations (3.35) and (3.22) in equation (3.36) and simplifying, one obtains

$$\frac{\mathcal{G}(\tau_1)}{\sigma T_0^4} = -(1 + \frac{2}{3}\tau_1)(e^{-\tau_1} - e^{-\tau_2}) \tag{3.36}$$

From equation (3.36), we obtain

$$\lim_{\tau_1 \to 0} \mathcal{G}(\tau_1)/\sigma T_0^4 = e^{-\tau_2} - 1 \tag{3.37}$$

Expression (3.37) is used to obtain numerical results for the dimensionless radiative flux at the inner layer when $\tau_1 = 0$.

Table 3.10

Values of the dimensionless radiative flux at the inner boundary for various differences of outer to inner optical radii

τ_1/τ_2	$-\mathcal{F}(\tau_1)/\sigma\tau_0^4$			
	$\tau_2-\tau_1=0.1$	$\tau_2-\tau_1=0.5$	$\tau_2-\tau_1=1.0$	$\tau_2-\tau_1=2.0$
0	0.095613	0.393469	0.632121	0.864665
0.01	0.095465	0.394482	0.633347	0.865565
0.10	0.098254	0.403724	0.644402	0.873474
0.20	0.101530	0.414355	0.656793	0.881904
0.30	0.105050	0.425506	0.669412	0.890010
0.40	0.108898	0.437362	0.682386	0.897838
0.50	0.113194	0.450167	0.695867	0.905421
0.60	0.118121	0.464277	0.710048	0.912782
0.70	0.123997	0.480241	0.725181	0.919927
0.80	0.131454	0.499018	0.741623	0.926841
0.90	0.142128	0.522592	0.759896	0.933477
0.95	0.150371	0.537609	0.769929	0.936660
0.99	0.161710	0.552488	0.778432	0.939128
Planar Layer	0.167417	0.556791	0.780616	0.939733

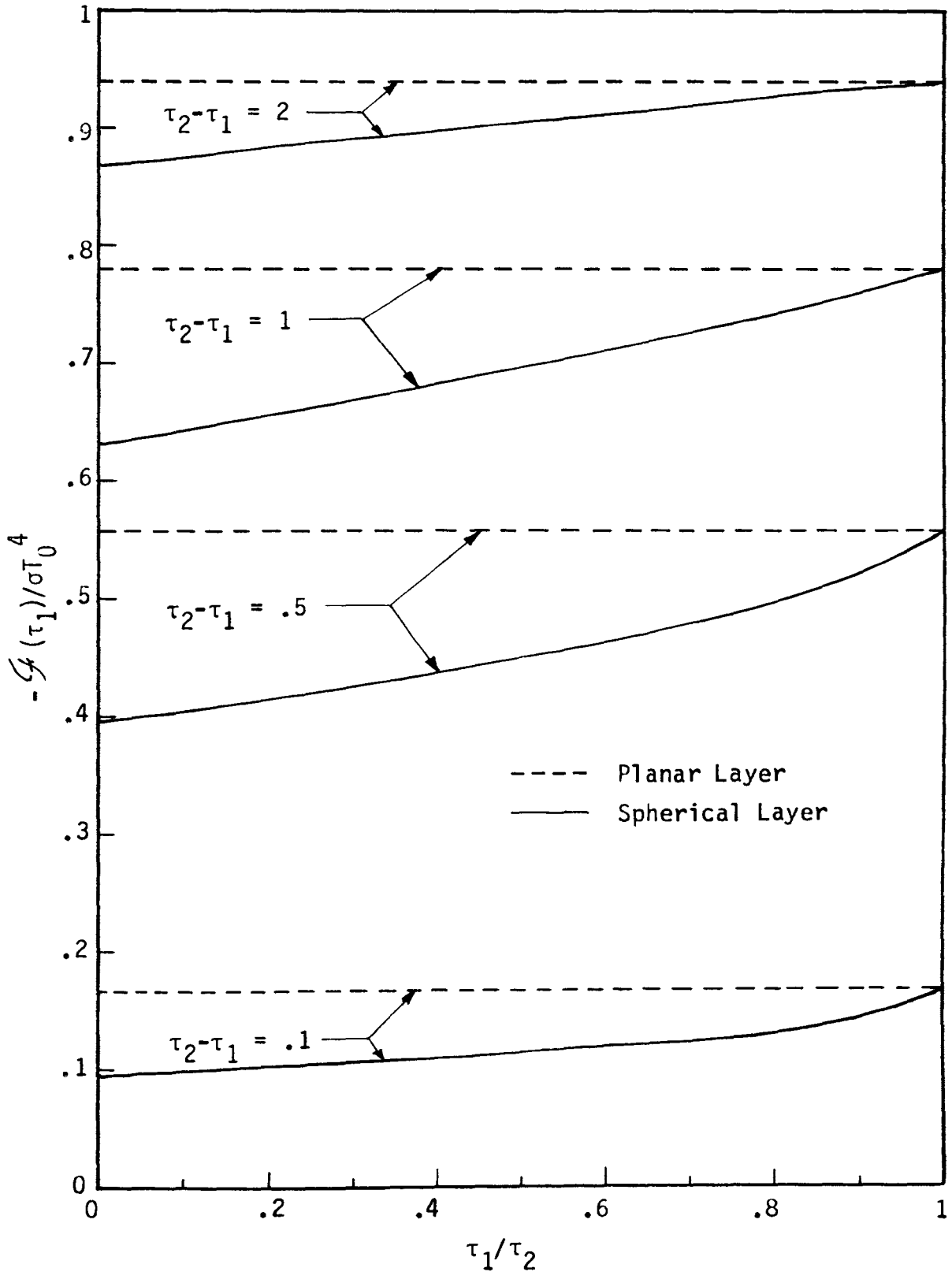

Figure 3.16 - Dimensionless radiative flux at the inner boundary versus ratio of inner to outer optical radii

Table 3.11

Values of the dimensionless radiative flux at the outer boundary for various differences of outer to inner optical radii

τ_1/τ_2	$\mathcal{F}(\tau_2)/\sigma\tau_0^4$			
	$\tau_2-\tau_1=0.1$	$\tau_2-\tau_1=0.5$	$\tau_2-\tau_1=1.0$	$\tau_2-\tau_1=2.0$
0	0.123845	0.471518	0.703003	0.886447
0.01	0.124996	0.474727	0.706224	0.888338
0.10	0.135496	0.503178	0.733954	0.904077
0.20	0.147323	0.533314	0.761574	0.918794
0.30	0.159066	0.560953	0.785043	0.930547
0.40	0.170407	0.585010	0.803575	0.939364
0.50	0.180940	0.604221	0.816433	0.945348
0.60	0.190108	0.617062	0.822943	0.948662
0.70	0.197064	0.621607	0.822557	0.949523
0.80	0.200328	0.615304	0.814986	0.948179
0.90	0.196519	0.594671	0.800523	0.944866
0.95	0.188834	0.577762	0.791111	0.942523
0.99	0.174529	0.561194	0.782791	0.940327
Planar Layer	0.167417	0.556791	0.780616	0.939733

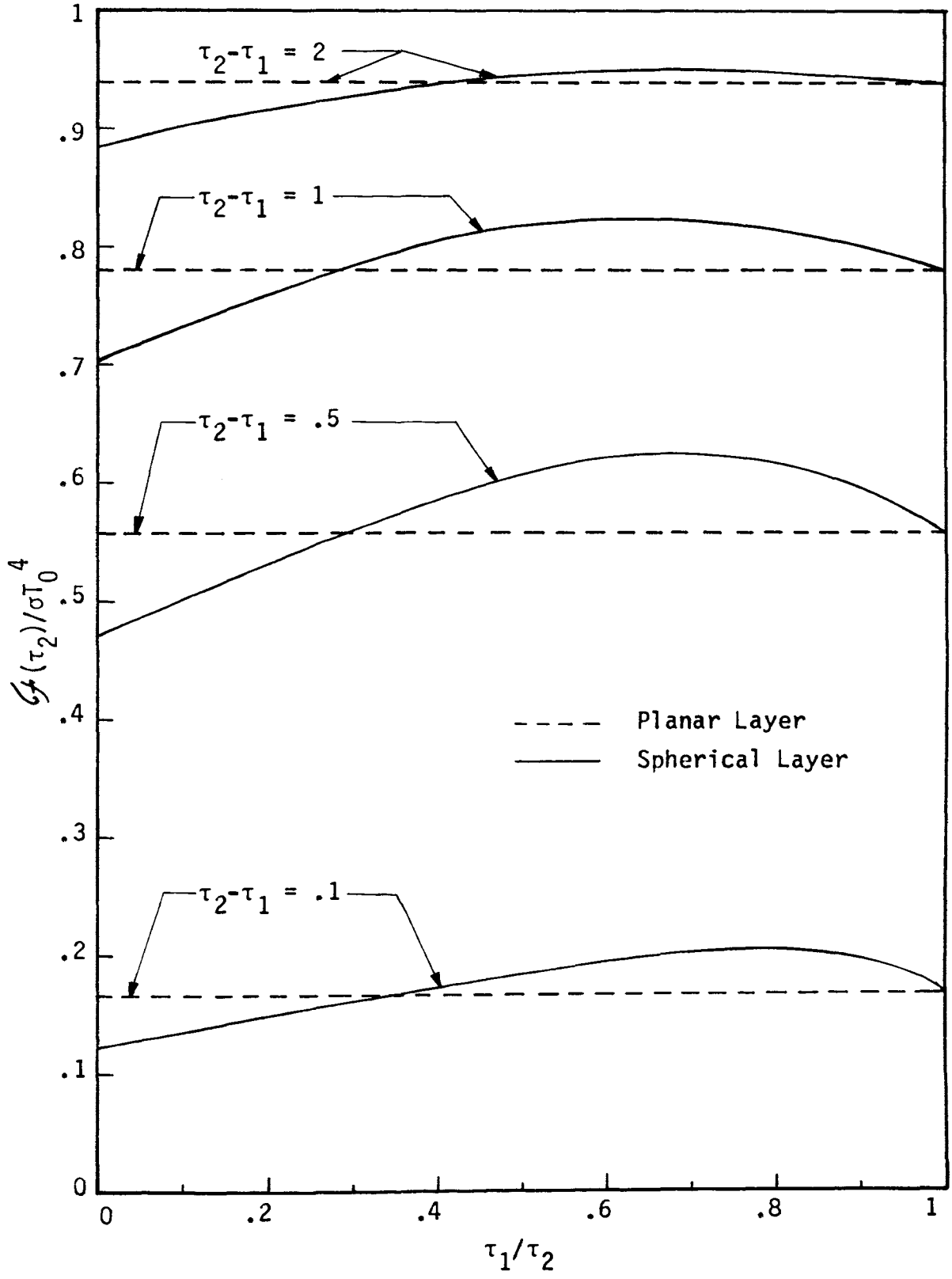

Figure 3.17 - Dimensionless radiative flux at the outer boundary versus ratio of inner to outer optical radii

E. Nonisothermal Case

In the previous sections, analysis of the local radiative flux was carried out for isothermal gas. That study turned out to be relatively simple because the term $T^4(t)$ in expression (3.1) could be pulled out, and mathematically, the problem became more tractable. Now, the case when the intervening medium is nonisothermal is studied.

To begin with, a conduction temperature distribution

$$T(r) = -\frac{C_1}{r} + C_2 \tag{3.38}$$

is assumed with the following boundary conditions

(1) at $r = r_1$, $T = T_1$ (3.39a)

(2) at $r = r_2$, $T = T_2$ (3.39b)

An expression for the dimensionless function $\Theta(\tau)$ in terms of Θ_1, Θ_2, τ_1 and τ_2 is obtained.

$$\Theta(\tau) = \frac{\Theta_2\tau_2 - \Theta_1\tau_1}{\tau_2-\tau_1} - \frac{\tau_1\tau_2(\Theta_2-\Theta_1)}{\tau(\tau_2-\tau_1)} \tag{3.40}$$

where

$$\Theta_1 = \frac{T_1}{T^*} \quad \text{and} \quad \Theta_2 = \frac{T_2}{T^*} \tag{3.41}$$

T^* is some reference temperature.

Moreover, if the bounding surfaces are assumed black, then

$$F_1 = \sigma T_1^4 \quad \text{and} \quad F_2 = \sigma T_2^4 \tag{3.42}$$

Knowing the incident fluxes F_1, F_2 and the temperature distribution $\Theta(\tau)$, numerical results are obtained for the dimensionless radiative fluxes at the inner and outer boundaries with the aid of expression (3.1). For some selected values of Θ_2, τ_1/τ_2 and $\tau_2-\tau_1$, different values of Θ_1 are obtained. To evaluate the integral in

expression (3.1) numerically, guassian quadrature is used. The numerical results obtained are tabulated in Table 3.12 and shown graphically in Figure 3.18. The term I in Table 3.12 stands for the following integral

$$2\int_{\tau_1}^{\tau_2} H(\tau,t;\tau_1)\Theta^4(t)dt \tag{3.43}$$

where Θ is given by expression (3.40).

Table 3.12

Values of the dimensionless radiative flux for the nonisothermal spherical layer (τ_1=1, τ_2=2 and Θ_2=1)

Θ_1	$-I/\tau_1^2$	I/τ_2^2	$-\mathcal{F}(\tau_1)/\sigma T_0^4$	$-\mathcal{F}(\tau_2)/\sigma T_0^4$
0	0.1325	0.4275	0.4366	0.4649
0.10	0.1474	0.4490	0.4515	0.4434
0.25	0.1773	0.4859	0.4776	0.4063
0.50	0.2607	0.5636	0.5046	0.3241
0.75	0.4173	0.6699	0.4050	0.1985
0.90	0.5660	0.7521	0.2141	0.0904
1.00	0.6959	0.8164	0	0

Figure 3.18 shows that I/τ_1^2 decreases as T_1 increases, while I/τ_2^2 increases as $T_1 \to T_2$. When $\Theta_1 = 1$, the results, $I/\tau_1^2 = -0.6959$ and $I/\tau_2^2 = 0.8164$, corresponds to the isothermal case and they compare quite well with the results obtained previously for the case when $\tau_2 - \tau_1 = 1$ and $\tau_1/\tau_2 = 0.5$ (see Tables 3.8 and 3.9). The dimensionless radiative fluxes at the inner and outer boundaries increases as T_1 increases.

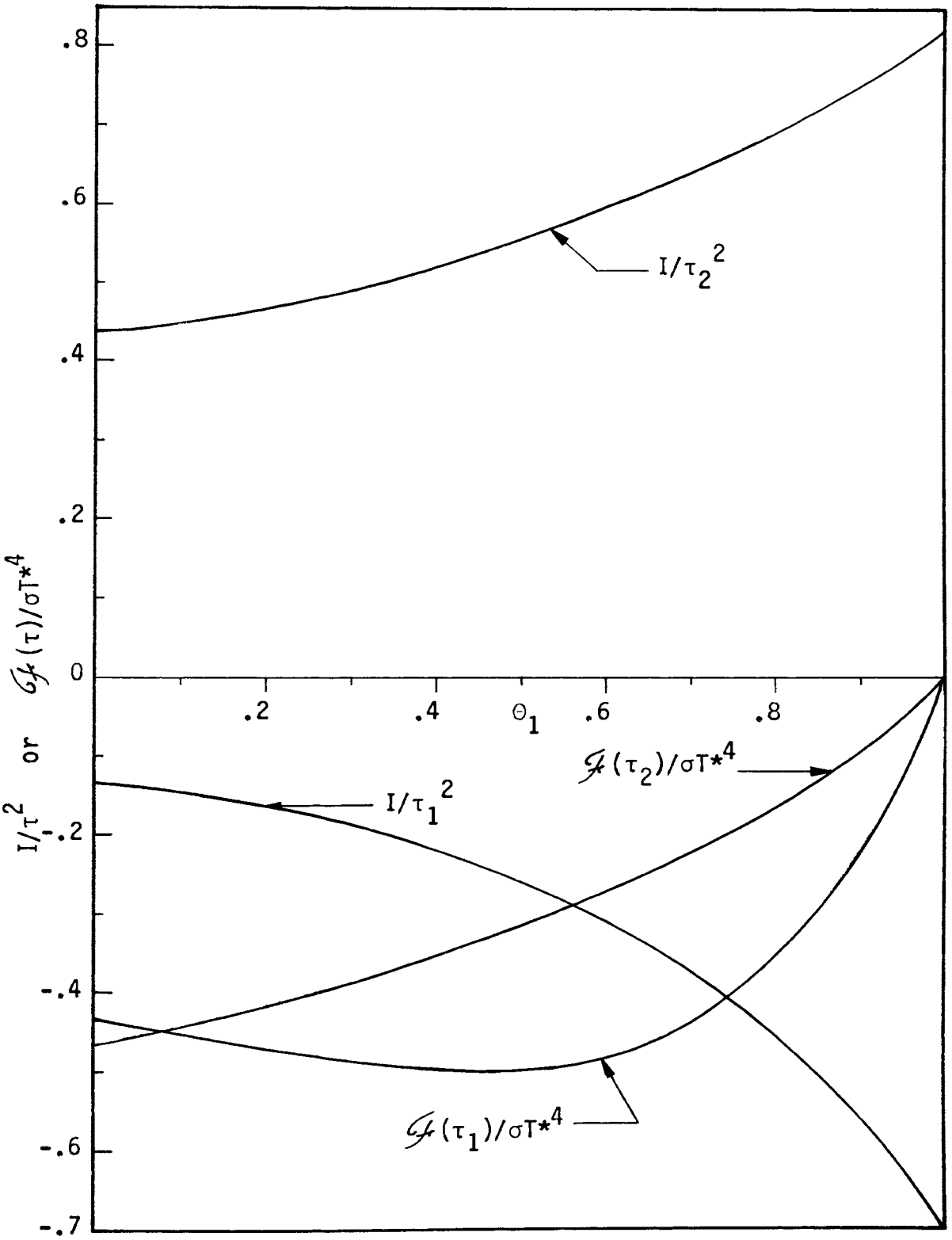

Figure 3.18 - Dimensionless radiative flux for the nonisothermal spherical layer

F. Conclusions

Comparison of the expressions for the local radiative flux in spherical and planar geometry reveals that the functions $h_1(\tau;\tau_1)/\tau^2$ and $h_2(\tau;\tau_1,\tau_2)/\tau^2$ of the spherical geometry are analogous to the functions $E_3(\tau-\tau_1)$ and $E_3(\tau_2-\tau)$ of the planar geometry, respectively. The mathematics of the isothermal analysis are tractable. Thus, by considering some simplified physical situations (Figures 3.3 and 3.4) one can gain some insight into the effect of various parameters on the heat transfer. By studying the limiting cases of the functions $h_1(\tau;\tau_1)$ and $h_2(\tau;\tau_1,\tau_2)$, one comes to know about the usefulness of the approximate expressions.

The shock layer example reveals that one can obtain closed form expressions for the radiative fluxes at the inner and outer boundaries. Numerical results obtained show that there is considerable difference between the results for the two geometries. The effect of curvature increases with decreasing τ_1/τ_2. The study of a particular noniso-thermal case shows that the temperature variations are important.

IV. NONGRAY ANALYSIS: SIMPLIFIED RECTANGULAR MODEL

The gray approximation employed in the previous chapter is the most frequently used in analysis of radiative transfer problems. The approximation is based upon the assumption of frequency independent radiation characteristics of the surfaces and the gases involved. The gray approximation is usually employed in most radiative transfer studies because of the mathematical complexity of the nongray analysis. Unfortunately, most of the substances in which radiation plays a dominant or an important role cannot be characterized as gray.

A. Physical Model and Governing Equations

1. Spherical Layer

In this and the next chapter a spherical layer of nongray gas is considered. The absorption coefficient is only a function of frequency, i.e. $\kappa_\nu=\alpha(\nu)\kappa$. For the simplified rectangular model, the function $\alpha(\nu)$ has only two values, zero and unity (see Figure 4.1). The rectangular model approximates a band by a rectangular box of calculable width (effective band width) with a suitably determined average absorption coefficient. The spectra of many substances, such as glass, carbon dioxide and water vapor have regions where the absorption coefficient is zero. Thus, an absorption coefficient of this type is of physical interest. The index of refraction of the medium is considered to be unity, and the medium is assumed to be in local thermodynamic equilibrium.

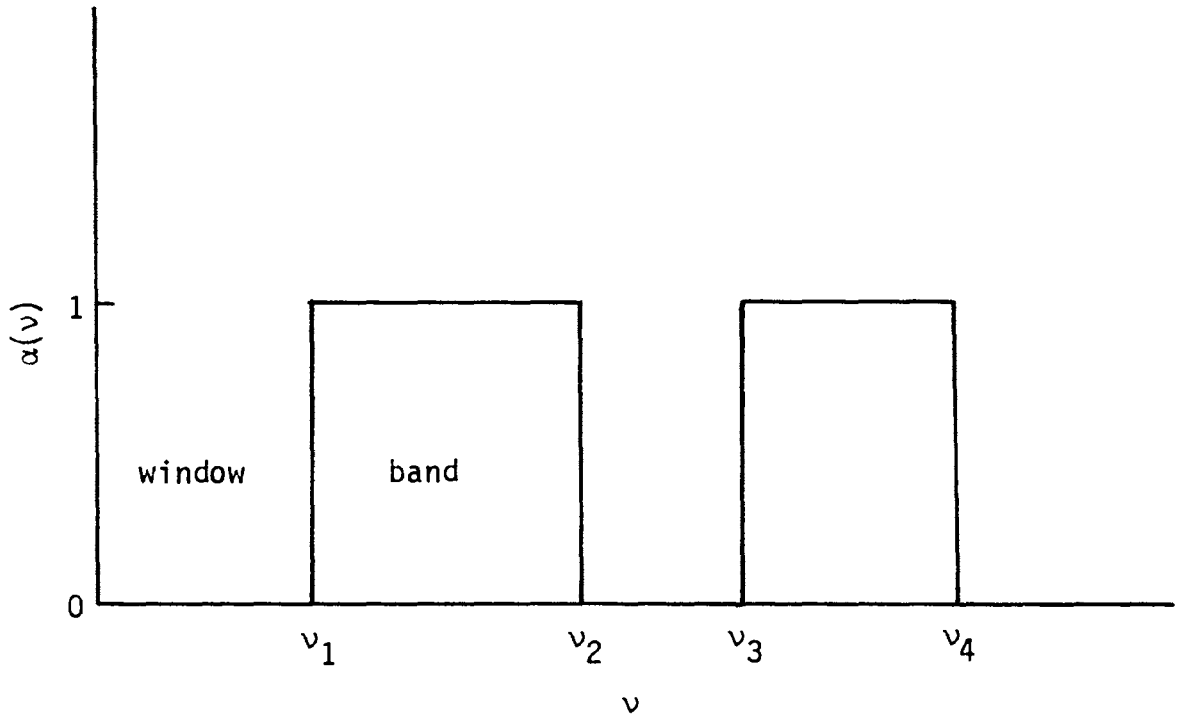

Figure 4.1 - Simplified rectangular model for spectral absorption coefficient

For the physical model and form of spectral absorption coefficient considered, the local radiative flux per unit frequency can be expressed as [6]

$$\tau_\nu^2 \mathcal{G}_\nu(\tau_\nu) = 2F_{1\nu}h_1(\tau_\nu;\tau_{1\nu}) - 2F_{2\nu}h_2(\tau_\nu;\tau_{1\nu},\tau_{2\nu}) + 2\int_{\tau_{1\nu}}^{\tau_{2\nu}} H(\tau_\nu,t;\tau_{1\nu})\, E_{b\nu}(t)dt \qquad (4.1)$$

where the optical radial distance τ_ν is defined as

$$\tau_\nu = \int_0^r \kappa_\nu dr = \kappa_\nu r \qquad (4.2)$$

and the inner and outer optical radii as

$$\tau_{1\nu} = \kappa_\nu r_1 \quad \text{and} \quad \tau_{2\nu} = \kappa_\nu r_2 \qquad (4.3)$$

In equation (4.1) $F_{1\nu}$ and $F_{2\nu}$ represent the radiative fluxes incident on the inside and outside of the layer, respectively, and $E_{b\nu}=\pi I_{b\nu}$ is the Planck function. The functions $h_1(\tau_\nu;\tau_{1\nu})$, $h_2(\tau_\nu;\tau_{1\nu},\tau_{2\nu})$ and $H(\tau_\nu,t;\tau_{1\nu})$ are defined as

$$h_1(\tau_\nu;\tau_{1\nu}) = \tau_\nu\tau_{1\nu}\, E_3(\tau_\nu-\tau_{1\nu}) - (\tau_\nu-\tau_{1\nu})\, E_4(\tau_\nu-\tau_{1\nu}) - E_5(\tau_\nu-\tau_{1\nu}) + (\tau_\nu^2-\tau_{1\nu}^2)^{1/2}\, E_4[(\tau_\nu^2-\tau_{1\nu}^2)^{1/2}] + E_5[(\tau_\nu^2-\tau_{1\nu}^2)^{1/2}] \tag{4.4}$$

$$h_2(\tau_\nu;\tau_{1\nu},\tau_{2\nu}) = \tau_\nu\tau_{2\nu}\, E_3(\tau_{2\nu}-\tau_\nu) - (\tau_{2\nu}-\tau_\nu)\, E_4(\tau_{2\nu}-\tau_\nu) - E_5(\tau_{2\nu}-\tau_\nu) + (\tau_{2\nu}^2-\tau_{1\nu}^2)^{1/2}(\tau_\nu^2-\tau_{1\nu}^2)^{1/2}\, E_3[(\tau_{2\nu}^2-\tau_{1\nu}^2)^{1/2} + (\tau_\nu^2-\tau_{1\nu}^2)^{1/2}] + [(\tau_{2\nu}^2-\tau_{1\nu}^2)^{1/2} + (\tau_\nu^2-\tau_{1\nu}^2)^{1/2}]E_4[(\tau_{2\nu}^2-\tau_{1\nu}^2)^{1/2} + (\tau_\nu^2-\tau_{1\nu}^2)^{1/2}] + E_5[(\tau_{2\nu}^2-\tau_{1\nu}^2)^{1/2} + (\tau_\nu^2-\tau_{1\nu}^2)^{1/2}] \tag{4.5}$$

$$H(\tau_\nu,t;\tau_{1\nu}) = \{\tau_\nu \mathrm{sign}(\tau_\nu-t)\, E_2(|\tau_\nu-t|) + E_3(|\tau_\nu-t|) - (\tau_\nu^2-\tau_{1\nu}^2)^{1/2}\, E_2[(t^2-\tau_{1\nu}^2)^{1/2} + (\tau_\nu^2-\tau_{1\nu}^2)^{1/2}] - E_3[(t^2-\tau_{1\nu}^2)^{1/2} + (\tau_\nu^2-\tau_{1\nu}^2)^{1/2}]\}t \tag{4.6}$$

By introducing new optical radial distance

$$\tau = \tau_\nu/\alpha(\nu) = \kappa r \tag{4.7}$$

and new inner and outer optical radii

$$\tau_1 = \frac{\tau_{1\nu}}{\alpha(\nu)} = \kappa r_1 \qquad \text{and} \qquad \tau_2 = \frac{\tau_{2\nu}}{\alpha(\nu)} = \kappa r_2 \tag{4.8}$$

equation (4.1) can be expressed as

$$\tau^2 \mathcal{G}_\nu(\tau) = 2F_{1\nu}\frac{h_1[\alpha(\nu)\tau;\alpha(\nu)\tau_1]}{\alpha^2(\nu)} - 2F_{2\nu}\frac{h_2[\alpha(\nu)\tau;\alpha(\nu)\tau_1,\alpha(\nu)\tau_2]}{\alpha^2(\nu)}$$

$$+ 2\int_{\tau_1}^{\tau_2} \frac{H[\alpha(\nu)\tau,\alpha(\nu)t;\alpha(\nu)\tau_1]}{\alpha(\nu)} E_{b\nu}(t)dt \qquad (4.9)$$

With the aid of the asymptotic expansions for functions $E_3[\alpha(\nu)\tau]$, $E_4[\alpha(\nu)\tau]$ and $E_5[\alpha(\nu)\tau]$ as $\alpha(\nu)\tau \to 0$, the expressions for the functions $h_1[\alpha(\nu)\tau;\alpha(\nu)\tau_1]/\alpha^2(\nu)$, $h_2[\alpha(\nu)\tau;\alpha(\nu)\tau_1,\alpha(\nu)\tau_2]/\alpha^2(\nu)$ and $H[\alpha(\nu)\tau,\alpha(\nu)t;\alpha(\nu)\tau_1]/\alpha(\nu)$ becomes

$$\frac{h_1[\alpha(\nu)\tau;\alpha(\nu)\tau_1]}{\alpha^2(\nu)} = \frac{\tau_1^2}{2} - \alpha(\nu)\tau\tau_1(\tau-\tau_1) - \frac{\alpha(\nu)(\tau-\tau_1)^3}{3}$$

$$+ \frac{\alpha(\nu)(\tau^2-\tau_1^2)^{3/2}}{3} \qquad (4.10)$$

$$\frac{h_2[\alpha(\nu)\tau;\alpha(\nu)\tau_1,\alpha(\nu)\tau_2]}{\alpha^2(\nu)} = \frac{\tau_1^2}{2} + \frac{\alpha(\nu)[(\tau_2^2-\tau_1^2)^{3/2} + (\tau^2-\tau_1^2)^{3/2}]}{3}$$

$$- \frac{\alpha(\nu)(\tau_2^3-\tau_1^3)}{3} \qquad (4.11)$$

$$\frac{H[\alpha(\nu)\tau,\alpha(\nu)t;\alpha(\nu)\tau_1]}{\alpha(\nu)} = \alpha(\nu)t\tau\ \mathrm{sign}[\alpha(\nu)(\tau-t)] - \frac{\alpha(\nu)t|\tau-t|}{2}$$

$$- \alpha(\nu)t(\tau^2-\tau_1^2)^{\frac{1}{2}}$$

$$+ \frac{\alpha(\nu)t[(t^2-\tau_1^2)^{\frac{1}{2}} + (\tau^2-\tau_1^2)^{\frac{1}{2}}]}{2} \qquad (4.12)$$

From equations (4.10) through (4.12) it is possible to deduce that

$$\lim_{\alpha(\nu)\to 0} \frac{h_1[\alpha(\nu)\tau;\alpha(\nu)\tau_1]}{\alpha^2(\nu)} = \frac{\tau_1^2}{2} \qquad (4.13)$$

$$\lim_{\alpha(\nu)\to 0} \frac{h_2[\alpha(\nu)\tau;\alpha(\nu)\tau_1,\alpha(\nu)\tau_2]}{\alpha^2(\nu)} = \frac{\tau_1^2}{2} \qquad (4.14)$$

$$\lim_{\alpha(\nu)\to 0} \frac{H[\alpha(\nu)\tau,\alpha(\nu)t;\alpha(\nu)\tau_1]}{\alpha(\nu)} = 0 \tag{4.15}$$

From equation (4.9), the local radiative flux,

$$\mathcal{F} = \int_0^\infty \mathcal{F}_\nu d\nu$$

can be written as

$$\tau^2 \mathcal{F}(\tau) = 2\int_0^\infty F_{1\nu} \frac{h_1[\alpha(\nu)\tau;\alpha(\nu)\tau_1]}{\alpha^2(\nu)} d\nu$$

$$- 2\int_0^\infty F_{2\nu} \frac{h_2[\alpha(\nu)\tau;\alpha(\nu)\tau_1,\alpha(\nu)\tau_2]}{\alpha^2(\nu)} d\nu$$

$$+ 2\int_0^\infty \int_{\tau_1}^{\tau_2} \frac{H[\alpha(\nu)\tau,\alpha(\nu)t;\alpha(\nu)\tau_1]}{\alpha(\nu)} E_{b\nu}(t)dtd\nu \tag{4.16}$$

Splitting the first integral of equation (4.16) into two parts, it can be expressed as

$$2\int_0^\infty F_{1\nu} \frac{h_1[\alpha(\nu)\tau;\alpha(\nu)\tau_1]}{\alpha^2(\nu)} d\nu$$

$$= 2\int_0^\infty [1-\alpha(\nu)]\, F_{1\nu} \frac{h_1[\alpha(\nu)\tau;\alpha(\nu)\tau_1]}{\alpha^2(\nu)} d\nu$$

$$+ 2\int_0^\infty \alpha(\nu)\, F_{1\nu} \frac{h_1[\alpha(\nu)\tau;\alpha(\nu)\tau_1]}{\alpha^2(\nu)} d\nu \tag{4.17}$$

Substituting for the function $h_1[\alpha(\nu)\tau;\alpha(\nu)\tau_1]$ and using equation (4.13), equation (4.17) can be written as

$$2\int_0^\infty F_{1\nu}\,\frac{h_1[\alpha(\nu)\tau;\alpha(\nu)\tau_1]}{\alpha^2(\nu)}\,d\nu = \tau_1^2 F_1^* + 2F_1 h_1(\tau;\tau_1) \tag{4.18}$$

where

$$F_1^* = \int_0^\infty [1-\alpha(\nu)]\,F_{1\nu}\,d\nu \tag{4.19}$$

$$F_1 = \int_0^\infty \alpha(\nu)\,F_{1\nu}\,d\nu \tag{4.20}$$

In equation (4.18), F_1^* and F_1 are the incident fluxes that do not act with the intervening medium and that do act with the intervening medium, respectively. Similarly, the next two integrals of equation can be written as

$$2\int_0^\infty F_{2\nu}\,\frac{h_2[\alpha(\nu)\tau;\alpha(\nu)\tau_1,\alpha(\nu)\tau_2]}{\alpha^2(\nu)}\,d\nu = \tau_1^2 F_2^* + 2F_2 h_2(\tau;\tau_1,\tau_2) \tag{4.21}$$

where

$$F_2^* = \int_0^\infty [1-\alpha(\nu)]\,F_{2\nu}\,d\nu \tag{4.22}$$

$$F_2 = \int_0^\infty \alpha(\nu)\,F_{2\nu}\,d\nu \tag{4.23}$$

and

$$2\int_0^\infty \int_{\tau_1}^{\tau_2} \frac{H[\alpha(\nu)\tau,\alpha(\nu)t;\alpha(\nu)\tau_1]}{\alpha(\nu)}\,E_{b\nu}(t)\,dt\,d\nu$$

$$= 2\int_{\tau_1}^{\tau_2} H(\tau,t;\tau_1)E(t)dt \tag{4.24}$$

where $E(\tau) = \int_0^\infty \alpha(\nu)\, E_{b\nu}\, d\nu$. (4.25)

Making use of the foregoing results, the expression for the local radiative flux becomes

$$\tau^2 \mathcal{F}(\tau) = \tau_1^2(F_1^*-F_2^*) + 2F_1 h_1(\tau;\tau_1) - 2F_2 h_2(\tau;\tau_1,\tau_2) + 2\int_{\tau_1}^{\tau_2} H(\tau,t;\tau_1)\, E(t)\, dt \; . \quad (4.26)$$

In equation (4.26) the functions $h_1(\tau;\tau_1)$, $h_2(\tau;\tau_1,\tau_2)$ and $H(\tau,t;\tau_1)$ are the same as defined previously in chapter three. Equation (4.26) is similar to equation (3.1) of the previous chapter except for an additional term $\tau_1^2(F_1^*-F_2^*)$. This term represents the net energy exchanged through the 'windows' (see Figure 4.1).

The case when $\alpha(\nu)\equiv 1$, corresponds to the gray medium situation. As $\alpha(\nu)\to 1$, examination of equations (4.19) and (4.22) shows that both F_1^* and $F_2^*\to 0$ and the term $\tau_1^2(F_1^*-F_2^*)$ vanishes. Thus the expression for the local radiative flux (4.26) becomes similar to the one given by equation (3.1). This shows that the gray case is a special case of the general nongray problem.

2. Planar Layer

Once again, in order to make a comparative study, the planar case is considered. For a similar problem in planar medium, the local radiative flux per unit frequency is given by [111]

$$\mathcal{G}_{p\nu}(\tau_\nu) = 2F_{1\nu}E_3(\tau_\nu-\tau_{1\nu}) - 2F_{2\nu}E_3(\tau_{2\nu}-\tau_\nu)$$

$$+ 2\int_{\tau_{1\nu}}^{\tau_{2\nu}} \text{sign}(\tau_\nu-t)\, E_2(|\tau_\nu-t|)\, E_{b\nu}(t)dt \qquad (4.27)$$

Equation (4.27) can also be expressed as

$$\mathcal{G}_{p\nu}(\tau) = 2\,F_{1\nu}\,E_3\,[\alpha(\nu)(\tau-\tau_1)] - 2\,F_{2\nu}\,E_3[\alpha(\nu)(\tau_2-\tau)]$$

$$+ 2\int_{\tau_1}^{\tau_2} \alpha(\nu)\,\text{sign}(\tau-t)\,E_2[\alpha(\nu)|\tau-t|]\,E_{b\nu}(t)dt \qquad (4.28)$$

By noting that $\alpha(\nu)$ has only two values, zero and unity, the local radiative flux can be written as

$$\mathcal{G}_p(\tau) = \int_0^\infty \mathcal{G}_{p\nu}d\nu = (F_1^*-F_2^*) + 2F_1E_3(\tau-\tau_1) - 2F_2E_3(\tau_2-\tau)$$

$$+ 2\int_{\tau_1}^{\tau_2} \text{sign}(\tau-t)\,E_2(|\tau-t|)\,E(t)dt \qquad (4.29)$$

where F_1^*, F_1, F_2^*, F_2 and $E(\tau)$ are given by equations (4.19), (4.20), (4.22), (4.23) and (4.25), respectively.

Equation (4.29) is similar to equation (3.7) encountered in the last chapter except for the first term $(F_1^*-F_2^*)$. The term $(F_1^*-F_2^*)$ represents the net flux exchanged through the 'windows' (see Figure 4.1).

B. Isothermal Analysis

When the nongray gas is isothermal, i.e. $E(t) = E_0$, equation (4.26) reduces to

$$\tau^2 \mathcal{G}(\tau) = \tau_1^2(F_1^*-F_2^*) + 2h_1(\tau;\tau_1)(F_1-E_0) - 2h_2(\tau;\tau_1,\tau_2)(F_2-E_0) \quad (4.30)$$

As in the previous chapter, relation (3.10) is used. Now, equation (4.30) is similar to equation (3.9) of the gray analysis except for the term $\tau_1^2(F_1^*-F_2^*)$.

The assumption of an isothermal planar medium reduces equation (4.29) to

$$\mathcal{G}_p(\tau) = (F_1^*-F_2^*) + 2E_3(\tau-\tau_1)(F_1-E_0) - 2E_3(\tau_2-\tau)(F_2-E_0) \quad (4.31)$$

Examination of equation (4.31) reveals that except for the term $(F_1^*-F_2^*)$, this equation is similar to equation (3.12).

Case 1: $F_2 = E_0$

Consider the physical situation illustrated by Figure 3.3 of the gray analysis. Since the outer boundary is black, the following identity results:

$$F_2 + F_2^* \equiv \sigma T_2^4 \quad (4.32)$$

Equations (4.30) and (4.31) simplify to

$$\tau^2 \mathcal{G}(\tau) = \tau_1^2(F_1^*-\sigma T_2^4+E_0) + 2h_1(\tau;\tau_1)(F_1-E_0) \quad (4.33)$$

$$\mathcal{G}_p(\tau) = (F_1^*-\sigma T_2^4+E_0) + 2E_3(\tau-\tau_1)(F_1-E_0) \quad (4.34)$$

respectively.

Case 2: $F_1 = E_0$

Referring to Figure 3.6 of the previous chapter, for the case when the inner wall is black, the following relation ensues:

$$F_1 + F_1^* \equiv \sigma T_1^4 \quad (4.35)$$

For this case, equation (4.30) reduces to

$$\tau^2 \mathcal{G}(\tau) = \tau_1^2(\sigma T_1^4 - E_0 - F_2^*) - 2h_2(\tau;\tau_1,\tau_2)(F_2 - E_0) \tag{4.36}$$

and equation (4.31) simplifies to

$$\mathcal{G}_p(\tau) = (\sigma T_1^4 - E_0 - F_2^*) - 2E_3(\tau_2 - \tau)(F_2 - E_0) \tag{4.37}$$

Case 3: Shock Layer

The incident fluxes F_1 and F_2 are essentially zero when the shock layer is considered. For this case, expressions (4.30) and (4.31) for the local radiative flux further simplifies to

$$\tau^2 \mathcal{G}(\tau) = -2E_0[h_1(\tau;\tau_1) - h_2(\tau;\tau_1,\tau_2)] \tag{4.38}$$

$$\mathcal{G}_p(\tau) = -2E_0[E_3(\tau - \tau_1) - E_3(\tau_2 - \tau)] \tag{4.39}$$

These expressions turn out to be similar to expressions (3.11) and (3.13) obtained in the previous chapter. Using expression (4.38), one can obtain the expressions for the radiative fluxes from the shock layer to the body and from the shock layer into the free stream, when the shock shape is taken to be concentric with the body.

Once again, the fact that the gray situation is a special case of the general nongray situation is reemphasized.

C. Nonisothermal Case

When the temperature variations are considered, numerical results can be obtained by using equation (4.26). The integral term in equation (4.26) is not the same as the one in equation (3.1) because of the fact that $E(t) \neq \sigma T^4(t)$. It is for this reason that the results obtained for the integral term of equation (3.1) cannot be

used for the nongray case. Moreover, the first term, $\tau_1^2(F_1^*-F_2^*)$, of equation (4.26) which does not appear in equation (3.1) should be accounted for.

D. Case of Radiative Equilibrium

If there is no heat generation in the medium and a steady state exists, the net emission of radiation from each volume vanishes, i.e. the radiant energy absorbed per unit time by a unit volume is equal to the radiant energy emitted per unit time by the same volume. Thus, the net emission during radiative equilibrium is zero.

1. Formulation

Mathematically speaking, radiative equilibrium for one dimensional spherical geometry is defined by

$$\frac{d[\tau^2 \mathcal{G}(\tau)]}{d\tau} = 0 \tag{4.40}$$

Upon differentiating equation (4.26) and making use of the fact that

$$\frac{d[h_1(\tau;\tau_1)]}{d\tau} = -\tau g_1(\tau;\tau_1) \tag{4.41}$$

$$\frac{d[h_2(\tau;\tau_1,\tau_2)]}{d\tau} = \tau g_2(\tau;\tau_1,\tau_2) \tag{4.42}$$

$$\frac{d}{d\tau}\int_{\tau_1}^{\tau_2} H(\tau,t;\tau_1)\, E(t)dt = 2\tau^2 E(\tau) - \tau \int_{\tau_1}^{\tau_2} K(\tau,t;\tau_1)\, E(t)dt \tag{4.43}$$

one obtains,

$$E(\tau) = \frac{1}{2\tau}\left[F_1 g_1(\tau;\tau_1) + F_2 g_2(\tau;\tau_1,\tau_2) + \int_{\tau_1}^{\tau_2} K(\tau,t;\tau_1)E(t)dt\right] \tag{4.44}$$

where

$$g_1(\tau;\tau_1) = \tau_1 E_2(\tau-\tau_1) - E_3(\tau-\tau_1) + E_3[(\tau^2-\tau_1^2)^{\frac{1}{2}}] \tag{4.45}$$

$$g_2(\tau;\tau_1,\tau_2) = \tau_2 E_2(\tau_2-\tau) + E_3(\tau_2-\tau) - (\tau_2^2-\tau_1^2)^{\frac{1}{2}} E_2[(\tau_2^2-\tau_1^2)^{\frac{1}{2}} + (\tau^2-\tau_1^2)^{\frac{1}{2}}] - E_3[(\tau_2^2-\tau_1^2)^{\frac{1}{2}} + (\tau^2-\tau_1^2)^{\frac{1}{2}}] \tag{4.46}$$

$$K(\tau,t;\tau_1) = t\{E_1(|\tau-t|) - E_1[(\tau^2-\tau_1^2)^{\frac{1}{2}} + (t^2-\tau_1^2)^{\frac{1}{2}}]\} \tag{4.47}$$

Inspection of equation (4.44) reveals that the energy equation has four independent parameters: τ_1, τ_2, F_1 and F_2. The radiative fluxes F_1 and F_2 cannot in general be evaluated before the temperature distribution has been completely determined.

The transformation

$$E(\tau) = F_2 + (F_1-F_2)\phi(\tau) \tag{4.48}$$

permits one to express the solution of the integral equation (4.44) in terms of an independent singular Fredholm integral equation of the second kind:

$$\phi(\tau) = \frac{1}{2\tau}\left[g_1(\tau;\tau_1) + \int_{\tau_1}^{\tau_2} K(\tau,t;\tau_1)\phi(t)dt\right] \tag{4.49}$$

Substitution of equation (4.48) into equation (4.26) results in the following expression for the local radiation flux

$$\tau^2 \mathcal{G}(\tau) = \tau_1^2(F_1^*-F_2^*) + (F_1-F_2)Q(\tau) \tag{4.50}$$

where

$$Q(\tau) = 2[h_1(\tau;\tau_1) + \int_{\tau_1}^{\tau_2} H(\tau,t;\tau_1)\phi(t)dt] \qquad (4.51)$$

Equation (4.49) represents the dimensionless energy equation. The function $\phi(\tau)$ is a universal function and depends only on the optical radial distances τ, τ_1 and τ_2. Equation (4.49) is independent of the parameters (except τ_1 and τ_2) affecting the particular conditions to be specified at the two walls. The functions $\phi(\tau)$ and $Q(\tau)$ defined in this analysis are different from the functions $\tilde{\phi}(\tau)$ and $\tilde{Q}(\tau)$ defined in Reference [17]. The following relation exists: $\phi(\tau) = 1-\tilde{\phi}(\tau)$; $Q(\tau) = -\tilde{Q}(\tau)$.

Radiative equilibrium for one-dimensional planar geometry is defined by

$$\frac{d[\mathcal{F}_p(\tau)]}{d\tau} = 0 \qquad (4.52)$$

Differentiation of equation (4.29) gives

$$E(\tau) = \frac{1}{2}[F_1E_2(\tau-\tau_1) + F_2E_3(\tau_2-\tau) + \int_{\tau_1}^{\tau_2} E_1(|\tau-t|)E(t)dt] \qquad (4.53)$$

The above integral equation defines the temperature distribution and therefore the radiative flux.

The transformation [111]

$$E(\tau) = F_2 + (F_1-F_2)\phi_p(\tau) \qquad (4.54)$$

reduces equation (4.53) to a simpler singular Fredholm integral equation of the second kind:

$$\phi_p(\tau) = \frac{1}{2}\left[E_2(\tau-\tau_1) + \int_{\tau_1}^{\tau_2} \phi_p(t)E_1(|\tau-t|)dt\right] \tag{4.55}$$

Equation (4.55) represents the dimensionless energy equation. The function $\phi_p(\tau)$ is a general function representing solutions of a class of problems for which the gray case is only one limiting solution. Once $\phi_p(\tau)$ is known, the temperature distribution in the medium can be obtained by solving equation (4.54). Substitution of equation (4.54) into equation (4.29) results in the following expression for the local radiation flux.

$$\mathcal{F}_p(\tau) = F_1^* - F_2^* + (F_1-F_2)Q_p(\tau) \tag{4.56}$$

where

$$Q_p(\tau) = 2\left[E_3(\tau-\tau_1) + \int_{\tau_1}^{\tau_2} \text{sign}(\tau-t)E_2(|\tau-t|)\phi_p(t)dt\right] \tag{4.57}$$

By comparing the energy equations (4.44) and (4.53) one finds that the functions $g_1(\tau;\tau_1)$, $g_2(\tau;\tau_1,\tau_2)$ and $K(\tau,t;\tau_1)$ which arise in the spherical geometry case are analogous to the functions $E_2(\tau-\tau_1)$, $E_2(\tau_2-\tau)$ and $E_1(|\tau-t|)$, respectively, of the planar geometry.

2. Function $g_1(\tau;\tau_1)$

Examination of the dimensionless energy equation for the spherical layer (4.49) and that for the planar layer (4.55) reveals that the function $g_1(\tau;\tau_1)/\tau$ is analogous to the function $E_2(\tau-\tau_1)$. In order to gain some insight into the behavior of the function $\phi(\tau)$ with respect to the optical distance τ and the optical radii τ_1, a

study of the function $g_1(\tau;\tau_1)$ is undertaken. The following cases are considered:

a. Exact Results

By utilizing the expression (4.45) for the function $g_1(\tau;\tau_1)$, numerical results are obtained for several values of τ_1. These results are obtained for several values of τ_1. These results are tabulated in Table 4.1 and presented graphically in Figure 4.2.

Examination of Figure 4.2 shows that all the four curves start at the same value when $\tau_1/\tau = 1$. As the ratio τ_1/τ decreases, the function $g_1(\tau;\tau_1)/\tau$ also decreases. For the first two cases, i.e. $\tau_1 = 0.01$ and 0.1, the decrease in the function $g_1(\tau;\tau_1)/\tau$ is quite gradual as $\tau_1/\tau \to 0$, while for the next two cases, i.e. $\tau_1 = 1$ and 5, the decrease in the function $g_1(\tau;\tau_1)/\tau$ is quite rapid as $\tau_1/\tau \to 0$. It is observed that the behavior of the function $g_1(\tau;\tau_1)/\tau$ is quite similar to that of the function $h_1(\tau;\tau_1)/\tau^2$. In Figure 4.2 the curves in broken lines represent the function $E_2(\tau-\tau_1)$ for four cases of τ_1.

b. Optically Thin

With the aid of the asymptotic expansions for the functions $E_2(\tau)$ and $E_3(\tau)$, the function $g_1(\tau;\tau_1)$ in the optically thin limit becomes

$$g_1(\tau;\tau_1) = \tau - [(\tau^2-\tau_1^2)^{\frac{1}{2}}] \tag{4.58}$$

From equation (4.58), one observes that

$$\lim_{\tau\to\tau_1} g_1(\tau;\tau_1) = \tau_1 \tag{4.59}$$

Substitution of $\tau = \tau_1$ in expression (4.45) also yields the same result, i.e. $g_1(\tau=\tau_1;\tau_1) = \tau_1$.

Table 4.1

Values of the function $g_1(\tau;\tau_1)/\tau$

τ_1/τ	$g_1(\tau;\tau_1)/\tau$			
	τ_1=0.01	τ_1=0.1	τ_1=1.0	τ_1=5.0
0.001	2.2858D-11			
0.002	1.3566D-08			
0.003	1.6161D-07			
0.004	6.6108D-07			
0.005	1.7030D-06			
0.006	3.4226D-06	1.0179D-11		
0.007	5.9109D-06	1.6539D-11		
0.008	9.2298D-06	1.2762D-10		
0.009	1.3422D-05	6.4738D-10		
0.010	1.8518D-05	2.4278D-09		
0.020	1.2214D-04	1.4417D-06		
0.030	3.2469D-04	1.7181D-05		
0.040	6.2752D-04	7.0312D-05		
0.050	1.0310D-03	1.8122D-04	1.3314D-10	
0.060	1.5355D-03	3.6438D-04	2.0448D-10	
0.070	2.1411D-03	6.2964D-04	3.1125D-09	
0.080	2.8480D-03	9.8379D-04	2.4307D-08	
0.090	3.6566D-03	1.4316D-03	1.2369D-07	
0.100	4.5670D-03	1.9765D-03	4.6511D-07	
0.200	1.9357D-02	1.3167D-02	2.8429D-04	7.1794D-09
0.300	4.4882D-02	3.5547D-02	3.5067D-03	1.5492D-07
0.400	8.2049D-02	7.0199D-02	1.4954D-02	1.9483D-05
0.500	1.3236D-01	1.1873D-01	4.0495D-02	4.1197D-04
0.600	1.9831D-01	1.8375D-01	8.6485D-02	3.5498D-03
0.700	2.8420D-01	2.6976D-01	1.6118D-01	1.8411D-02
0.800	3.9853D-01	3.8557D-01	2.7825D-01	7.0810D-02
0.900	5.6306D-01	5.5368D-01	4.6912D-01	2.3404D-01
1.000	1.0000D+00	1.0000D+00	1.0000D+00	1.0000D+00

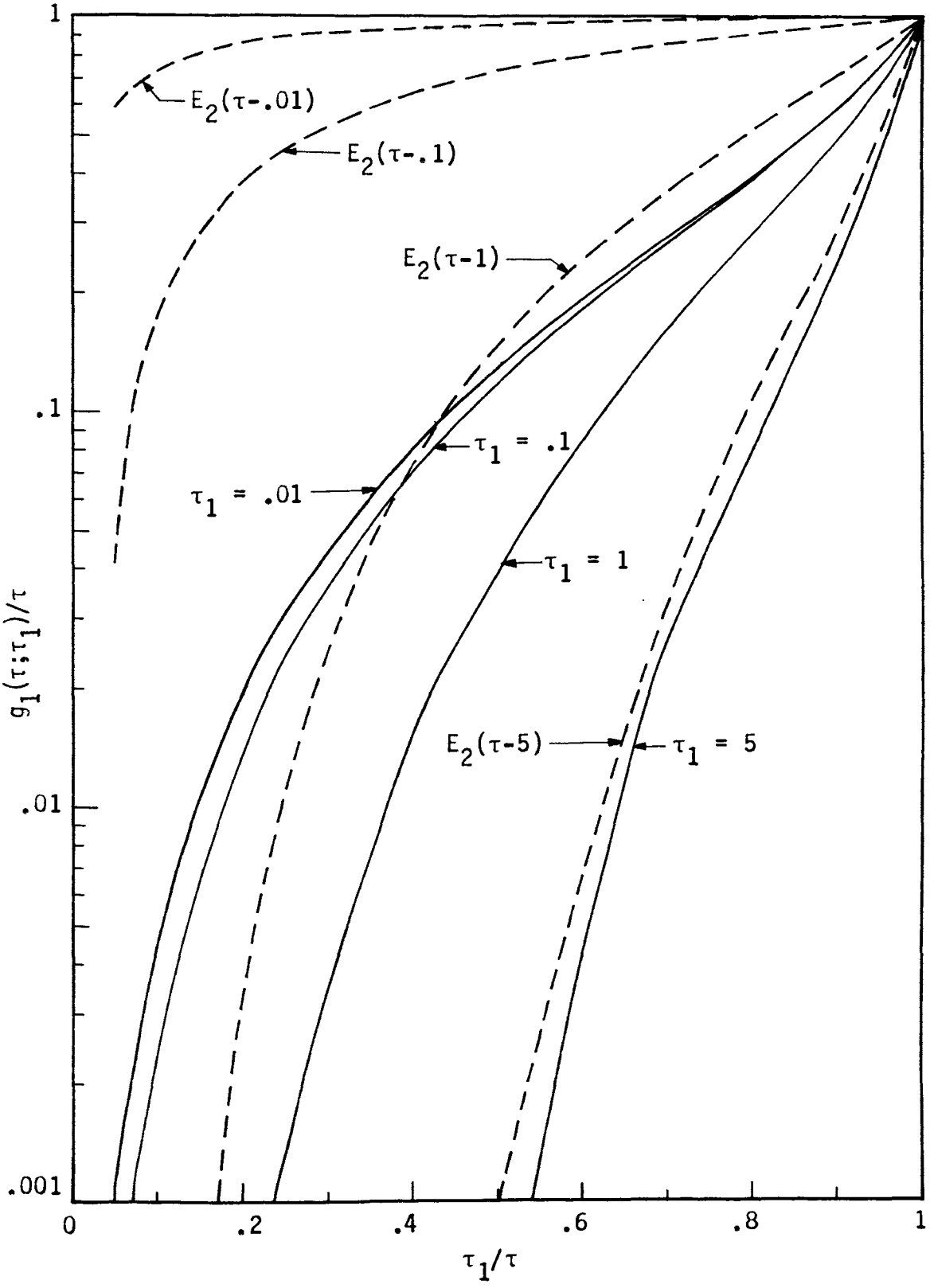

Figure 4.2 - Function $g_1(\tau;\tau_1)$ versus τ_1/τ

3. An Example: Carbon Monoxide

The object of this example is to illustrate how the rectangular model can be used to analyze radiative heat transfer in a nongray gas. For this purpose, both the planar and spherical media will be bounded by black walls at temperatures T_1 and T_2. The analysis is restricted to gases having a single fundamental vibration-rotation band; that is, diatomic gases.

Diatomic absorbing-emitting gases, such as carbon monoxide, have a single fundamental band as well as overtone bands. The first overtone band of carbon monoxide has roughly one percent of the intensity of the fundamental band. Therefore, overtone bands may be neglected and only the fundamental band will be included in the following development.

The band intensity, S, and the effective band width, $\Delta\omega$, for the CO fundamental band may be expressed by the following relations [112],

$$S(T) = 237 \left(\frac{300}{T}\right) \tag{4.60}$$

$$\Delta\omega = 214 \left(\frac{T}{300}\right)^{1/2} \tag{4.61}$$

respectively. The center of the CO fundamental band is located at

$$\omega_c = 2143 \text{ cm}^{-1} \tag{4.62}$$

With the aid of the expressions (4.60) through (4.62), the rectangular models are plotted for different temperatures as shown in Figure 4.3. The rectangular model is a very simple band approximation which assumes that the spectral absorption coefficient κ_ω is constant over an effective band width. Observation of Figure 4.3 shows that κ_ω/P decreases as temperature increases while the reverse is true for the

effective band width. One may say that the rectangle is 'compressed' as the temperature increases. The values for ν_1, ν_2 and $\Delta\nu$ for various temperatures are tabulated in Table 4.2.

Table 4.2
Values of the quantities $\overline{\nu}_c$, $\overline{\nu}_1$ and $\overline{\nu}_2$ for various temperatures

T (°K)	$\nu_c \times 10^{-13}$ (sec^{-1})	$\nu_1 \times 10^{-13}$ (sec^{-1})	$\nu_2 \times 10^{-13}$ (sec^{-1})	$\Delta\nu \times 10^{-13}$ (sec^{-1})
300	6.43	6.12	6.74	0.62
400	6.43	6.06	6.80	0.74
500	6.43	6.02	6.84	0.82
600	6.43	5.99	6.87	0.88
700	6.43	5.94	6.92	0.98
800	6.43	5.90	6.96	1.06
900	6.43	5.88	6.98	1.10

The following identities result for black walls:

$$F_1 + F_1^* \equiv \sigma T_1^4 \tag{4.63}$$

$$F_2 + F_2^* \equiv \sigma T_2^4 \tag{4.64}$$

where F_1, F_2, F_1^* and F_2^* denote the quantities used in expressions (4.26) and (4.29). Utilizing the identities (4.63) and (4.64) in expression (4.56), the following dimensionless function results in case of a planar layer:

$$\mathcal{G}_p^*(\tau) = \frac{\mathcal{G}_p(\tau)}{\sigma T_1^4 - \sigma T_2^4} = 1 - \frac{F_1 - F_2}{\sigma T_1^4 - \sigma T_2^4}\,[1 - Q_p(\tau)] \tag{4.65}$$

Similarly, making use of the identities (4.63) and (4.64), one obtains from expression (4.51) the following form for the dimensionless

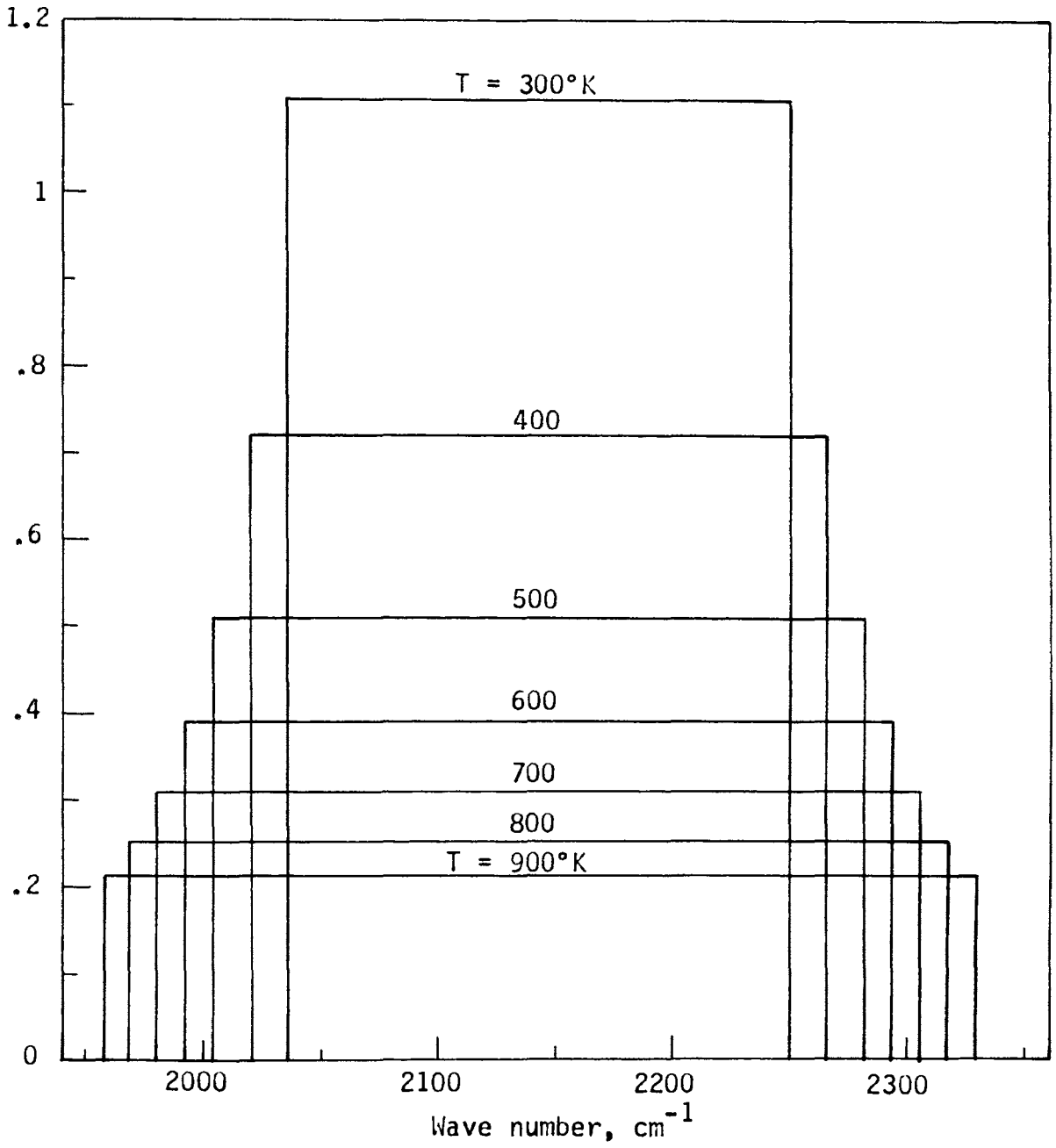

Figure 4.3 - Rectangular model for spectral absorption coefficient of carbon monoxide

function for a spherical layer.

$$\mathcal{G}^*(\tau) = \frac{\tau_1^2}{\tau^2}\left[1 - \frac{F_1 - F_2}{\sigma T_1^4 - \sigma T_2^4}\left(1 + \frac{Q(\tau)}{\tau_1^2}\right)\right] \tag{4.66}$$

The flux incident on the boundary is given by

$$F = \int_0^\infty F_{1\nu}\,\alpha(\nu)\,d\nu \tag{4.67}$$

For a black wall, equation (4.67) reduces to

$$F = \int_0^\infty E_{b\nu}(T)\,\alpha(\nu)\,d\nu \tag{4.68}$$

In equation (4.61), Planck's function $E_{b\nu}$ is given by

$$E_{b\nu}(T) = \frac{2\Pi h\nu^3}{C_0^2\left[\exp\left(\frac{h\nu}{kT}\right) - 1\right]} \tag{4.69}$$

where k is Boltzmann's constant, h is Planck's constant and C_0 is the speed of light in vacuum.

By introducing a dimensionless frequency

$$\bar{\nu} = \frac{h\nu}{kT} \tag{4.70}$$

and rearranging, equation (4.69) reduces to

$$\frac{E_{b\bar{\nu}}(T)}{T^3} = \frac{2\Pi k^3}{C_0^2 h^2} \cdot \frac{\bar{\nu}^3}{(e^{\bar{\nu}} - 1)} \tag{4.71}$$

By noting that $\alpha(\nu)$ has only two values zero and unity, equation (4.68) with the aid of equation (4.71) reduces to

$$\frac{F}{\sigma T^4} = \frac{15}{\Pi^4}\int_{\bar{\nu}_1}^{\bar{\nu}_2} \frac{\bar{\nu}^3 d\bar{\nu}}{e^{\bar{\nu}} - 1} \tag{4.72}$$

In Figure 4.4, the variation of the integrand of equation (4.72) is shown with the dimensionless frequency $\bar{\nu}$. The figure shows that the integrand increases as $\bar{\nu}$ increases. It has a maximum at $\bar{\nu} = 2.8$. The integrand decreases as $\bar{\nu}$ increases beyond 2.8. The cut-offs shown from left to right correspond to the temperatures 900°K, 600°K and 300°K respectively. Figure 4.5 shows the variation of the dimensionless flux $F/\sigma T^4$ with respect to dimensionless frequency $\bar{\nu}$ for various values of $\Delta\bar{\nu}$. The technique used to evaluate the integral in equation (4.72) is outlined in the Appendix of Reference [111]. Examination of Figure 4.5 shows that for a given $\bar{\nu}$ the dimensionless flux increases as $\Delta\bar{\nu}$ is increased. Table 4.3 shows the variation of the quantities $\bar{\nu}_C$, $\bar{\nu}_1$, $\bar{\nu}_2$ and $F/\sigma T^4$ with the absolute temperature T.

Table 4.3

Values of the quantities $\bar{\nu}_c$, $\bar{\nu}_1$, $\bar{\nu}_2$ and $F/\sigma T^4$ for various temperatures

T (°K)	$\bar{\nu}_C$	$\bar{\nu}_1$	$\bar{\nu}_2$	$\Delta\bar{\nu}$	$F/\sigma T^4$
300	10.30	9.80	10.80	1.00	0.0058
400	7.72	7.28	8.16	0.88	0.0280
500	6.16	5.76	6.56	0.80	0.0613
600	5.14	4.78	5.50	0.72	0.0860
700	4.40	4.07	4.73	0.66	0.1075
800	3.86	3.54	4.18	0.64	0.1217
900	3.43	3.13	3.73	0.60	0.1244

Letting $T_1 = 800°K$ and $T_2 = 400°K$, one can proceed to evaluate the dimensionless function $\mathcal{G}_p^*$ for the nongray planar layer. In this analysis the values of $F_1 = 36{,}300$ erg/sec cm^2 and

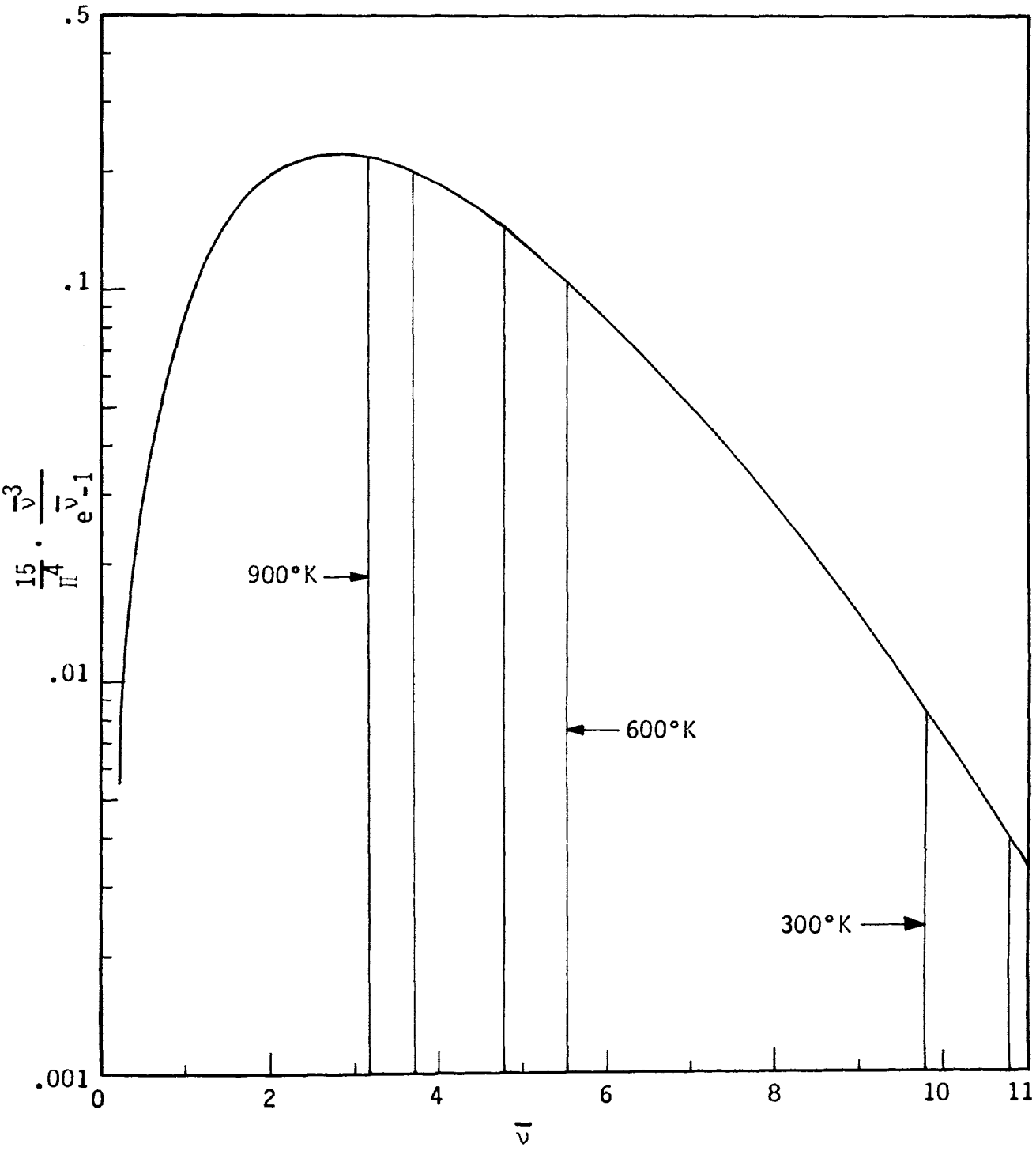

Figure 4.4 - Effect of $\bar{\nu}$ on the dimensionless spectral emissive power

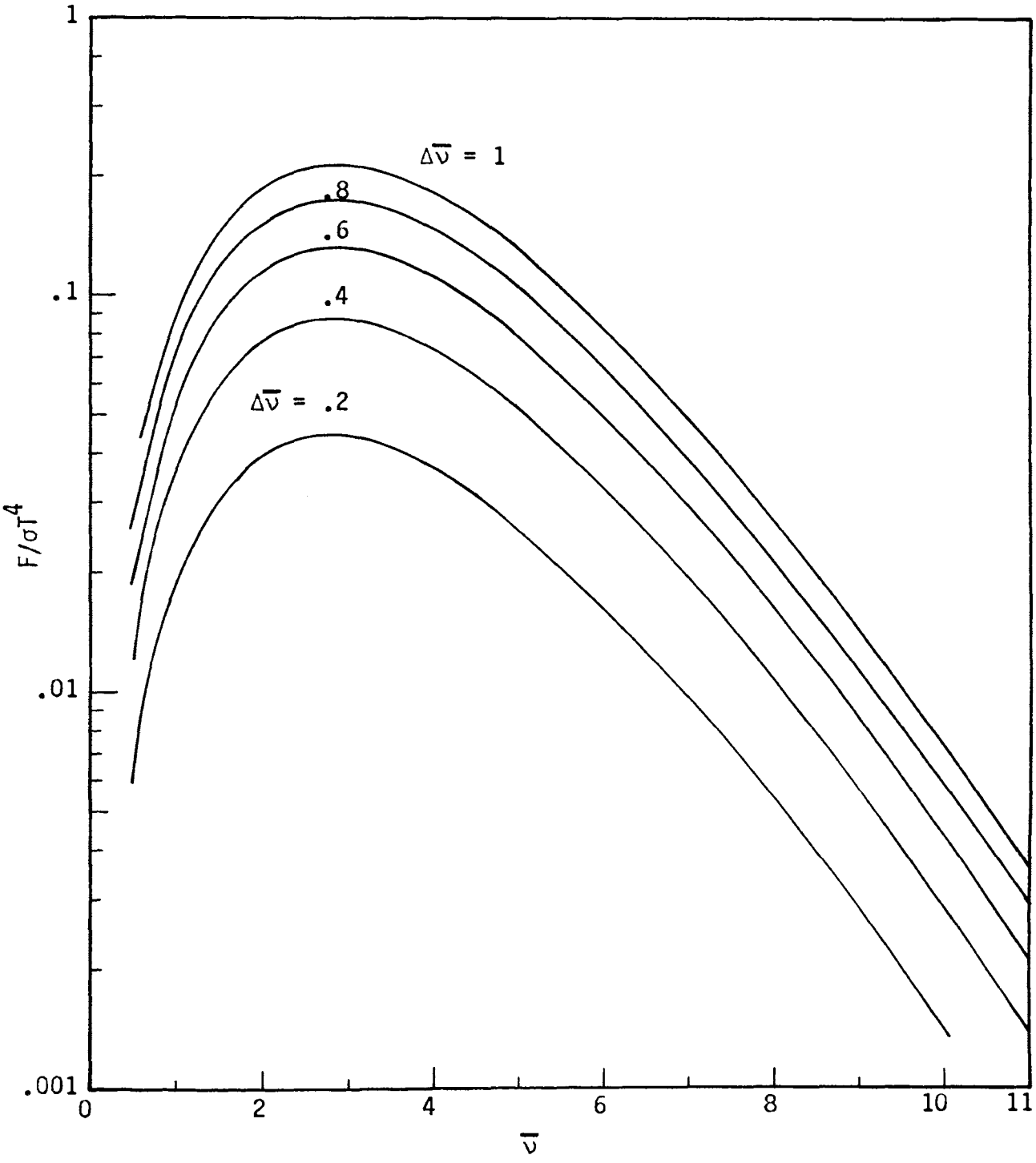

Figure 4.5 - Effect of $\Delta\bar{\nu}$ and $\bar{\nu}$ on the dimensionless radiative flux

F_2 = 3,035 erg/sec cm^2 used are those obtained by using $\nu_1 = 5.99 \times 10^{13}$ sec^{-1} and $\nu_2 = 6.87 \times 10^{13}$ sec^{-1} corresponding to an average temperature of 600°K. The variation of Q_p with respect to the optical thickness $\tau_2-\tau_1$ is known from Reference [113]. Thus, knowing all the quantities in equation (4.65) values of $\mathcal{F}_p^*$ for a range of optical thickness $\tau_2-\tau_1$ are obtained. These results are tabulated in Table 4.4 and presented graphically in Figure 4.7.

For the sake of comparison, a gray layer is considered. For this case, equation (4.65) reduces to

$$\mathcal{F}_p^*(\tau) = Q(\tau) \tag{4.73}$$

Instead of using the value of the absorption coefficient κ as shown in Figure 4.6, an average value (κ_p) is used. This average value, known as the Planck mean absorption coefficient, is expressed as

$$\kappa_p = \frac{\int_0^\infty \kappa_\nu E_{b\nu}(T)\, d\nu}{E_b(T)} \tag{4.74}$$

The Planck mean dimensionless function is expressed as

$$\alpha_p(\nu) = \frac{\int_0^\infty \alpha(\nu) E_{b\nu}(T)\, d\nu}{E_b(T)} \tag{4.75}$$

For the case under consideration

$$\alpha_p(\nu) = \frac{F}{\sigma T^4} = 0.086 \tag{4.76}$$

From the graph of Q versus $\tau_2-\tau_1$, values of $\mathcal{F}_p^*$ are determined for a range of optical thickness corresponding to values of $Q[0.086(\tau_2-\tau_1)]$. The results for the gray layer are tabulated in Table 4.4 and presented graphically in Figure 4.7.

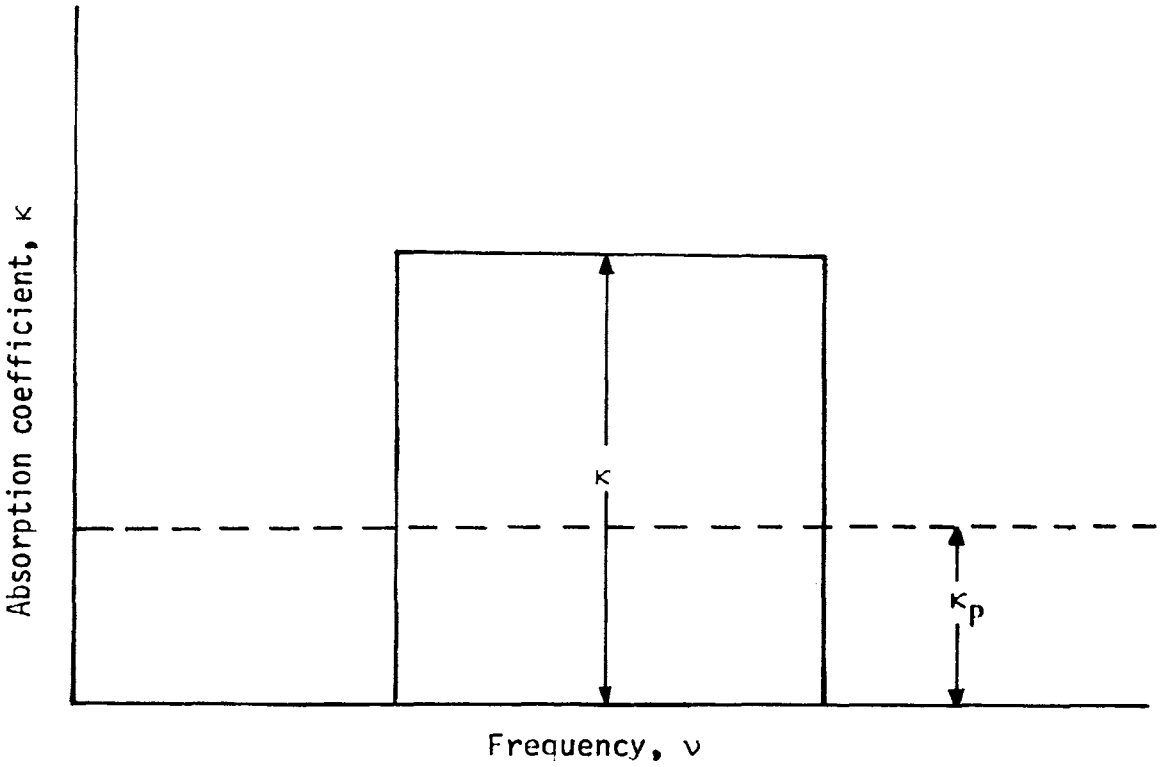

Figure 4.6 - Planck mean absorption coefficient

In a similar manner, values of $\mathcal{G}^*$ for the nongray and gray spherical layer are obtained for a range of inner optical radius τ_1. In this case, the quantity $-Q(\tau_1)/\tau_1^2$ for inner to outer optical radii ratio of 0.5 is obtained from Reference [17]. Results are tabulated in Table 4.5 and presented graphically in Figure 4.8.

Examination of Figures 4.7 and 4.8 show that there is considerable difference between the nongray and gray results for both the planar and the spherical layers. As $\tau_2-\tau_1 \to \infty$ (i.e. $Q \to 0$), $\mathcal{G}^* \to 0.878$ for the nongray medium and it tends to zero for the gray medium. The nongray results indicate that the gray analysis is of limited utility and should be used with extreme caution.

Table 4.4

Comparison of the gray and nongray values of the dimensionless radiative flux from a planar layer

$\tau_2-\tau_1$	$\mathcal{G}^*(\tau)$	
	Nongray	Gray
0.1	0.9870	
0.2	0.9816	
0.3	0.9748	
0.4	0.9690	
0.5	0.9640	0.960
0.6	0.9594	0.955
0.7	0.9554	0.950
0.8	0.9518	0.940
0.9	0.9485	0.935
1.0	0.9457	0.930
2.0	0.9266	0.870
3.0	0.9148	0.820
4.0	0.9080	0.770
5.0	0.9034	0.735
6.0	0.9000	0.700
7.0	0.8972	0.670
8.0	0.8952	0.640
9.0	0.8938	0.615
10.0	0.8922	0.590
20.0	0.8855	0.420
30.0	0.8831	0.330
40.0	0.8820	0.275
50.0	0.8811	0.235
60.0	0.8807	0.205
70.0	0.8804	0.180
80.0	0.8800	0.160
90.0	0.8798	0.145
100.0	0.8795	0.130

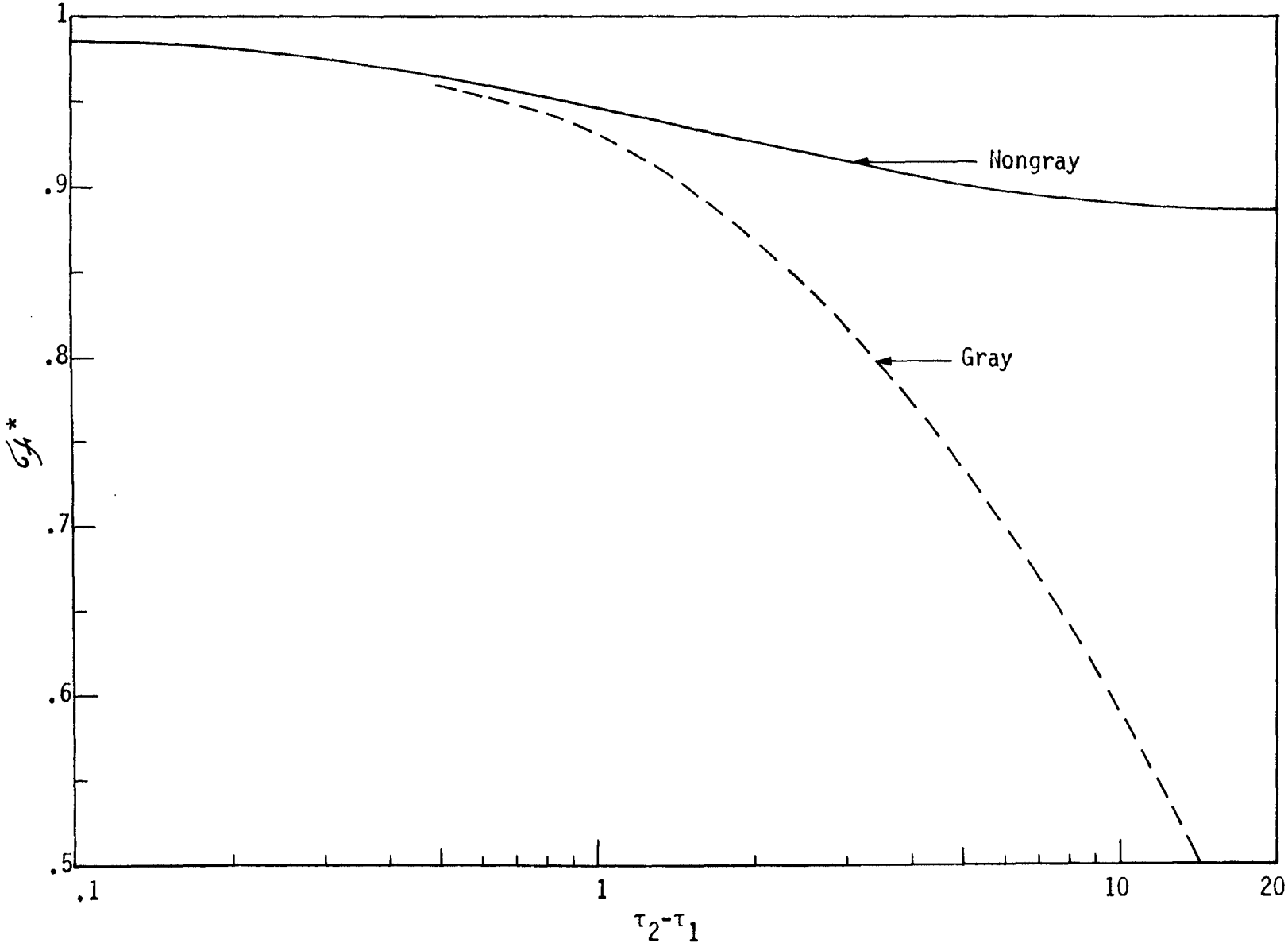

Figure 4.7 - Comparison between gray and nongray results for the radiative flux from a planar layer

Table 4.5

Comparison of the gray and nongray values of the dimensionless radiative flux at the inner boundary of the spherical layer

$\tau_2-\tau_1$	$-\mathcal{G}^*(\tau_1)$	
	Nongray	Gray
0.1	0.9982	
0.2	0.9951	
0.3	0.9929	
0.4	0.9916	
0.5	0.9878	
0.6	0.9854	0.995
0.7	0.9829	0.994
0.8	0.9805	0.993
0.9	0.9780	0.992
1.0	0.9756	0.990
2.0	0.9561	0.970
3.0	0.9415	0.950
4.0	0.9316	0.930
5.0	0.9244	0.910
6.0	0.9220	0.895
7.0	0.9146	0.875
8.0	0.9110	0.860
9.0	0.9080	0.845
10.0	0.9055	0.830
20.0		0.680
30.0		0.570
40.0		0.480
50.0		0.420
60.0		0.375
70.0		0.335
80.0		0.300
90.0		0.280
100.0		0.255

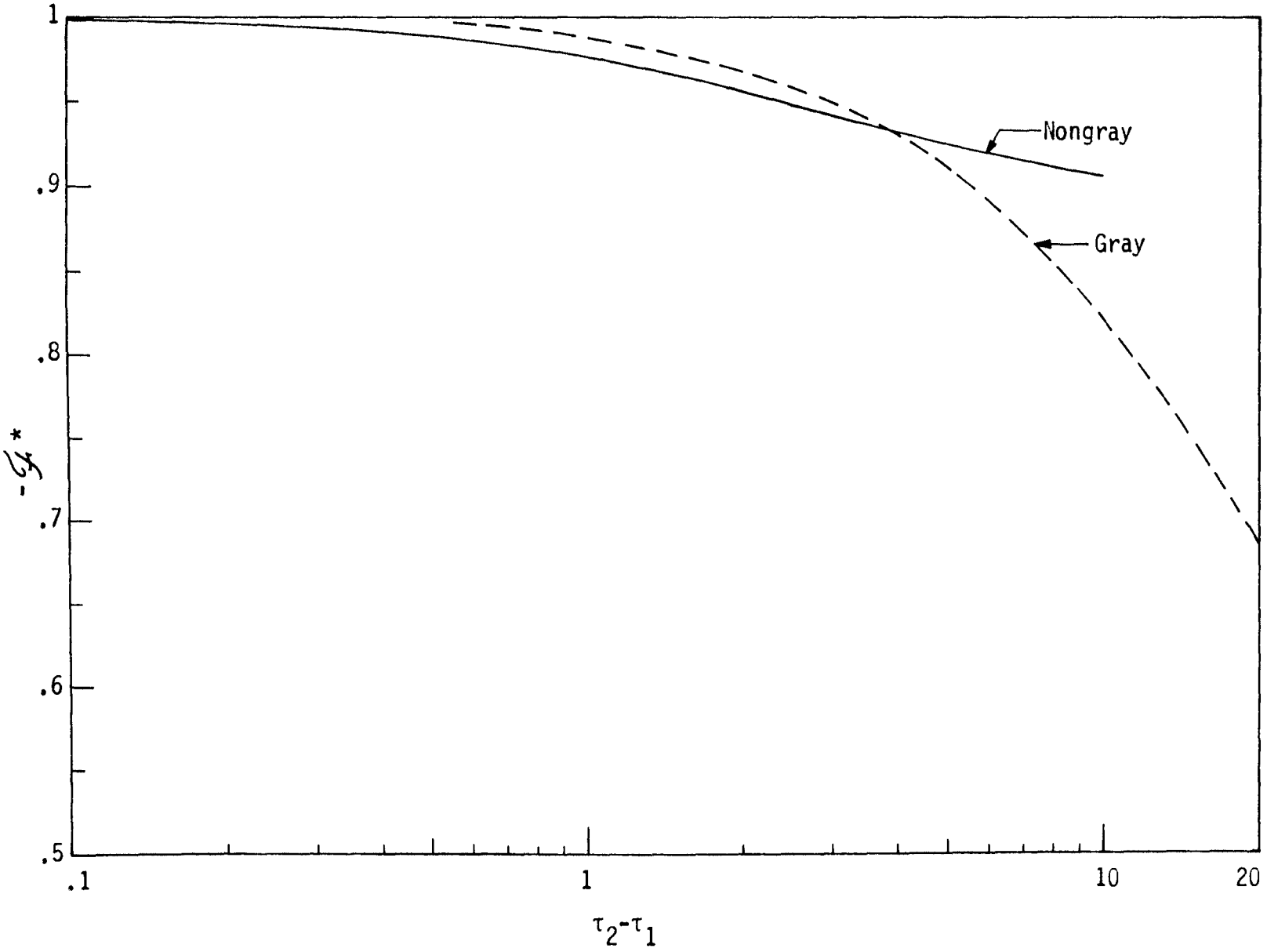

Figure 4.8 - Comparison between gray and nongray results for the radiative flux at the inner boundary of the spherical layer

E. Conclusions

The expressions for the simplified rectangular model turns out to be similar to the expressions for the gray analysis. The local radiative flux for the simplified nongray analysis can be expressed in terms of the functions of the gray analysis, $h_1(\tau;\tau_1)$, $h_2(\tau;\tau_1,\tau_2)$ and $H(\tau,t;\tau_1)$. The influence of the 'bands' occurs in the functions F_1. F_2 and E and the effect of the 'windows' is accounted for in the term $\tau_1^2/\tau^2(F_1^*-F_2^*)$ for the spherical geometry and $(F_1^*-F_2^*)$ for the planar geometry. Thus, with a small amount of additional computational time one can obtain the results for the simplified rectangular model. The isothermal case simplifies the analysis to the point where one can directly use the results of the gray analysis.

The radiative flux from a shock layer composed of nongray medium with simplified rectangular model absorption coefficient is proportional to the flux from a gray shock layer. The example of carbon monoxide analyzed in the study of the radiative equilibrium case reveals that the influence of the 'windows' is quite profound, thus exposing the limitations of the gray analysis.

V. NONGRAY ANALYSIS: EFFECT OF BAND OR LINE SHAPE

In this chapter the effect of line or band shape on the radiative transfer in a nonplanar medium is studied. The method of Reference [113] is extended to the nonplanar region. Five different models for the absorption coefficient have been selected to determine the effect of the absorption coefficient on the radiative transfer. The rectangular, triangular and exponential profiles are usually associated with bands, while the Doppler and Lorentz profiles characterize spectral lines. These models have been selected because they approximate the absorption characteristics of a wide range of substances.

A. Physical Model and Governing Equations

1. Spherical Layer

The medium can absorb and emit but is unable to scatter thermal radiation. The absorption coefficient is written in the form $\kappa_\nu = \alpha(\nu)\kappa$. The dimensionless function $\alpha(\nu)$ can range from zero to unity (see Figure 5.1). The index of refraction of the medium is considered to be unity and the medium is assumed to be in local thermodynamic equilibrium.

The mathematical definition of the models is given in Table 5.1 [114]. Each model is the superposition of m symmetric lines or bands. In Table 5.1, α_i is the amplitude, ν_i is the center, d_i is the damping factor and $\Delta\nu_i$ is the width of the i^{th} band or line. The unit step function is defined as $u(t) = 0$ for $t < 0$ and $u(t) = 1$ for $t > 0$. In all models frequency ν_{i+1} is larger than frequency ν_i.

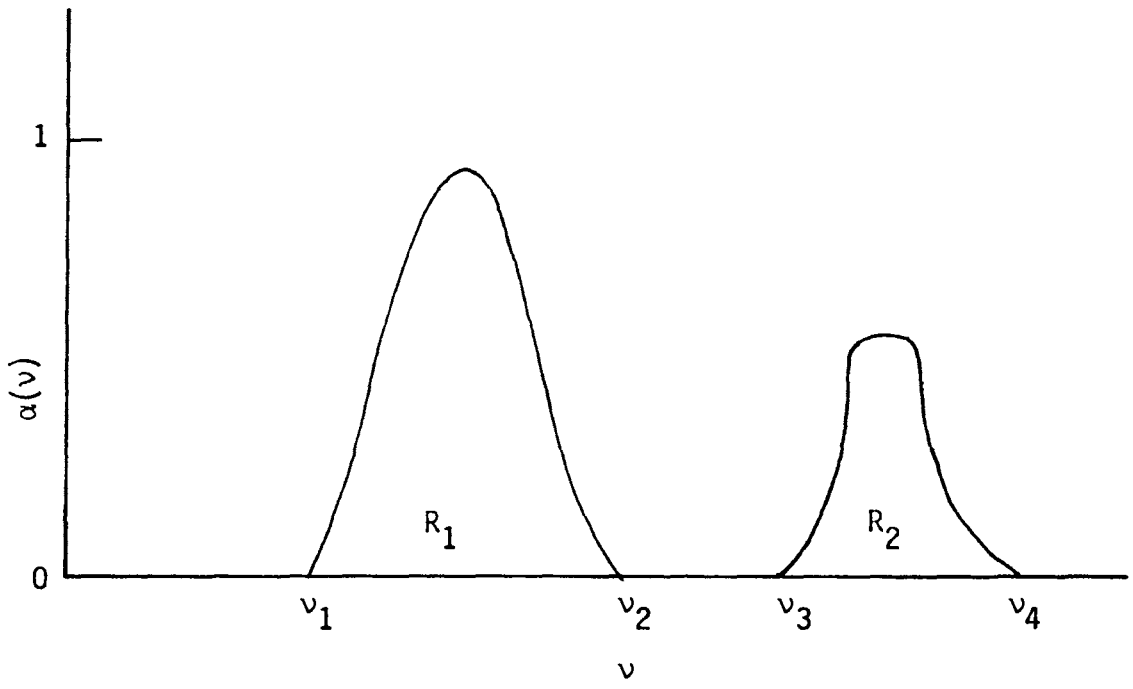

Figure 5.1 - Arbitrary model for spectral absorption coefficient

From equations (4.7) and (4.8) of the previous chapter, we know that

$$\tau_\nu = \alpha(\nu)\tau \quad ; \quad \tau_{1\nu} = \alpha(\nu)\tau_1 \quad ; \quad \tau_{2\nu} = \alpha(\nu)\tau_2$$

Substituting for τ_ν, $\tau_{1\nu}$ and $\tau_{2\nu}$ into equation (4.1) of the preceding chapter, we obtain

$$\alpha^2(\nu)\tau^2 \mathcal{G}_\nu(\tau) = 2 F_{1\nu} h_1[\alpha(\nu)\tau;\alpha(\nu)\tau_1] - 2 F_{2\nu} h_2[\alpha(\nu)\tau;\alpha(\nu)\tau_1,\alpha(\nu)\tau_2] + 2 \int_{\tau_1}^{\tau_2} \alpha(\nu) H[\alpha(\nu)\tau,\alpha(\nu)t;\alpha(\nu)\tau_1] E_{b\nu}(t)dt \quad (5.1)$$

where

Table 5.1

Models for the absorption coefficient $\alpha(\nu)$

Model	Mathematical Definition
Rectangular	$\alpha(\nu) = \sum_{i=1}^{m} \alpha_i [u(\nu - \nu_i + \frac{1}{2}\Delta\nu_i) - u(\nu - \nu_i - \frac{1}{2}\Delta\nu_i)]$
Triangular	$\alpha(\nu) = \sum_{i=1}^{m} \alpha_i (1 - \frac{2}{\Delta\nu_i} \lvert\nu - \nu_i\rvert)[u(\nu - \nu_i + \frac{1}{2}\Delta\nu_i) - u(\nu - \nu_i - \frac{1}{2}\Delta\nu_i)]$
Exponential	$\alpha(\nu) = \sum_{i=1}^{m} \alpha_i \exp[-d_i \lvert\nu - \nu_i\rvert]$
Doppler	$\alpha(\nu) = \sum_{i=1}^{m} \alpha_i \exp[-d_i (\nu - \nu_i)^2]$
Lorentz	$\alpha(\nu) = \sum_{i=1}^{m} \alpha_i \frac{1}{1 + d_i(\nu - \nu_i)^2}$

$$h_1[\alpha(\nu)\tau;\alpha(\nu)\tau_1] = \alpha^2(\nu)\tau\tau_1 E_3[\alpha(\nu)(\tau-\tau_1)] - \alpha(\nu)(\tau-\tau_1) E_4[\alpha(\nu)(\tau-\tau_1)]$$
$$- E_5[\alpha(\nu)(\tau-\tau_1)] + \alpha(\nu)(\tau^2-\tau_1^2)^{\frac{1}{2}} E_4[\alpha(\nu)(\tau^2-\tau_1^2)^{\frac{1}{2}}]$$
$$+ E_5[\alpha(\nu)(\tau^2-\tau_1^2)^{\frac{1}{2}}] \qquad (5.2)$$

$$h_2[\alpha(\nu)\tau;\alpha(\nu)\tau_1,\alpha(\nu)\tau_2] = \alpha^2(\nu)\tau\tau_2 E_3[\alpha(\nu)(\tau_2-\tau)]$$
$$-\alpha(\nu)(\tau_2-\tau) E_4[\alpha(\nu)(\tau_2-\tau)] - E_5[\alpha(\nu)(\tau_2-\tau)]$$
$$+ \alpha^2(\nu)(\tau_2^2-\tau_1^2)^{\frac{1}{2}}(\tau^2-\tau_1^2)^{\frac{1}{2}} E_3[\alpha(\nu)\{(\tau_2^2-\tau_1^2)^{\frac{1}{2}} + (\tau^2-\tau_1^2)^{\frac{1}{2}}\}]$$
$$+ \alpha(\nu)[(\tau_2^2-\tau_1^2)^{\frac{1}{2}} + (\tau^2-\tau_1^2)^{\frac{1}{2}}] E_4[\alpha(\nu)\{(\tau_2^2-\tau_1^2)^{\frac{1}{2}} + (\tau^2-\tau_1^2)^{\frac{1}{2}}\}]$$
$$+ E_5[\alpha(\nu)\{(\tau_2^2-\tau_1^2)^{\frac{1}{2}} + (\tau^2-\tau_1^2)^{\frac{1}{2}}\}] \qquad (5.3)$$

$$H[\alpha(\nu)\tau,\alpha(\nu)t;\alpha(\nu)\tau_1] = \{\alpha(\nu)\tau \ \text{sign}[\alpha(\nu)(\tau-t)]\ E_2[\alpha(\nu)|\tau-t|]$$

$$+ E_3[\alpha(\nu)|\tau-t|]$$

$$- \alpha(\nu)(\tau^2-\tau_1^2)^{\frac{1}{2}}\ E_2[\alpha(\nu)\{(t^1-\tau_1^2)^{\frac{1}{2}} + (\tau^2-\tau_1^2)^{\frac{1}{2}}\}]$$

$$- E_3[\alpha(\nu)\{(t^2-\tau_1^2)^{\frac{1}{2}} + (\tau^2-\tau_1^2)^{\frac{1}{2}}\}]\alpha(\nu)t \qquad (5.4)$$

Substituting for the functions $h_1[\alpha(\nu)\tau;\alpha(\nu)\tau_1]$, $h_2[\alpha(\nu)\tau;\alpha(\nu)\tau_1,\alpha(\nu)\tau_2]$ and $H[\alpha(\nu)\tau,\alpha(\nu)t;\alpha(\nu)\tau_1]$ in equation (5.1) yields

$$\tau^2 \mathcal{G}_\nu(\tau) = 2\ F_{1\nu}\{\tau\tau_1\ E_3[\alpha(\nu)(\tau-\tau_1)] - \frac{(\tau-\tau_1)}{\alpha(\nu)}\ E_4[\alpha(\nu)(\tau-\tau_1)]$$

$$- \frac{1}{\alpha^2(\nu)}\ E_5[\alpha(\nu)(\tau-\tau_1)] + \frac{(\tau^2-\tau_1^2)^{\frac{1}{2}}}{\alpha(\nu)}\ E_4[\alpha(\nu)(\tau^2-\tau_1^2)^{\frac{1}{2}}]$$

$$+ \frac{1}{\alpha^2(\nu)}\ E_5[\alpha(\nu)(\tau^2-\tau_1^2)^{\frac{1}{2}}]\ \}$$

$$- 2\ F_{2\nu}\{\tau\tau_2\ E_3[\alpha(\nu)(\tau_2-\tau)] - \frac{(\tau_2-\tau)}{\alpha(\nu)}\ E_4[\alpha(\nu)(\tau_2-\tau)]$$

$$- \frac{1}{\alpha^2(\nu)}\ E_5\ \alpha(\nu)(\tau_2-\tau)$$

$$+ (\tau_2^2-\tau_1^2)^{\frac{1}{2}}(\tau^2-\tau_1^2)^{\frac{1}{2}}\ E_3[\alpha(\nu)\{(\tau_2^2-\tau_1^2)^{\frac{1}{2}}$$

$$+ (\tau^2-\tau_1^2)^{\frac{1}{2}}\}]$$

$$+ \frac{[(\tau_2^2-\tau_1^2)^{\frac{1}{2}} + (\tau^2-\tau_1^2)^{\frac{1}{2}}]}{\alpha(\nu)}\ E_4[\alpha(\nu)\{(\tau_2^2-\tau_1^2)^{\frac{1}{2}}$$

$$+ (\tau^2-\tau_1^2)^{\frac{1}{2}}\}]$$

$$+ \frac{1}{\alpha^2(\nu)}\ E_5[\alpha(\nu)\{(\tau_2^2-\tau_1^2)^{\frac{1}{2}} + (\tau^2-\tau_1^2)^{\frac{1}{2}}\}]\ \}$$

$$+ 2 \left\{ \int_{\tau_1}^{\tau_2} \alpha(\nu)\tau t \; \text{sign}[\alpha(\nu)(\tau-t)] \; E_2[\alpha(\nu)|\tau-t|] \; E_{b\nu}(t)dt \right.$$

$$+ \int_{\tau_1}^{\tau_2} t \; E_3[\alpha(\nu)|\tau-t|] \; E_{b\nu}(t)dt$$

$$- \int_{\tau_1}^{\tau_2} \alpha(\nu)t(\tau^2-\tau_1{}^1)^{\frac{1}{2}} \; E_2[\alpha(\nu)\{(t^2-\tau_1{}^2)^{\frac{1}{2}} + (\tau^2-\tau_1{}^2)^{\frac{1}{2}}\}] \; E_{b\nu}(t)dt$$

$$\left. - \int_{\tau_1}^{\tau_2} t \; E_3[\alpha(\nu)\{(t^2-\tau_1{}^2)^{\frac{1}{2}} + (\tau^2-\tau_1{}^2)^{\frac{1}{2}}\}] \; E_{b\nu}(t)dt \right. \quad (5.5)$$

The total flux over all wavelengths is obtained by integrating equation (5.5). The portion of the spectrum which is capable of absorbing radiation [$\alpha(\nu) \neq 0$] is divided into m regions. The number of regions considered is such that the narrow band approximation is valid in each region.

Narrow band approximation - The narrow band approximation assumes that Planck's function does not vary greatly across the band or line. Mathematically, this approximation can be stated as follows

$$\int_{R_i} E_{b\nu}(t) \; f(\nu,t) \; d\nu \simeq E_{bi}(t) \int_{R_i} f(\nu,t) \; d\nu \quad (5.6)$$

where R_i is the region of the spectrum over which the integration is performed and E_{bi} is the function $E_{b\nu}$ evaluated at the center of the band or line. The validity of the narrow band approximation is investigated in Reference [115].

Application of the narrow band approximation yields

$$\tau^2 \mathcal{G}(\tau) = \tau_1^2(F_1' - F_2') + 2\{\tau\tau_1 \sum_{i=1}^{m} \gamma_i F_{1i} K_3^i(\tau-\tau_1) - (\tau-\tau_1) \sum_{i=1}^{m} \gamma_i F_{1i} K_4^i(\tau-\tau_1) - \sum_{i=1}^{m} \gamma_i F_{1i} K_5^i(\tau-\tau_1) + (\tau^2-\tau_1^2)^{1/2} \sum_{i=1}^{m} \gamma_i F_{1i} K_4^i[(\tau^2-\tau_1^2)^{1/2}] - \sum_{i=1}^{m} \gamma_i F_{1i} K_5^i [(\tau^2-\tau_1^2)^{1/2}] \}$$

$$- 2\{\tau\tau_2 \sum_{i=1}^{m} \gamma_i F_{2i} K_3^i(\tau_2-\tau) - (\tau_2-\tau) \sum_{i=1}^{m} \gamma_i F_{2i} K_4^i(\tau_2-\tau) - \sum_{i=1}^{m} \gamma_i F_{2i} K_5^i(\tau_2-\tau) + (\tau_2^2-\tau_1^2)^{1/2}(\tau^2-\tau_1^2)^{1/2} \sum_{i=1}^{m} \gamma_i F_{2i} K_3^i[(\tau_2^2-\tau_1^2)^{1/2} + (\tau^2-\tau_1^2)^{1/2}] + [(\tau_2^2-\tau_1^2)^{1/2} + (\tau^2-\tau_1^2)^{1/2}] \sum_{i=1}^{m} \gamma_i F_{2i} K_4^i[(\tau_2^2-\tau_1^2)^{1/2} + (\tau^2-\tau_1^2)^{1/2}] + \sum_{i=1}^{m} \gamma_i F_{2i} K_5^i [(\tau_2^2-\tau_1^2)^{1/2} + (\tau^2-\tau_1^2)^{1/2}] \}$$

$$+ 2 \{ \sum_{i=1}^{m} \gamma_i \int_{\tau_1}^{\tau_2} \tau\, t\, \mathrm{sign}(\tau-t)\, K_2^{\,i}(|\tau-t|)\, E_{bi}(t)\, dt$$

$$+ \sum_{i=1}^{m} \gamma_i \int_{\tau_1}^{\tau_2} t\, K_3^{\,i}(|\tau-t|)\, E_{bi}(t)\, dt$$

$$- \sum_{i=1}^{m} \gamma_i \int_{\tau_1}^{\tau_2} t(\tau^2-\tau_1^{\,2})^{\frac{1}{2}}\, K_2^{\,i}[(t^2-\tau_1^{\,2})^{\frac{1}{2}} + (\tau^2-\tau_1^{\,2})^{\frac{1}{2}}]\, E_{bi}(t)\, dt$$

$$- \sum_{i=1}^{m} \gamma_i \int_{\tau_1}^{\tau_2} t\, K_3^{\,i}[(t^2-\tau_1^{\,2})^{\frac{1}{2}} + (\tau^2-\tau_1^{\,2})^{\frac{1}{2}}]\, E_{bi}(t)\, dt \,\} \quad (5.7)$$

where the kernels $K_2^{\,i}(\tau)$, $K_3^{\,i}(\tau)$, $K_4^{\,i}(\tau)$, $K_5^{\,i}(\tau)$ and quantity γ_i are defined as follows (see Appendix B for mathematical properties of the functions $K_n(\tau)$):

$$K_2^{\,i}(\tau) = \int_{R_i} \alpha(\nu) E_2[\alpha(\nu)\tau] d\nu \,/\, \gamma_i \quad (5.8)$$

$$K_3^{\,i}(\tau) = \int_{R_i} \{E_3[\alpha(\nu)\tau] - \tfrac{1}{2}\} d\nu \,/\, \gamma_i \quad (5.9)$$

$$K_4^{\,i}(\tau) = \int_{R_i} \{E_4[\alpha(\nu)\tau] - \tfrac{1}{3} + [\alpha(\nu)\tau]/2\} \,/\, \alpha(\nu)\, d\nu \,/\, \gamma_i \quad (5.10)$$

$$K_5^{\,i}(\tau) = \int_{R_i} \{E_5[\alpha(\nu)\tau] - \tfrac{1}{4} + [\alpha(\nu)\tau]/3 - [\alpha^2(\nu)\tau^2]/4\} \,/\, \alpha^2(\nu)\, d\nu \,/\, \gamma_i \quad (5.11)$$

$$\gamma_i = \int_{R_i} \alpha(\nu)\, d\nu \tag{5.12}$$

where R_i is the i^{th} region of the spectrum. In equation (5.7) E_{bi} is the function $E_{b\nu}$ evaluated at the center of the i^{th} region of the spectrum and

$$F_1' = \int_0^\infty F_{1\nu}\, d\nu \tag{5.13}$$

$$F_2' = \int_0^\infty F_{2\nu}\, d\nu \tag{5.14}$$

If the absorption coefficient in each region is identical in shape and intensity and the profiles are nonoverlapping (see Figure 5.2), the quantities $K_2^i(\tau)$, $K_3^i(\tau)$, $K_4^i(\tau)$, $K_5^i(\tau)$ and γ_i are independent of i. Thus, equation 5.7 reduces to

$$\tau^2 \mathcal{G}(\tau) = \tau_1^2(F_1' - F_2') + 2\gamma F_1 \mathcal{h}_1(\tau;\tau_1) - 2\gamma F_2 \mathcal{h}_2(\tau;\tau_1,\tau_2) + 2\gamma \int_{\tau_1}^{\tau_2} \mathcal{H}(\tau,t;\tau_1)\psi(t)\, dt \tag{5.15}$$

where

$$\mathcal{h}_1(\tau;\tau_1) = \tau\tau_1 K_3(\tau-\tau_1) - (\tau-\tau_1)K_4(\tau-\tau_1) - K_5(\tau-\tau_1) + (\tau^2-\tau_1^2)^{\frac{1}{2}}K_4[(\tau^2-\tau_1^2)^{\frac{1}{2}}] + K_5[(\tau^2-\tau_1^2)^{\frac{1}{2}}] \tag{5.16}$$

$$\mathcal{h}_2(\tau;\tau_1,\tau_2) = \tau\tau_2 K_3(\tau_2-\tau) - (\tau_2-\tau)K_4(\tau_2-\tau) - K_5(\tau-\tau_1) + (\tau_2^2-\tau_1^2)^{\frac{1}{2}}(\tau^2-\tau_1^2)^{\frac{1}{2}}K_3[(\tau_2^2-\tau_1^2)^{\frac{1}{2}} + (\tau^2-\tau_1^2)^{\frac{1}{2}}] + [(\tau_2^2-\tau_1^2)^{\frac{1}{2}} + (\tau^2-\tau_1^2)^{\frac{1}{2}}]K_4[(\tau_2^2-\tau_1^2)^{\frac{1}{2}} + (\tau^2-\tau_1^2)^{\frac{1}{2}}]$$

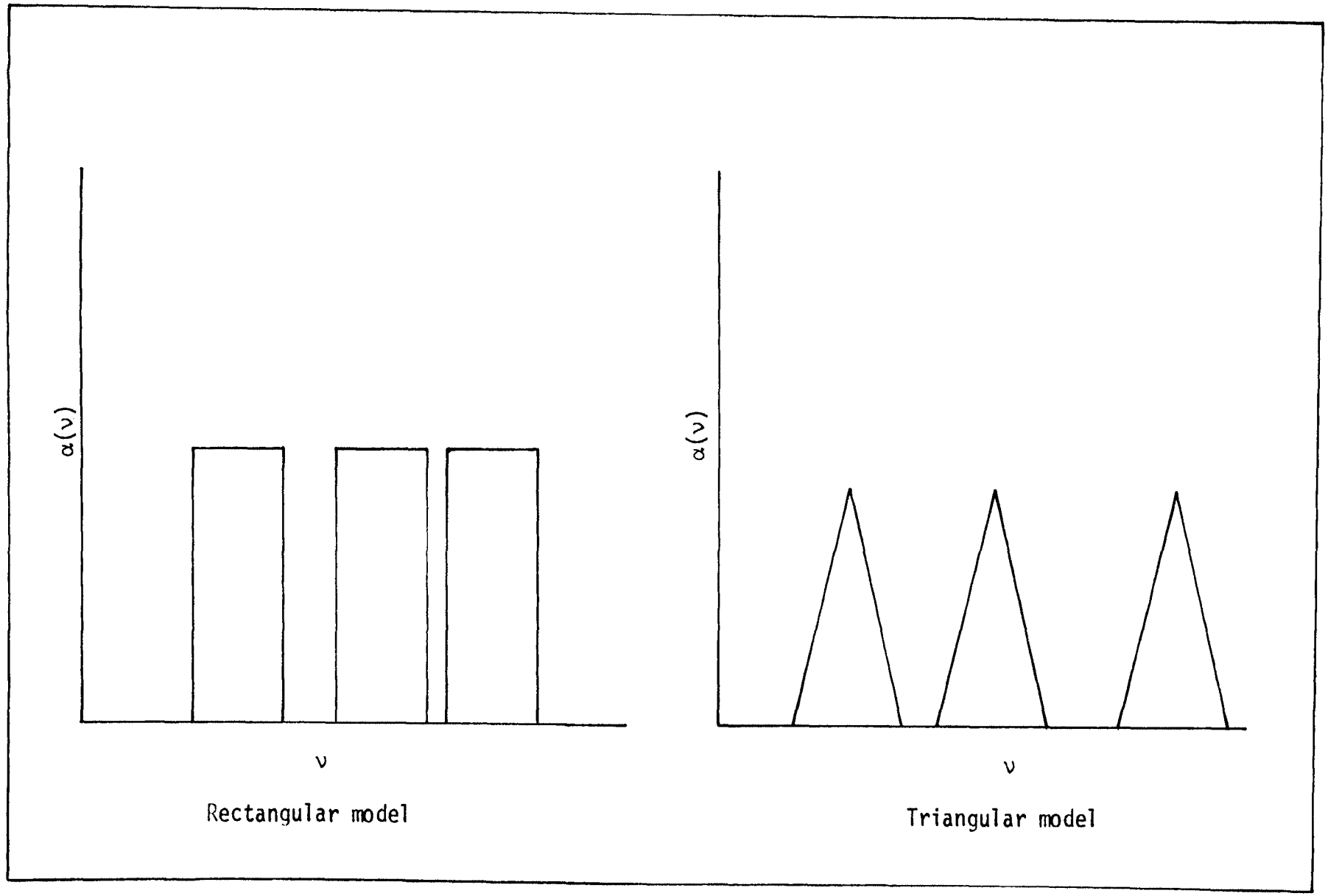

Figure 5.2 - Models for absorption coefficient of bands identical in shape and intensity

$$+ K_5[(\tau_2^2-\tau_1^2)^{\frac{1}{2}} + (\tau^2-\tau_1^2)^{\frac{1}{2}}] \tag{5.17}$$

$$\mathcal{H}(\tau,t;\tau_1) = \{ \tau \, \text{sign}(\tau-t)K_2(|\tau-t|) + K_3(|\tau-t|)$$

$$- (\tau^2-\tau_1^2)^{\frac{1}{2}}K_2[(t^2-\tau_1^2)^{\frac{1}{2}} + (\tau^2-\tau_1^2)^{\frac{1}{2}}]$$

$$- K_3[(t^2-\tau_1^2)^{\frac{1}{2}} + (\tau^2-\tau_1^2)^{\frac{1}{2}}] \} \, t \tag{5.18}$$

$$F_1 = \sum_{i=1}^{m} F_{1i} \tag{5.19}$$

$$F_2 = \sum_{i=1}^{m} F_{2i} \tag{5.20}$$

$$\psi(t) = \sum_{i=1}^{m} E_{bi}(t) \tag{5.21}$$

2. Planar Layer

Consideration of a similar problem in planar medium yields the following expression for local radiative flux [113]

$$\mathcal{F}_p(\tau) = F_1'-F_2' + 2\gamma F_1 K_3(\tau-\tau_1) - 2\gamma F_2 K_3(\tau_2-\tau)$$

$$+ 2\gamma \int_{\tau_1}^{\tau_2} \text{sign}(\tau-t)K_2(|\tau-t|)\psi(t)\, dt \tag{5.22}$$

where F_1' and F_2' are given by equations (5.13) and (5.14) respectively, while F_1, F_2 and $\psi(t)$ are given by equations (5.19) through (5.21). Equation (5.22) is obtained from equation (4.27) of the previous chapter in a manner similar to the one which is used for the spherical geometry as discussed earlier in this chapter.

Comparison of equation (5.15) with equation (5.22) shows that the functions $\mathcal{L}_1(\tau;\tau_1)/\tau^2$ and $\mathcal{L}_2(\tau;\tau_1,\tau_2)/\tau^2$ in spherical geometry

corresponds to the functions $K_3(\tau-\tau_1)$ and $K_3(\tau_2-\tau)$ in planar geometry respectively. This pattern is very similar to the one observed in chapter three during the study of gray medium problem.

3. Isothermal Layer

For the isothermal case, i.e. when $\psi(t) = \psi_0$, equation (5.15) reduces to

$$\tau^2 \mathcal{G}(\tau) = \tau_1^2(F_1'-F_2') + 2\gamma \mathcal{h}_1(\tau;\tau_1)[F_1-\psi_0] - 2\gamma \mathcal{h}_2(\tau;\tau_1,\tau_2)[F_2-\psi_0] \quad (5.23)$$

To arrive at the above expression, the following relation is used

$$\int_{\tau_1}^{\tau_2} \mathcal{H}(\tau,t;\tau_1)\, dt = -\mathcal{h}_1(\tau;\tau_1) + \mathcal{h}_2(\tau;\tau_1,\tau_2) \quad (5.24)$$

The above relation (5.24) is similar to relation (3.10) used in the study of gray medium problem.

The expression for local radiative flux in a planar medium reduces to

$$\mathcal{G}_p(\tau) = F_1'-F_2' + 2\gamma K_3(\tau-\tau_1)[F_1-\psi_0] - 2\gamma K_3(\tau_2-\tau)[F_2-\psi_0] \quad (5.25)$$

Inspection of equation (5.23) reveals that the local radiative flux depends on the functions $\mathcal{h}_1(\tau;\tau_1)$ and $\mathcal{h}_2(\tau;\tau_1,\tau_2)$. Therefore, to gain some insight into the local radiative flux, it seems appropriate to study the functions $\mathcal{h}_1(\tau;\tau_1)$ and $\mathcal{h}_2(\tau;\tau_1,\tau_2)$.

B. Isothermal Analysis: Function $\mathcal{h}_1(\tau;\tau_1)$

Considering the same physical situation as illustrated in Figure

3.3 of chapter three, we find from equation (5.23), that in order to predict the variation in $\mathcal{G}(\tau)$, some knowledge of the function $\mathcal{h}_1(\tau;\tau_1)$ is essential. The following cases of the function $\mathcal{h}_1(\tau;\tau_1)$ are studied:

1. Exact Results

Numerical results are obtained using the exact expression (5.16) for the function $\mathcal{h}_1(\tau;\tau_1)$. The results for four different cases, i.e. τ_1 = 0.01, 0.1, 1 and 5 are tabulated in Tables 5.2 through 5.5 and presented graphically in Figures 5.3 through 5.6. Inspection of the results reveal that while the values for the rectangular profile are always less than that of the other four profiles, the values for the triangular and Doppler profiles do not defer much. Graphically, the curves begin to separate around different values of τ_1/τ, depending upon the inner optical radius τ_1. For τ_1 = 0.01 separation occurs around τ_1/τ = 0.06, for τ_1 = 0.1 separation occurs around τ_1/τ = 0.6, for τ_1 = 1 separation occurs around τ_1/τ = 0.8, and for τ_1 = 5 separation occurs around τ_1/τ = 0.95. Therefore one can infer that the results become independent of the shape of the absorption coefficient as $\tau_1 \to 0$.

It is worth noting that the following relation holds good always for the rectangular profile:

$$\mathcal{h}_1(\tau;\tau_1) = h_1(\tau;\tau_1) - \frac{\tau_1^2}{2} \qquad (5.26)$$

Table 5.2

Values of the function $\mathcal{H}_1(\tau,\tau_1)/\tau^2$ for $_1$ = 0.01

τ_1/τ	$-\mathcal{H}_1(\tau;\tau_1)/\tau^2$				
	Rectangular	Triangular	Exponential	Doppler	Lorentz
			(i) τ_1=0.01		
0.01	3.1482D-5	3.6611D-5	3.9618D-5	3.6081D-5	3.9857D-5
0.02	7.7876D-5	8.4253D-5	8.7709D-5	8.3534D-5	8.7849D-5
0.03	1.2538D-4	1.3219D-4	1.3579D-4	1.3140D-4	1.3589D-4
0.04	1.7273D-4	1.7972D-4	1.8336D-4	1.7890D-4	1.8344D-4
0.05	2.1961D-4	2.2668D-4	2.3033D-4	2.2584D-4	2.3039D-4
0.06	2.6591D-4	2.7299D-4	2.7663D-4	2.7215D-4	2.7667D-4
0.07	3.1156D-4	3.1863D-4	3.2224D-4	3.1778D-4	3.2228D-4
0.08	3.5654D-4	3.6356D-4	3.6714D-4	3.6273D-4	3.6718D-4
0.09	4.0083D-4	4.0779D-4	4.1134D-4	4.0696D-4	4.1137D-4
0.10	4.4440D-4	4.5130D-4	4.5480D-4	4.5047D-4	4.5483D-4
0.20	8.3847D-4	8.4447D-4	8.4749D-4	8.4375D-4	8.4750D-4
0.30	1.1507D-3	1.1557D-4	1.1582D-3	1.1551D-3	1.1582D-3
0.40	1.3724D-3	1.3764D-3	1.3784D-3	1.3759D-3	1.3784D-3
0.50	1.4940D-3	1.4971D-3	1.4986D-3	1.4967D-3	1.4986D-3
0.60	1.5046D-3	1.5068D-3	1.5079D-3	1.5065D-3	1.5079D-3
0.70	1.3901D-3	1.3915D-3	1.3922D-3	1.3913D-3	1.3922D-3
0.80	1.1312D-3	1.1319D-3	1.1323D-3	1.1318D-3	1.1323D-3
0.90	6.9629D-4	6.9651D-4	6.9663D-4	6.9648D-4	6.9663E-4
0.95	3.9341D-4	3.9348D-4	3.9351D-4	3.9347D-4	3.9351D-4
1.00	0	0	0	0	0

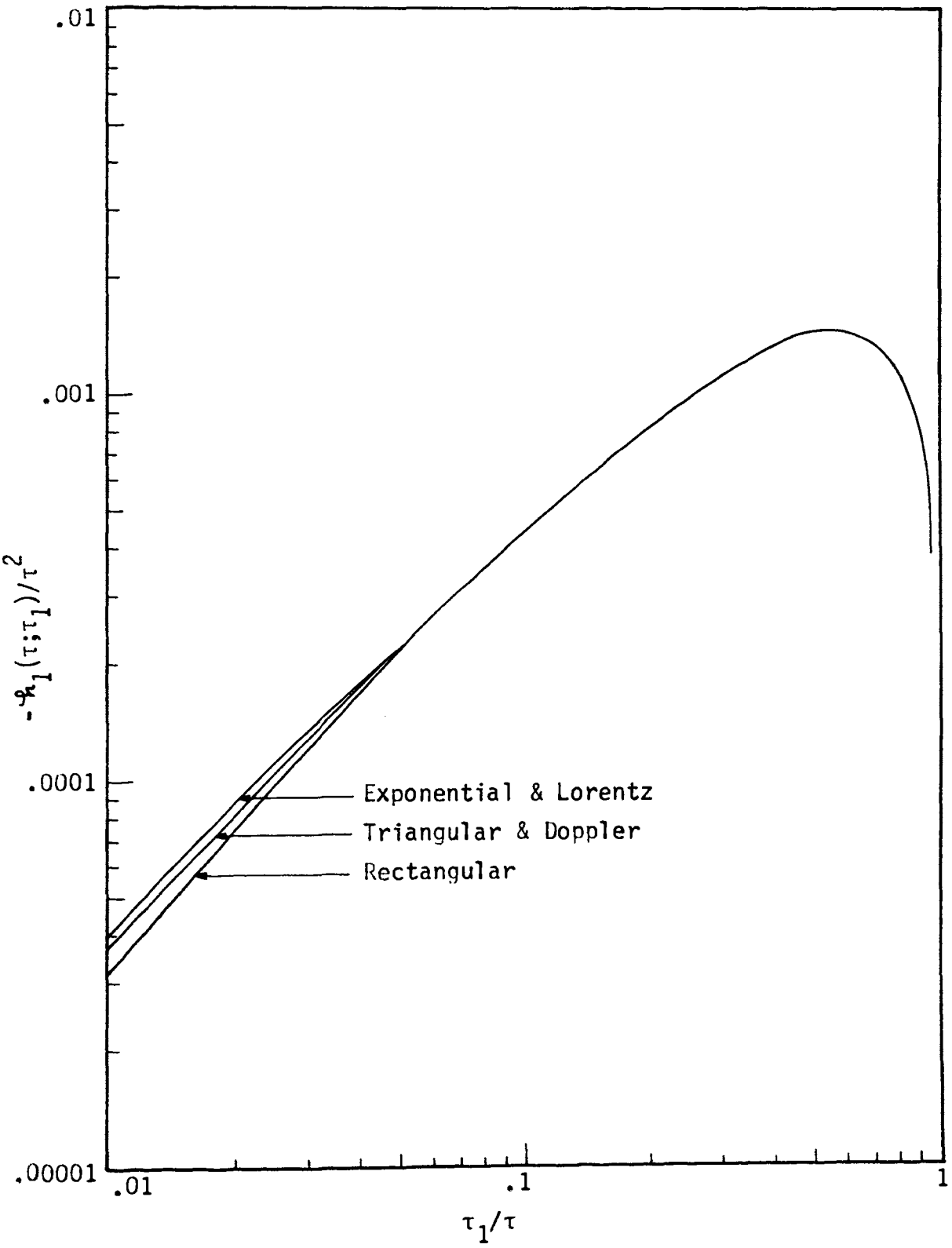

Figure 5.3 - Function $\mathcal{h}_1(\tau;\tau_1)/\tau^2$ versus τ_1/τ for $\tau_1 = 0.01$

Table 5.3

Values of the function $\Phi_1(\tau;\tau_1)/\tau^2$ for $\tau_1 = 0.1$

τ_1/τ	$-\Phi_1(\tau;\tau_1)/\tau^2$				
	Rectangular	Triangular	Exponential	Doppler	Lorentz
			(ii) τ_1=0.1		
0.01	4.9998D-5	8.9933D-5	1.4365D-4	9.3355D-5	1.7314D-4
0.02	1.9856D-4	3.1949D-4	4.3487D-4	3.1752D-4	4.7299D-4
0.03	4.3282D-4	6.3493D-4	7.9653D-4	6.2393D-4	8.3457D-4
0.04	7.2972D-4	9.9995D-4	1.1946D-3	9.8017D-4	1.2301D-3
0.05	1.0689D-3	1.3934D-3	1.6119D-3	1.3661D-3	1.6442D-3
0.06	1.4359D-3	1.8032D-3	2.0389D-3	1.7697D-3	2.0682D-3
0.07	1.8211D-3	2.2218D-3	2.4702D-3	2.1833D-3	2.4967D-3
0.08	2.2178D-3	2.6447D-3	2.9023D-3	2.6021D-3	2.9264D-3
0.09	2.6213D-3	3.0687D-3	3.3330D-3	3.0229D-3	3.3550D-3
0.10	3.0284D-3	3.4917D-3	3.7608D-3	3.4433D-3	3.7809D-3
0.20	6.9649D-3	7.4615D-3	7.7279D-3	7.4049D-3	7.7373D-3
0.30	1.0263D-2	1.0708D-2	1.0940D-2	1.0656D-2	1.0945D-2
0.40	1.2702D-2	1.3071D-2	1.3262D-2	1.3028D-2	1.3265D-2
0.50	1.4149D-2	1.4437D-2	1.4585D-2	1.4403D-2	1.4586D-2
0.60	1.4478D-2	1.4686D-2	1.4791D-2	1.4661D-2	1.4792D-2
0.70	1.3536D-2	1.3670D-2	1.3738D-2	1.3654D-2	1.3738D-2
0.80	1.1121D-2	1.1191D-2	1.1227D-2	1.1182D-2	1.1227D-2
0.90	6.9020D-3	6.9245D-3	6.9358D-3	6.9218D-3	6.9358D-3
0.95	3.9154D-3	3.9223D-3	3.9258D-3	3.9215D-3	3.9258D-3
1.00	0	0	0	0	0

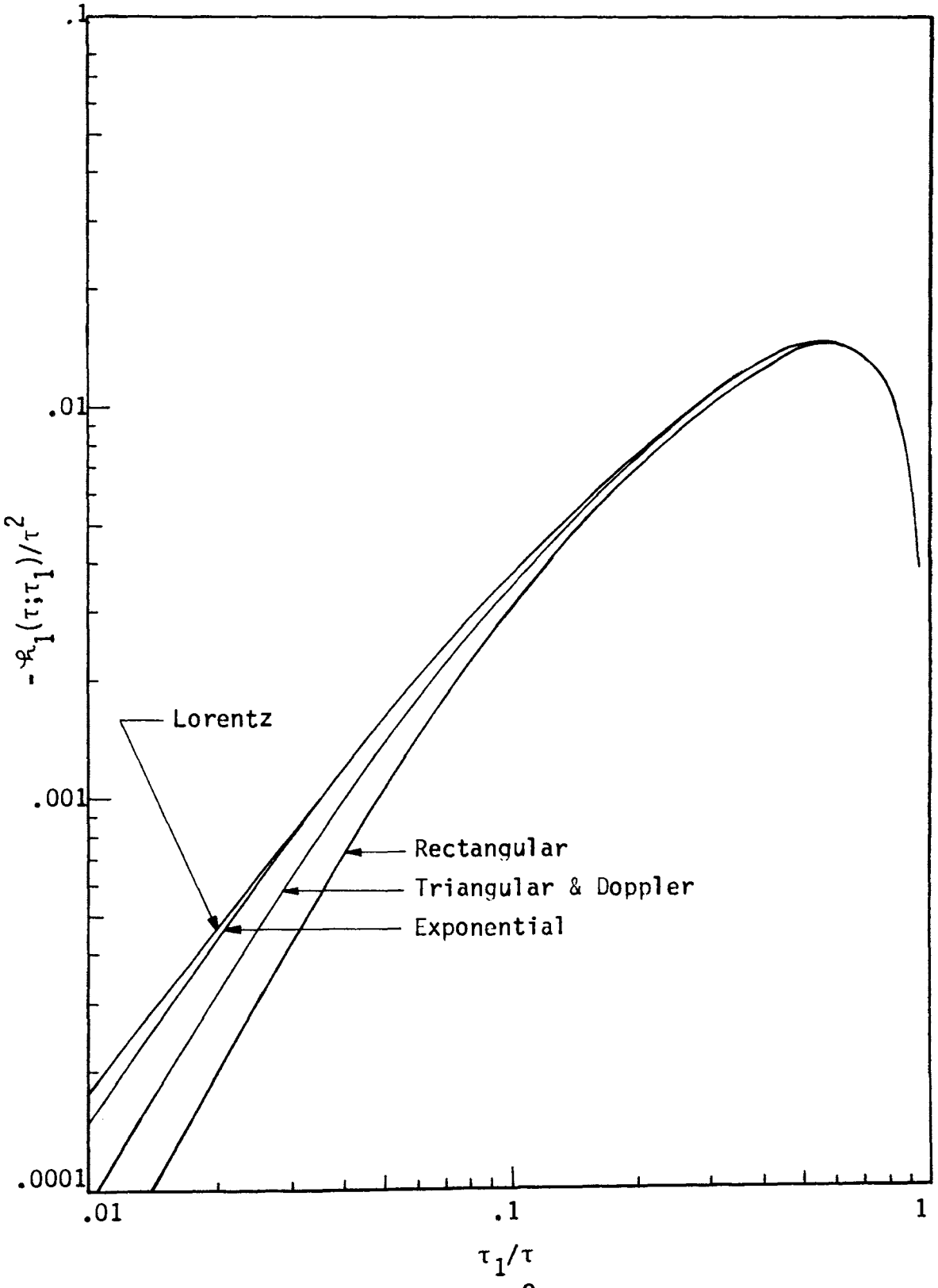

Figure 5.4 - Function $\mathcal{R}_1(\tau;\tau_1)/\tau^2$ versus τ_1/τ for $\tau_1 = 0.1$

Table 5.4

Values of the function $\mathcal{L}_1(\tau;\tau_1)/\tau^2$ for $\tau_1 = 1$

τ_1/τ	$-\mathcal{L}_1(\tau;\tau_1)/\tau^2$				
	Rectangular	Triangular	Exponential	Doppler	Lorentz
			(iii) τ_1=1.0		
0.01					
0.02					
0.03	4.4805D-4	8.7235D-4	1.8283D-3		2.8792D-3
0.04	8.0000D-4	1.5342D-3	3.0149D-3		4.4055D-3
0.05	1.2500D-3	2.3706D-3	4.4229D-3		6.1178D-3
0.06	1.8000D-3	3.3747D-3	6.0278D-3	3.6718D-3	7.9900D-3
0.07	2.4500D-3	4.5396D-3	7.8088D-3	4.8381D-3	1.0002D-2
0.08	3.2000D-3	5.8580D-3	9.7480D-3	6.1687D-3	1.2138D-2
0.09	4.0499D-3	7.3225D-3	1.1830D-2	7.6307D-3	1.4384D-2
0.10	4.9995D-3	8.9252D-3	1.4039D-2	9.2173D-3	1.6727D-3
0.20	1.9718D-2	3.0773D-2	4.0670D-2	3.0430D-2	4.3595D-2
0.30	4.1566D-2	5.7773D-2	6.9715D-2	5.6649D-2	7.2027D-2
0.40	6.5611D-2	8.3688D-2	9.5555D-2	8.2100D-2	9.7164D-2
0.50	8.6983D-2	1.0413D-1	1.1456D-1	1.0244D-1	1.1558D-1
0.60	1.0150D-1	1.1576D-1	1.2398D-1	1.1426D-1	1.2456D-1
0.70	1.0534D-1	1.1558D-1	1.2124D-1	1.1445D-1	1.2153D-1
0.80	9.4432D-2	1.0032D-1	1.0346D-1	9.9645D-2	1.0357D-1
0.90	6.3366D-2	6.5399D-2	6.6453D-2	6.5160D-2	6.6473D-2
0.95	3.7367D-2	3.8018D-2	3.8350D-2	3.7940D-2	3.8354D-2
1.00	0	0	0	0	0

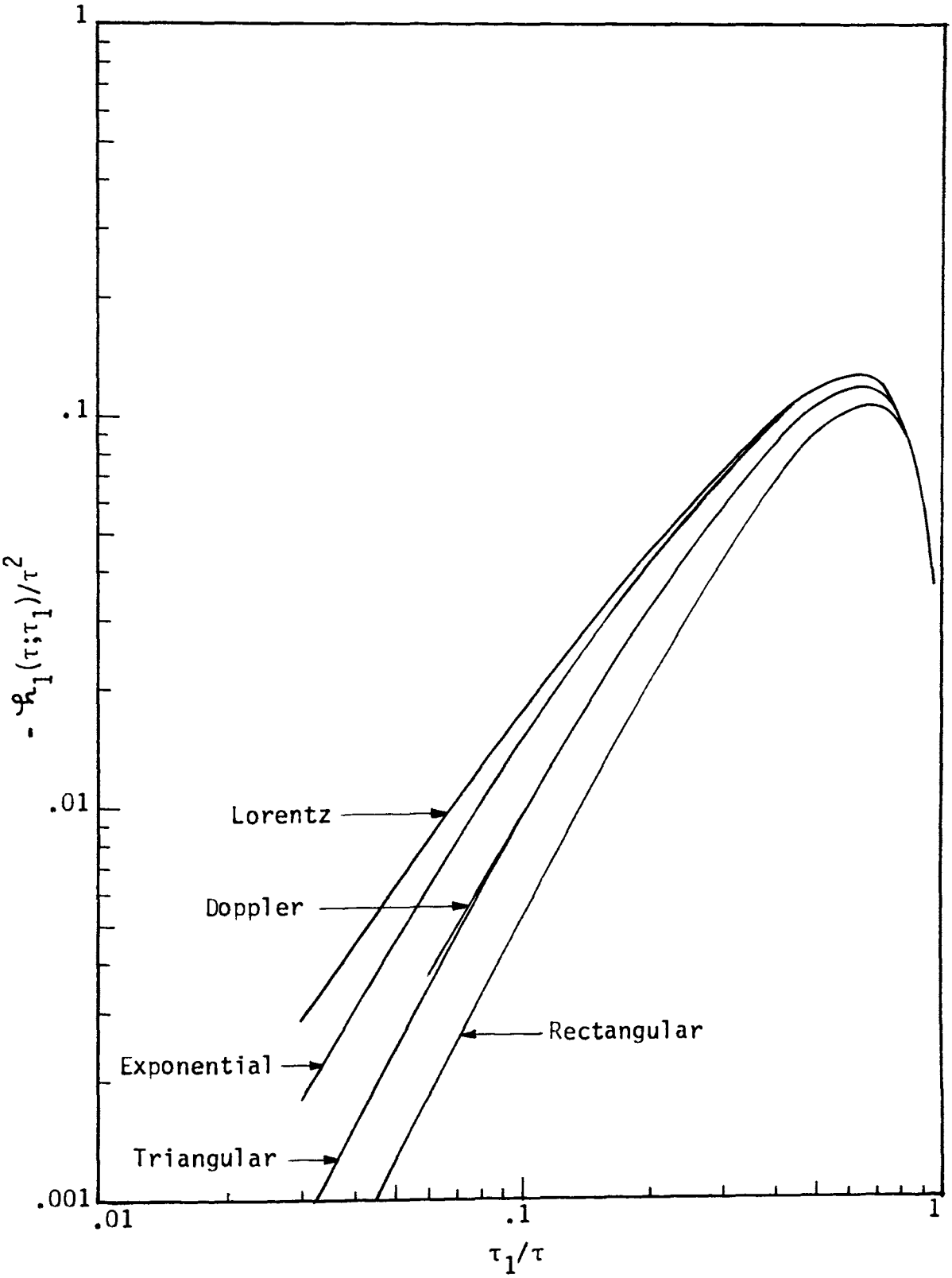

Figure 5.5 - Function $\mathcal{R}_1(\tau;\tau_1)/\tau^2$ versus τ_1/τ for $\tau_1 = 1$

Table 5.5

Values of the function $\mathcal{L}_1(\tau;\tau_1)/\tau^2$ for $\tau_1 = 5$

τ_1/τ	$-\mathcal{L}_1(\tau;\tau_1)/\tau^2$				
	Rectangular	Triangular	Exponential	Doppler	Lorentz
			(iv) τ_1=5.0		
0.15	1.1250D-2	2.1744D-2	4.4679D-2		6.8711D-2
0.20	2.0000D-2	3.8128D-2	7.2803D-2		1.0316D-1
0.30	4.5000D-2	8.3015D-2	1.4111D-1	8.8100D-2	1.7897D-1
0.40	7.9981D-2	1.4133D-1	2.1841D-1	1.4514D-1	2.5708D-1
0.50	1.2461D-1	2.0788D-1	2.9540D-1	2.0859D-1	3.2938D-1
0.60	1.7669D-1	2.7375D-1	3.6042D-1	2.7070D-1	3.8610D-1
0.70	2.2849D-1	3.2396D-1	3.9752D-1	3.1812D-1	4.1358D-1
0.80	2.6010D-1	3.3382D-1	3.8345D-1	3.2763D-1	3.9087D-1
0.90	2.2625D-1	2.6032D-1	2.8049D-1	2.5684D-1	2.8220D-1
0.95	1.5429D-1	1.6705D-1	1.7410D-1	1.6564D-1	1.7447D-1
1.00	0	0	0	0	0

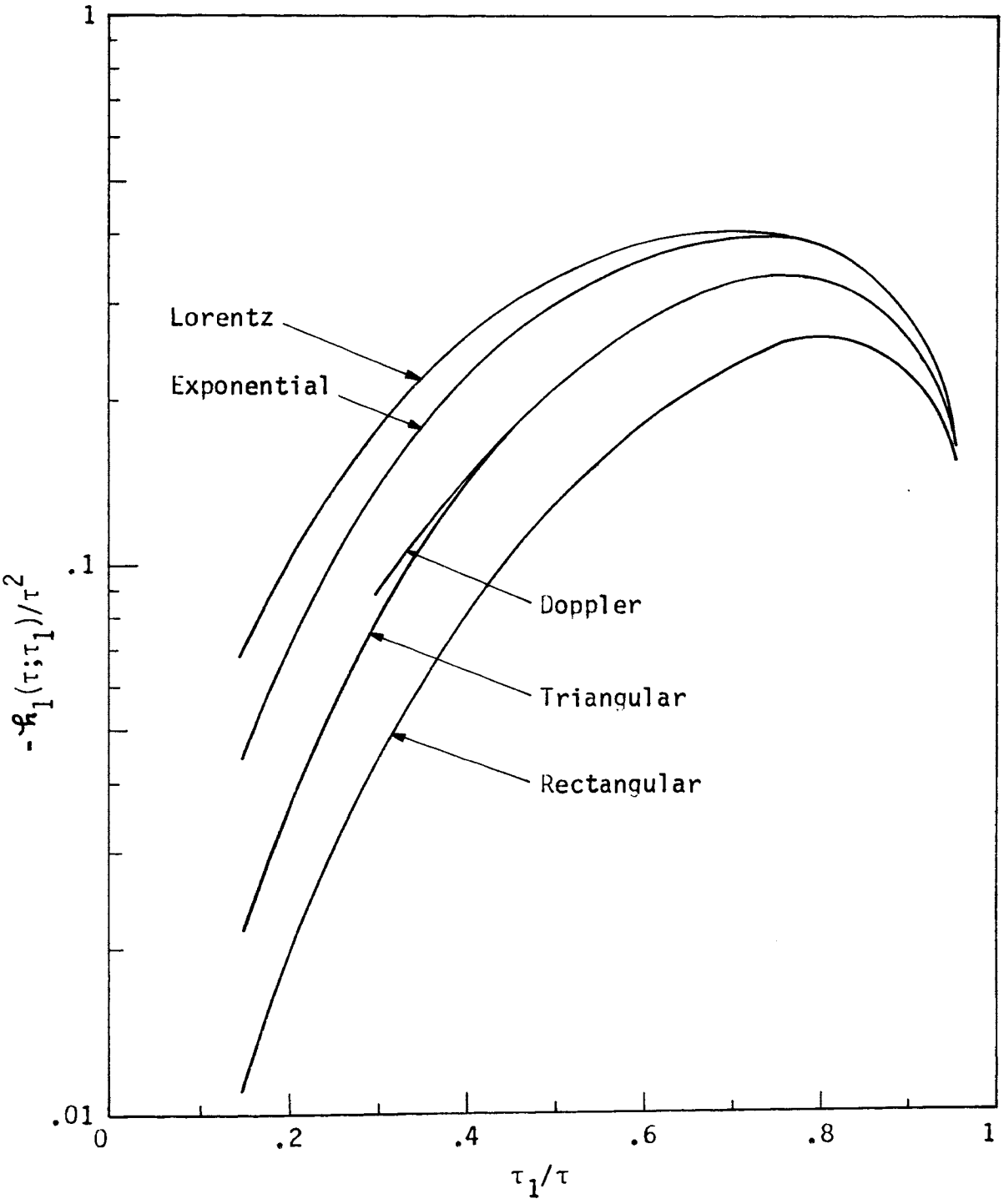

Figure 5.6 - Function $\mathcal{R}_1(\tau;\tau_1)/\tau^2$ versus τ_1/τ for $\tau_1 = 5$

2. Special Limiting Results

a. Optically Thin

By utilizing the asymptotic expansions for functions $K_3(\tau)$, $K_4(\tau)$ and $K_5(\tau)$ as $\tau \to 0$ (see Appendix B), function $\mathcal{h}_1(\tau;\tau_1)$ in the optically thin approximation becomes

$$\mathcal{h}_1(\tau;\tau_1) = -\frac{(\tau^3-\tau_1^3)}{3} + \frac{(\tau^2-\tau_1^2)^{3/2}}{3} \tag{5.27}$$

Inspection of equation (5.27) reveals that in the optically thin approximation, the function $\mathcal{h}_1(\tau;\tau_1)$ becomes independent of the shape of $\alpha(\nu)$. Comparison of equations (5.27) and (3.14) shows that relation (5.26) holds good for all the five profiles in the optically thin approximation. From equation (5.27) it is possible to deduce that

$$\lim_{\tau\to\tau_1} \mathcal{h}_1(\tau;\tau_1) = 0 \tag{5.28}$$

Substitution of $\tau = \tau_1$ in expression (5.16) leads to the same result as in (5.27), i.e. $\mathcal{h}_1(\tau=\tau_1;\tau_1) = 0$.

b. Optically Thick

By utilizing the approximate expressions for large τ for functions $K_3(\tau)$, $K_4(\tau)$ and $K_5(\tau)$ as $\tau \to \infty$ (see Appendix B), the expression (5.16) for the function $\mathcal{h}_1(\tau;\tau_1)$ in the optically thick limit becomes

(a) Rectangular profile

$$\mathcal{h}_1(\tau;\tau_1) = -\frac{\tau_1^2}{2} \tag{5.29a}$$

(b) Triangular profile

$$\mathcal{h}_1(\tau;\tau_1) = \frac{2}{3}\left[\frac{\tau\tau_1}{(\tau-\tau_1)} + (\tau-\tau_1) - (\tau^2-\tau_1^2)^{\frac{1}{2}}\right] - \tau_1^2 \quad (5.29b)$$

(c) Exponential profile

$$\mathcal{h}_1(\tau;\tau_1) = -\frac{\tau_1^2}{2}\{\gamma + \ln(\tau-\tau_1) + \ln[(\tau^2-\tau_1^2)^{\frac{1}{2}}]\} - \frac{\tau\tau_1}{4} \quad (5.29c)$$

Approximate results for the three profiles are presented in Table 5.6 along with the exact results. It is found that for the case when $\tau_1 = 0.01$, the error in using the optically thick expression is less than 5% in case of the rectangular profile for values of $\tau \geq 4$, and in case of the triangular profile for values of $\tau \geq 3$, while in case of the exponential profile the error is less than 5% for values of $\tau \geq 2$.

c. Small Sphere

Expansion of the function $\mathcal{h}_1(\tau;\tau_1)$ (5.16) in a Taylor's series about $\tau_1 = 0$ yields

$$\mathcal{h}_1(\tau;\tau_1) = \frac{\tau_1^2}{2}[2\,K_3(\tau) + \tau\,K_2(\tau)] + \frac{\tau_1^3}{3}[\tau\,K_1(\tau) + K_2(\tau)] \quad (5.30)$$

By comparing equation (5.30) with equation (3.16) of the gray analysis, one finds that equation (5.30) is similar to equation (3.16) with $E_n(\tau)$ functions replaced by $K_n(\tau)$ functions.

C. Isothermal Analysis: Function $\mathcal{h}_2(\tau;\tau_1,\tau_2)$

The study of the function $\mathcal{h}_2(\tau;\tau_1,\tau_2)$ is undertaken in this section. In order to give the function $\mathcal{h}_2(\tau;\tau_1,\tau_2)$ a physical

Table 5.6

Comparison of the exact and optically thick values of the function $\mathcal{H}_1(\tau;\tau_1)$ for $\tau_1 = 0.01$

τ	$-\mathcal{H}_1(\tau;\tau_1)$					
	Rectangular		Triangular		Exponential	
	Exact	Approximate	Exact	Approximate	Exact	Approximate
	(i) τ_1=0.01					
1	3.1482D-5	-2.2250D-5	3.6611D-5	-6.7423D-7	3.9618D-5	2.8525D-5
2	4.3188D-5	2.4305D-5	5.6667D-5	4.9832D-5	6.5819D-5	6.3351D-5
3	4.7494D-5	4.1486D-5	6.8267D-5	6.6592D-5	8.4338D-5	8.3680D-5
4	4.9078D-5	4.7208D-5	7.5420D-5	7.4958D-5	9.8283D-5	9.8092D-5
5	4.9661D-5	4.9079D-5	8.0109D-5	7.9973D-5	1.0932D-4	1.0927D-4
6	4.9875D-5	4.9693D-5	8.3356D-5	8.3315D-5	1.1841D-4	1.1839D-4
7	4.9954D-5	4.9897D-5	8.5714D-5	8.5701D-5	1.2611D-4	1.2611D-4
8	4.9983D-5	4.9965D-5	8.7494D-5	8.7490D-5	1.3279D-4	1.3279D-4
9	4.9994D-5	4.9988D-5	8.8882D-5	8.8881D-5	1.3869D-4	1.3868D-4
10	4.9998D-5	4.9996D-5	8.9994D-5	8.9993D-5	1.4396D-4	1.4396D-4

interpretation, consider the case described in Figure 3.6 of chapter three. The following cases are considered:

1. Exact Results

Numerical results are obtained by using expression (5.17) for four different values of τ_1 and three different ratios of the inner to outer optical radii. The function $\mathcal{h}_2(\tau;\tau_1,\tau_2)$ changes sign and in order to facilitate the drawing of the graphs, values of $\mathcal{h}_2(\tau;\tau_1,\tau_2) + \frac{\tau_1^2}{2}$ are shown tabulated in Tables 5.7 through 5.10.

Inspection of the results reveal that the values for the rectangular profile are always less than the values for the other four profiles. There is very little difference in the values for the triangular and Doppler profiles. It is only for the ratio $\tau_1/\tau_2 = 0.1$ that the results for the five different profiles are somewhat different. For large ratios of τ_1/τ_2, e.g. $\tau_1/\tau_2 = 0.5$ and 0.9, the results become independent of the shape of $\alpha(\nu)$.

The following relation for the rectangular profile always holds good:

$$\mathcal{h}_2(\tau;\tau_1,\tau_2) = h_2(\tau;\tau_1,\tau_2) + \frac{\tau_1^2}{2} \tag{5.31}$$

2. Special Limiting Results

a. Optically Thin

With the aid of the asymptotic expansions for functions $K_3(\tau)$, $K_4(\tau)$ and $K_5(\tau)$ as $\tau \to 0$, the function $\mathcal{h}_2(\tau;\tau_1,\tau_2)$ in the optically thin approximation becomes

Table 5.7

Values of the function $\mathcal{L}_2(\tau;\tau_1,\tau_2) + \tau_1^2/2$ for $\tau_1 = 0.01$

τ/τ_2	$\mathcal{L}_2(\tau;\tau_1,\tau_2) + \tau_1^2/2$				
	Rectangular	Triangular	Exponential	Doppler	Lorentz
			(a) τ_1/τ_2=0.1		
0.10	4.5556D-5	4.5487D-5	4.5452D-5	4.5495D-5	4.5452D-5
0.20	4.9245D-5	4.9298D-5	4.9326D-5	4.9292D-5	4.9327D-5
0.30	6.0271D-5	6.0688D-5	6.0902D-5	6.0639D-5	6.0905D-5
0.40	8.2246D-5	8.3372D-5	8.3949D-5	8.3238D-5	8.3956D-5
0.50	1.1888D-4	1.2115D-4	1.2232D-4	1.2088D-4	1.2233D-4
0.60	1.7398D-4	1.7790D-4	1.7991D-4	1.7743D-4	1.7993D-4
0.70	2.5143D-4	2.5753D-4	2.6066D-4	2.5681D-4	2.6070D-4
0.80	3.5531D-4	3.6410D-4	3.6861D-4	3.6306D-4	3.6867D-4
0.90	4.8993D-4	5.0182D-4	5.0792D-4	5.0041D-4	5.0800D-4
1.00	6.6018D-4	6.7528D-4	6.8303D-4	6.7349D-4	6.8313D-4
			(b) τ_1/τ_2=0.5		
0.50	4.9402D-5	4.9401D-5	4.9401D-5	4.9401D-5	4.9401D-5
0.60	4.9738D-5	4.9738D-5	4.9738D-5	4.9738D-5	4.9738D-5
0.70	5.0285D-5	5.0288D-5	5.0289D-5	5.0287D-5	5.0289D-5
0.80	5.1061D-5	5.1067D-5	5.1071D-5	5.1067D-5	5.1071D-5
0.90	5.2095D-5	5.2106D-5	5.2111D-5	5.2104D-5	5.2111D-5
0.95	5.2719D-5	5.2732D-5	5.2738D-5	5.2730D-5	5.2738D-5
1.00	5.3420D-5	5.3434D-5	5.3442D-5	5.3433D-5	5.3442D-5
			(c) τ_1/τ_2=0.9		
0.90	4.9914D-5	4.9914D-5	4.9914D-5	4.9914D-5	4.9914D-5
0.91	4.9926D-5	4.9926D-5	4.9926D-5	4.9926D-5	4.9926D-5
0.92	4.9940D-5	4.9940D-5	4.9940D-5	4.9940D-5	4.9940D-5
0.93	4.9954D-5	4.9954D-5	4.9954D-5	4.9954D-5	4.9954D-5
0.94	4.9969D-5	4.9969D-5	4.9970D-5	4.9969D-5	4.9970D-5
0.95	4.9985D-5	4.9985D-5	4.9985D-5	4.9985D-5	4.9985D-5
0.96	5.0002D-5	5.0002D-5	5.0002D-5	5.0002D-5	5.0002D-5
0.97	5.0019D-5	5.0019D-5	5.0020D-5	5.0019D-5	5.0020D-5
0.98	5.0037D-5	5.0038D-5	5.0038D-5	5.0038D-5	5.0038D-5
0.99	5.0056D-5	5.0056D-5	5.0056D-5	5.0056D-5	5.0056D-5
1.00	5.0075D-5	5.0076D-5	5.0076D-5	5.0076D-5	5.0076D-5

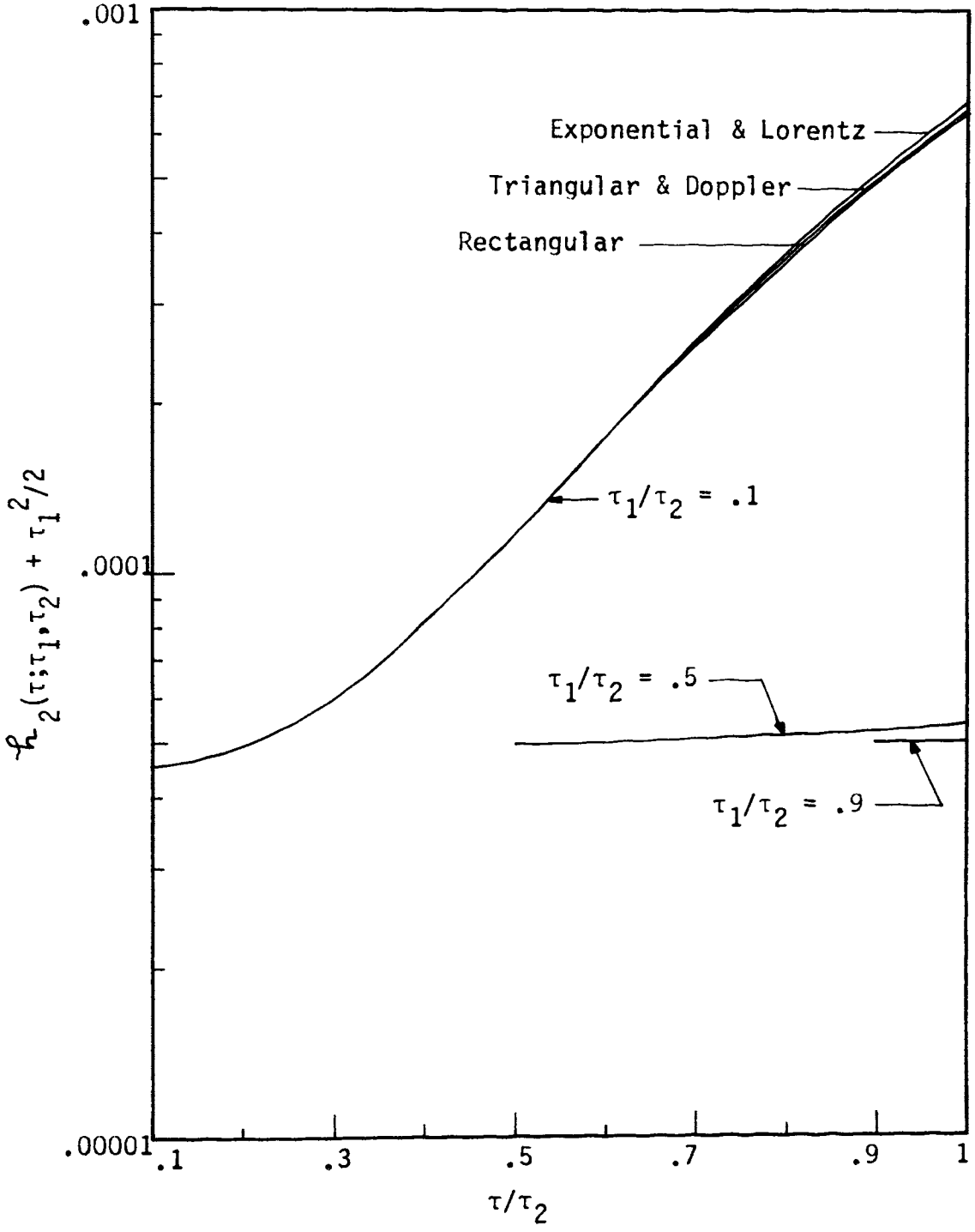

Figure 5.7 - Function $\mathcal{h}_2(\tau;\tau_1,\tau_2) + \tau_1^2/2$ versus τ/τ_2 for $\tau_1 = 0.01$

Table 5.8

Values of the function $\mathcal{R}_2(\tau;\tau_1,\tau_2) + \tau_1^2/2$ for $\tau_1 = 0.1$

τ/τ_2	$\mathcal{R}_2(\tau;\tau_1,\tau_2) + \tau_1^2/2$				
	Rectangular	Triangular	Exponential	Doppler	Lorentz
			(a) τ_1/τ_2=0.1		
0.10	1.9716D-3	1.5083D-3	1.2392D-3	1.5567D-3	1.2191D-3
0.20	3.5155D-3	3.6974D-3	3.8420D-3	3.6868D-3	3.8722D-3
0.30	8.1825D-3	1.0277D-2	1.1648D-2	1.0091D-2	1.1827D-2
0.40	1.7725D-2	2.3564D-2	2.7331D-2	2.3035D-2	2.7802D-2
0.50	3.4238D-2	4.6154D-2	5.3799D-2	4.5065D-2	5.4734D-2
0.60	6.0304D-2	8.1014D-2	9.4248D-2	7.9111D-2	9.5847D-2
0.70	9.9256D-2	1.3167D-1	1.5231D-1	1.2867D-1	1.5478D-1
0.80	1.5561D-1	2.0249D-1	2.3227D-1	1.9815D-1	2.3581D-1
0.90	2.3598D-1	2.9935D-1	3.3956D-1	2.9347D-1	3.4434D-1
1.00	3.5218D-1	4.3166D-1	4.8230D-1	4.2434D-1	4.8843D-1
			(b) τ_1/τ_2=0.5		
0.50	4.4340D-3	4.4225D-3	4.4166D-3	4.4239D-3	4.4166D-3
0.60	4.7290D-3	4.7319D-3	4.7335D-3	4.7315D-3	4.7336D-3
0.70	5.2115D-3	5.2376D-3	5.2512D-3	5.2345D-3	5.2516D-3
0.80	5.9019D-3	5.9587D-3	5.9884D-3	5.9521D-3	5.9891D-3
0.90	6.8341D-3	6.9274D-3	6.9762D-3	6.9165D-3	6.9773D-3
0.95	7.4040D-3	7.5165D-3	7.5754D-3	7.5034D-3	7.5767D-3
1.00	8.0528D-3	8.1837D-3	8.2522D-3	8.1685D-3	8.2538D-3
			(c) τ_1/τ_2=0.9		
0.90	4.9148D-3	4.9145D-3	4.9144D-3	4.9145D-3	4.9144D-3
0.91	4.9268D-3	4.9267D-3	4.9266D-3	4.9267D-3	4.9266D-3
0.92	4.9400D-3	4.9400D-3	4.9399D-3	4.9400D-3	4.9399D-3
0.93	4.9541D-3	4.9542D-3	4.9542D-3	4.9542D-3	4.9542D-3
0.94	4.9690D-3	4.9692D-3	4.9693D-3	4.9692D-3	4.9693D-3
0.95	4.9846D-3	4.9849D-3	4.9851D-3	4.9849D-3	4.9851D-3
0.96	5.0009D-3	5.0013D-3	5.0016D-3	5.0013D-3	5.0016D-3
0.97	5.0179D-3	5.0185D-3	5.0188D-3	5.0184D-3	5.0188D-3
0.98	5.0356D-3	5.0363D-3	5.0366D-3	5.0362D-3	5.0366D-3
0.99	5.0540D-3	5.0548D-3	5.0552D-3	5.0547D-3	5.0552D-3
1.00	5.0731D-3	5.0739D-3	5.0744D-3	5.0738D-3	5.0744D-3

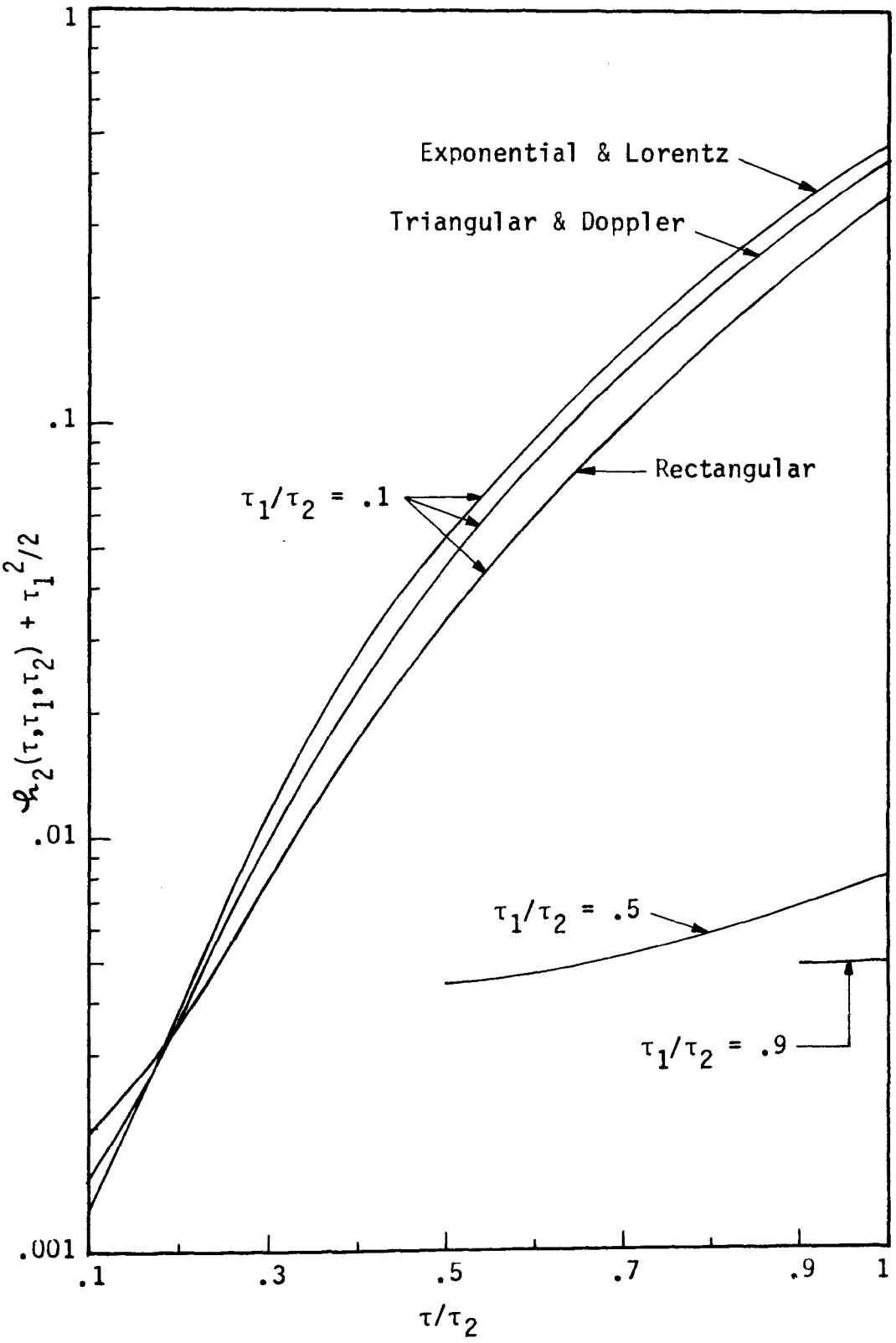

Figure 5.8 - Function $\mathcal{L}_2(\tau;\tau_1,\tau_2) + \tau_1^2/2$ versus τ/τ_2 for $\tau_1 = 0.1$

Table 5.9

Values of the function $\Phi_2(\tau;\tau_1,\tau_2) + \tau_1^2/2$ for $\tau_1 = 1$

τ/τ_2	$\Phi_2(\tau;\tau_1,\tau_2) + \tau_1^2/2$				
	Rectangular	Triangular	Exponential	Doppler	Lorentz
			(a) τ_1/τ_2=0.1		
0.10	4.6408D-5				
0.20	3.8466D-4				
0.30	2.1407D-3		8.0173D-1	1.9947D-1	1.8792D+0
0.40	9.6109D-3	5.8480D-1	3.4654D+0	1.1880D+0	6.5317D+0
0.50	3.9271D-2	1.7750D+0	8.1854D+0	2.9916D+0	1.4515D+1
0.60	1.5383D-1	3.9944D+0	1.5933D+1	6.1039D+0	2.7045D+1
0.70	5.9545D-1	8.1820D+0	2.8272D+1	1.1514D+1	4.5824D+1
0.80	2.3393D+0	1.6560D+1	4.8120D+1	2.1611D+1	7.3685D+1
0.90	9.7158D+0	3.5360D+1	8.2091D+1	4.3375D+1	1.1667D+2
1.00	4.9750D+1	9.0050D+1	1.5249D+2	1.0559D+2	1.9544D+2
			(b) τ_1/τ_2=0.5		
0.50	1.5207D-1	8.3477D-2	4.1748D-2	9.0235D-2	3.7670D-2
0.60	2.3935D-1	2.2673D-1	2.2559D-1	2.2943D-1	2.2890D-1
0.70	3.9390D-1	4.6949D-1	5.3243D-1	4.6585D-1	5.4760D-1
0.80	6.4896D-1	8.4254D-1	9.9040D-1	8.3025D-1	1.0211D+0
0.90	1.0667D+0	1.4007D+0	1.6487D+0	1.3780D+0	1.6977D+0
0.95	1.3723D+0	1.7780D+0	2.0775D+0	1.7501D+0	2.1361D+0
1.00	1.7849D+0	2.2523D+0	2.5980D+0	2.2203D+0	2.6662D+0
			(c) τ_1/τ_2=0.9		
0.90	4.2177D-1	4.1926D-1	4.1796D-1	4.1956D-1	4.1794D-1
0.91	4.3149D-1	4.2979D-1	4.2893D-1	4.3000D-1	4.2892D-1
0.92	4.4212D-1	4.4131D-1	4.4093D-1	4.4141D-1	4.4094D-1
0.93	4.5349D-1	4.5362D-1	4.5375D-1	4.5361D-1	4.5378D-1
0.94	4.6557D-1	4.6665D-1	4.6731D-1	4.6655D-1	4.6737D-1
0.95	4.7836D-1	4.8041D-1	4.8160D-1	4.8019D-1	4.8168D-1
0.96	4.9188D-1	4.9488D-1	4.9660D-1	4.9456D-1	4.9671D-1
0.97	5.0615D-1	5.1009D-1	5.1232D-1	5.0966D-1	5.1246D-1
0.98	5.2123D-1	5.2605D-1	5.2877D-1	5.2553D-1	5.2894D-1
0.99	5.3717D-1	5.4281D-1	5.4599D-1	5.4220D-1	5.4618D-1
1.00	5.5411D-1	5.6045D-1	5.6403D-1	5.5976D-1	5.6426D-1

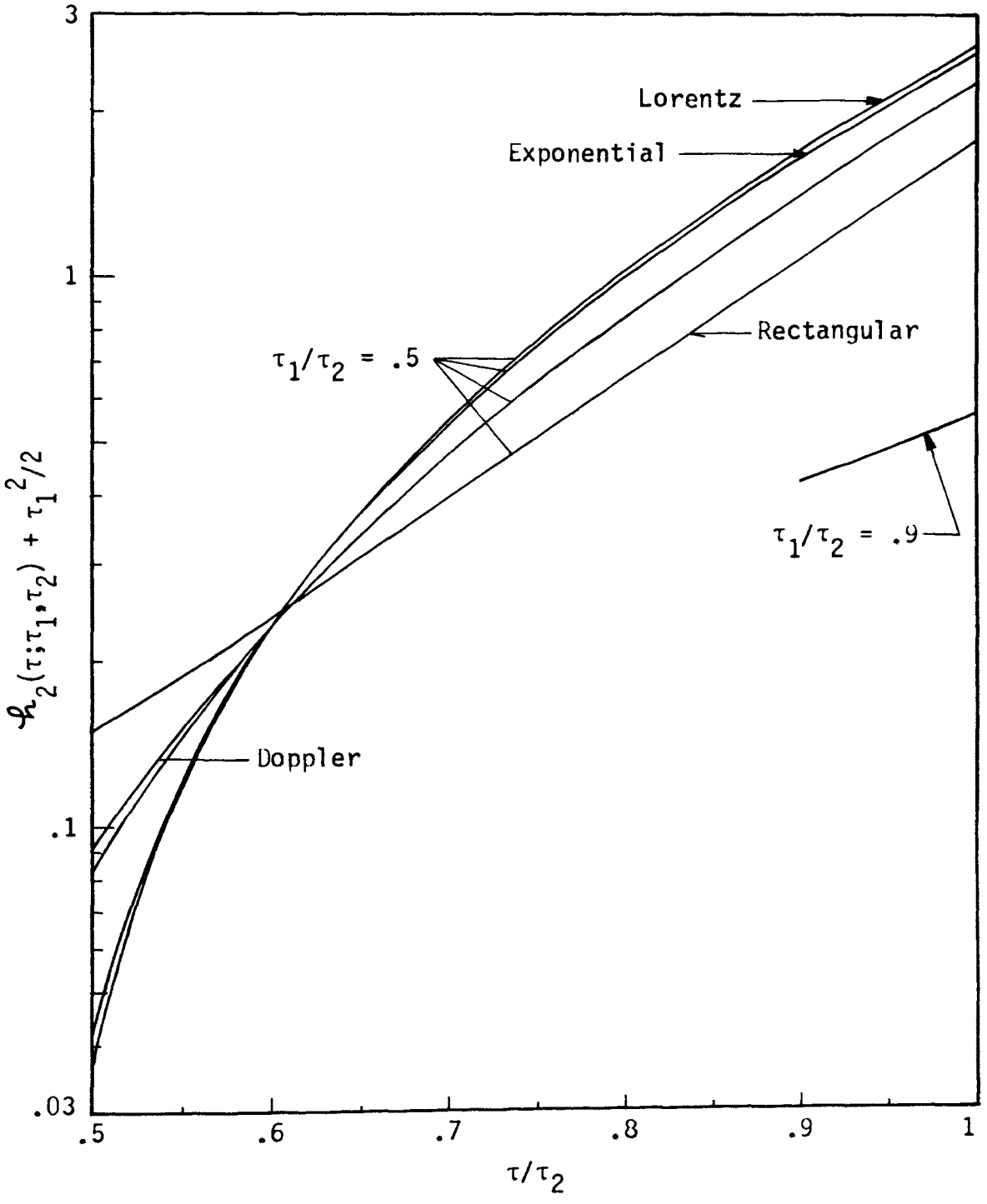

Figure 5.9 - Function $\mathcal{h}_2(\tau;\tau_1,\tau_2) + \tau_1^2/2$ versus τ/τ_2 for $\tau_1 = 1$

Table 5.10

Values of the function $\mathcal{L}_2(\tau;\tau_1,\tau_2) + \tau_1^2/2$ for $\tau_1 = 5$

τ/τ_2	$\mathcal{L}_2(\tau;\tau_1,\tau_2) + \tau_1^2/2$				
	Rectangular	Triangular	Exponential	Doppler	Lorentz
			(b) τ_1/τ_2=0.5		
0.50	3.9404D-2				
0.60	1.5385D-1				
0.70	5.9546D-1		6.4128D-1		5.7913D+0
0.80	2.3393D+0	6.0230D+0	1.9610D+1	8.5540D+0	3.1651D+1
0.90	9.7158D+0	2.4730D+1	5.2792D+1	2.8048D+1	7.2779D+1
0.95	2.0839D+1	4.3597D+1	7.9831D+1	4.7076D+1	1.0374D+2
1.00	4.9750D+1	7.9340D+1	1.2247D+2	8.3003D+1	1.4979D+2
			(c) τ_1/τ_2=0.9		
0.90	5.5170D+0	4.4655D+0	3.8430D+0	4.5727D+0	3.7901D+0
0.91	6.0492D+0	5.2294D+0	4.7692D+0	5.3187D+0	4.7439D+0
0.92	6.6458D+0	6.0722D+0	5.7871D+0	6.1430D+0	5.7931D+0
0.93	7.3124D+0	6.9923D+0	6.8882D+0	7.0443D+0	6.9275D+0
0.94	8.0581D+0	7.9950D+0	8.0746D+0	8.0281D+0	8.1481D+0
0.95	8.8945D+0	9.0880D+0	9.3510D+0	9.1022D+0	9.4590D+0
0.96	9.8363D+0	1.0282D+1	1.0725D+1	1.0277D+1	1.0867D+1
0.97	1.0903D+1	1.1589D+1	1.2206D+1	1.1568D+1	1.2382D+1
0.98	1.2119D+1	1.3029D+1	1.3808D+1	1.2992D+1	1.4017D+1
0.99	1.3524D+1	1.4629D+1	1.5552D+1	1.4578D+1	1.5792D+1
1.00	1.5194D+1	1.6439D+1	1.7475D+1	1.6381D+1	1.7745D+1

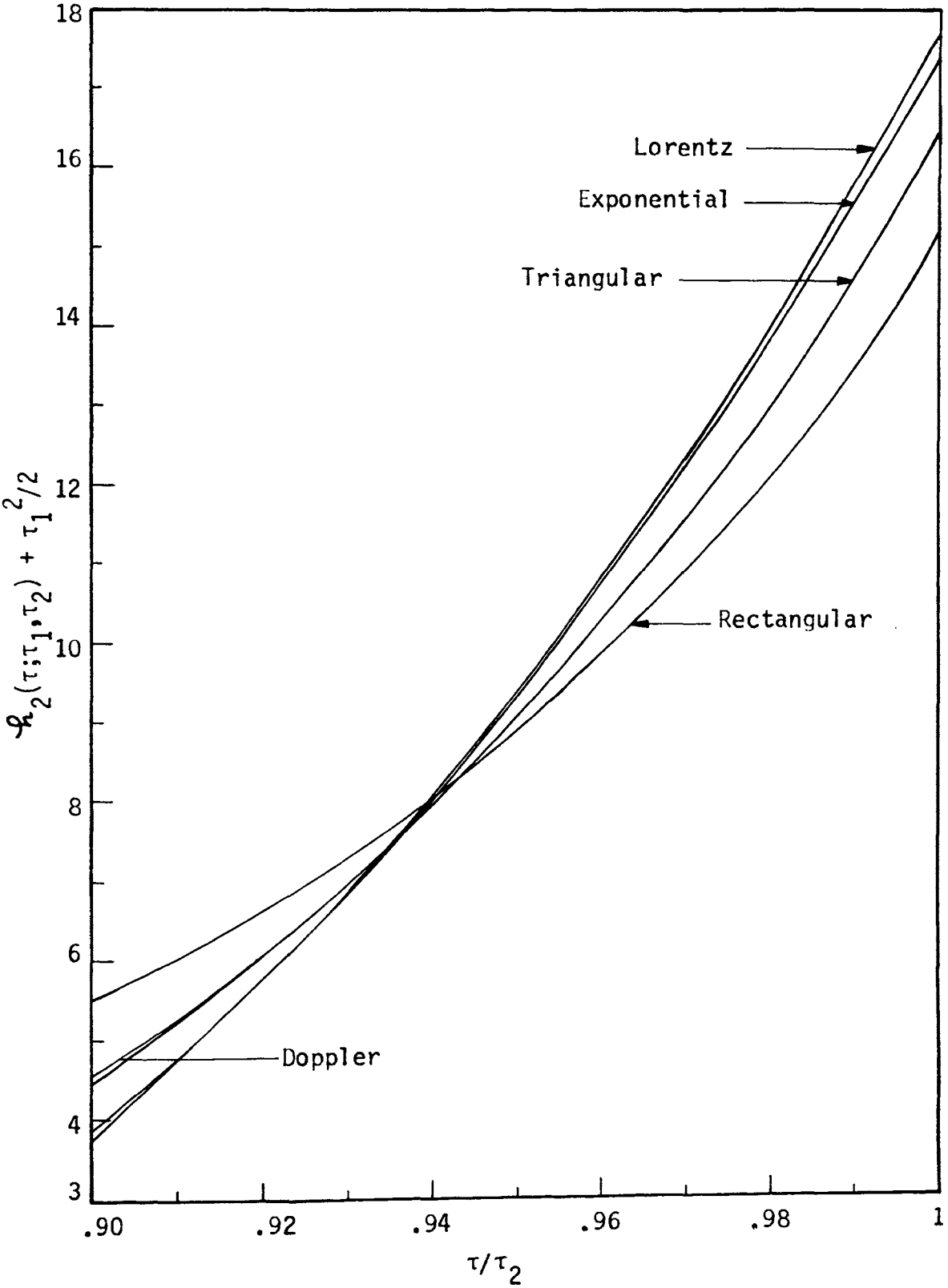

Figure 5.10 - Function $\mathcal{L}_2(\tau;\tau_1,\tau_2) + \tau_1^2/2$ versus τ/τ_2 for $\tau_1 = 5$

$$\mathcal{h}_2(\tau;\tau_1,\tau_2) = -\frac{(\tau_2^3-\tau^3)}{3} + \frac{(\tau_2^2-\tau_1^2)^{3/2}}{3} + \frac{(\tau^2-\tau_1^2)^{3/2}}{3} \qquad (5.32)$$

Examination of expression (5.32) shows that in the optically thin approximation, the function $\mathcal{h}_2(\tau;\tau_1,\tau_2)$ becomes independent of the shape of the absorption coefficient. Comparison of equations (5.29) and (3.19) reveals that relation (5.31) holds good for all the five profiles in the optically thin approximation. From equation (5.32) one observes that

$$\lim_{\substack{\tau\to\tau_1 \\ \tau_2\to\tau_1}} \mathcal{h}_2(\tau;\tau_1,\tau_2) = 0 \qquad (5.33)$$

The limits of expressions for the function $\mathcal{h}_1(\tau;\tau_1)$ and $\mathcal{h}_2(\tau;\tau_1,\tau_2)$ in the optically thin approximation tend to the same value, 0.

b. Function $\mathcal{h}_2(\tau;\tau_1,\tau_2)$ evaluated at $\tau = \tau_1$

This case is studied in order to gain some idea about the variation of the flux at the inner boundary. The following relation exist for the functions $\mathcal{h}_1(\tau;\tau_1)$ and $\mathcal{h}_2(\tau;\tau_1,\tau_2)$:

$$\mathcal{h}_2(\tau=\tau_1;\tau_1,\tau_2) = \mathcal{h}_1(\tau=\tau_2;\tau_1) \qquad (5.34)$$

Expansion of the function $\mathcal{h}_2(\tau=\tau_1;\tau_1,\tau_2)$ in a Taylor's series about $\tau_1 = 0$ yields

$$\mathcal{h}_2(\tau=\tau_1;\tau_1,\tau_2) = \frac{\tau_1^2}{2}\,[2\,K_3(\tau_2) + \tau_2\,K_2(\tau)] + \frac{\tau_1^3}{3}\,[\tau_2\,K_1(\tau_2) + K_2(\tau_2)] \qquad (5.35)$$

Comparison of expressions (5.30) and (5.35) reveal similarity.

c. Function $\mathcal{h}_2(\tau;\tau_1,\tau_2)$ evaluated at $\tau = \tau_2$

For this case, the expression (5.17) reduces to

$$\mathcal{h}_2(\tau=\tau_2;\tau_1,\tau_2) = (\tau_2^2-\tau_1^2)K_3[2(\tau_2^2-\tau_1^2)^{\frac{1}{2}}] + 2(\tau_2^2-\tau_1^2)^{\frac{1}{2}}K_4[2(\tau_2^2-\tau_1^2)^{\frac{1}{2}}] + K_5[2(\tau_2^2-\tau_1^2)^{\frac{1}{2}}] \quad (5.36)$$

From equation (5.36) we find that

$$\lim_{\tau_2 \to \tau_1} \mathcal{h}_2(\tau=\tau_2;\tau_1,\tau_2) = 0 \quad (5.37)$$

Results obtained are tabulated in Tables 5.11 through 5.14 and presented graphically in Figures 5.11 through 5.14. The results reveal that the values for the rectangular profile are always less than the values for the other four profiles. The values for the triangular and Doppler profiles are more or less identical. For the case when $\tau_1 = 5$, the results break down around $\tau_1/\tau_2 = 0.2$.

D. Case of Radiative Equilibrium

1. Formulation

Under the conditions of radiative equilibrium we know from equation (4.32) that

$$\frac{d[\tau^2 \mathcal{G}_r(\tau)]}{d\tau} = 0$$

Upon differentiating equation (5.15) and making use of the fact that

$$\frac{d[\mathcal{h}_1(\tau;\tau_1)]}{d\tau} = -\tau \mathcal{g}_1(\tau;\tau_1) \quad (5.38)$$

$$\frac{d[\mathcal{h}_2(\tau;\tau_1,\tau_2)]}{d\tau} = \tau \mathcal{g}_2(\tau;\tau_1,\tau_2) \quad (5.39)$$

Table 5.11

Values of the function $\mathcal{L}_2(\tau=\tau_2;\tau_1,\tau_2)/\tau_2^2$ for $\tau_1 = 0.01$

τ_1/τ_2	$\mathcal{L}_2(\tau=\tau_2;\tau_1,\tau_2)/\tau_2^2$				
	Rectangular	Triangular	Exponential	Doppler	Lorentz
			(i) τ_1=0.01		
0.01	3.5146D-1	4.3228D-1	4.8381D-1	4.2484D-1	4.9008D-1
0.02	2.3563D-1	2.6409D-1	2.8026D-1	2.6104D-1	2.8129D-1
0.03	1.7510D-1	1.8938D-1	1.9717D-1	1.8778D-1	1.9750D-1
0.04	1.3887D-1	1.4741D-1	1.5197D-1	1.4644D-1	1.5212D-1
0.05	1.1489D-1	1.2056D-1	1.2355D-1	1.1990D-1	1.2363D-1
0.06	9.7866D-2	1.0190D-1	1.0400D-1	1.0143D-1	1.0405D-1
0.07	8.5159D-2	8.8169D-2	8.9732D-2	8.7816D-2	8.9761D-2
0.08	7.5309D-2	7.7639D-2	7.8843D-2	7.7364D-2	7.8862D-2
0.09	6.7445D-2	6.9300D-2	7.0255D-2	6.9080D-2	7.0269D-2
0.10	6.1018D-2	6.2528D-2	6.3303D-2	6.2349D-2	6.3313D-2
0.20	3.0231D-2	3.0600D-2	3.0787D-2	3.0556D-2	3.0789D-2
0.30	1.8838D-2	1.8988D-2	1.9063D-2	1.8970D-2	1.9064D-2
0.40	1.2613D-2	1.2686D-2	1.2722D-2	1.2677D-2	1.2722D-2
0.50	8.5488D-3	8.5858D-3	8.6043D-3	8.5813D-3	8.6044D-3
0.60	5.6324D-3	5.6512D-3	5.6606D-3	5.6489D-3	5.6606D-3
0.70	3.4423D-3	3.4511D-3	3.4555D-3	3.4500D-3	3.4555D-3
0.80	1.7899D-3	1.7933D-3	1.7950D-3	1.7929D-3	1.7950D-3
0.90	6.1125D-4	6.1199D-4	6.1236D-4	6.1190D-4	6.1236D-4
1.00	0	0	0	0	0

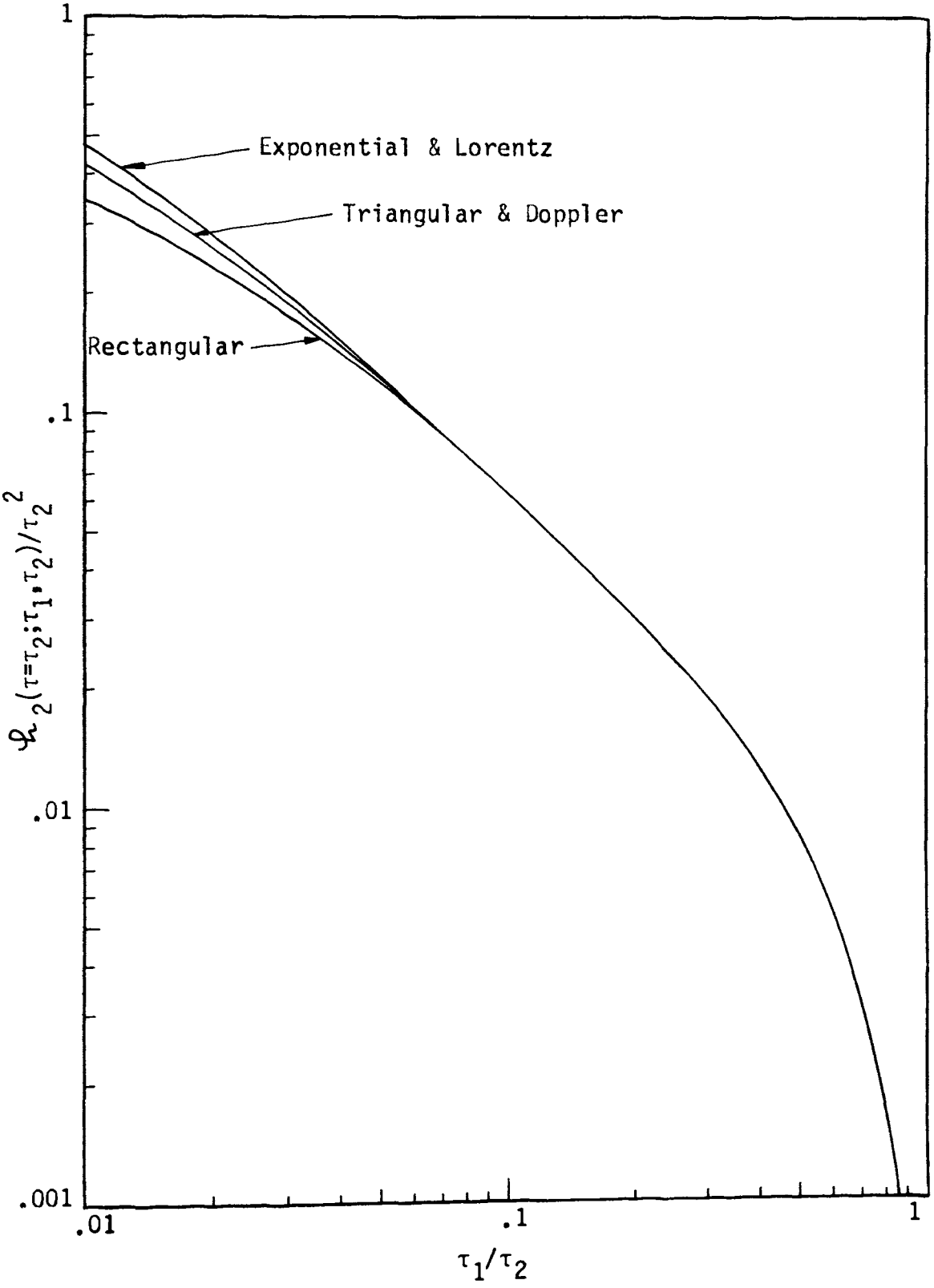

Figure 5.11 - Function $\mathcal{L}_2(\tau=\tau_2;\tau_1,\tau_2)/\tau_2^2$ versus τ_1/τ_2 for $\tau_1 = 0.01$

Table 5.12

Values of the function $\mathcal{L}_2(\tau=\tau_2;\tau_1,\tau_2)/\tau_2^2$ for $\tau_1 = 0.1$

τ_1/τ_2	$\mathcal{L}_2(\tau=\tau_2;\tau_1,\tau_2)/\tau_2^2$				
	Rectangular	Triangular	Exponential	Doppler	Lorentz
			(ii) τ_1=0.1		
0.01	4.9745D-1	9.0491D-1	1.5375D+0	1.0744D+0	1.9740D+0
0.02	4.8981D-1	8.1964D-1	1.1943D+0	8.2989D-1	1.3614D+0
0.03	4.7727D-1	7.4418D-1	9.9728D-1	7.3957D-1	1.0817D+0
0.04	4.6082D-1	6.7818D-1	8.6134D-1	6.6869D-1	9.1024D-1
0.05	4.4200D-1	6.2082D-1	7.5957D-1	6.1012D-1	7.9045D-1
0.06	4.2218D-1	5.7102D-1	6.7971D-1	5.6049D-1	7.0044D-1
0.07	4.0233D-1	5.2765D-1	6.1501D-1	5.1782D-1	6.2959D-1
0.08	3.8303D-1	4.8969D-1	5.6137D-1	4.80710D-1	5.7200D-1
0.09	3.6460D-1	4.5627D-1	5.1609D-1	4.4814D-1	5.2407D-1
0.10	3.4718D-1	4.2666D-1	4.7730D-1	4.1934D-1	4.8343D-1
0.20	2.2319D-1	2.4963D-1	2.6462D-1	2.4679D-1	2.6555D-1
0.30	1.5377D-1	1.6576D-1	1.7227D-1	1.6441D-1	1.7254D-1
0.40	1.0872D-1	1.1486D-1	1.1812D-1	1.1416D-1	1.1822D-1
0.50	7.6321D-2	7.9594D-2	8.1306D-2	7.9212D-2	8.1345D-2
0.60	5.1583D-2	5.3290D-2	5.4174D-2	5.3089D-2	5.4189D-2
0.70	3.2171D-2	3.2987D-2	3.3407D-2	3.2891D-2	3.3412D-2
0.80	1.7027D-2	1.7345D-2	1.7507D-2	1.7307D-2	1.7509D-2
0.90	5.9175D-3	5.9890D-3	6.0252D-3	5.9804D-3	6.0254D-3
1.00	0	0	0	0	0

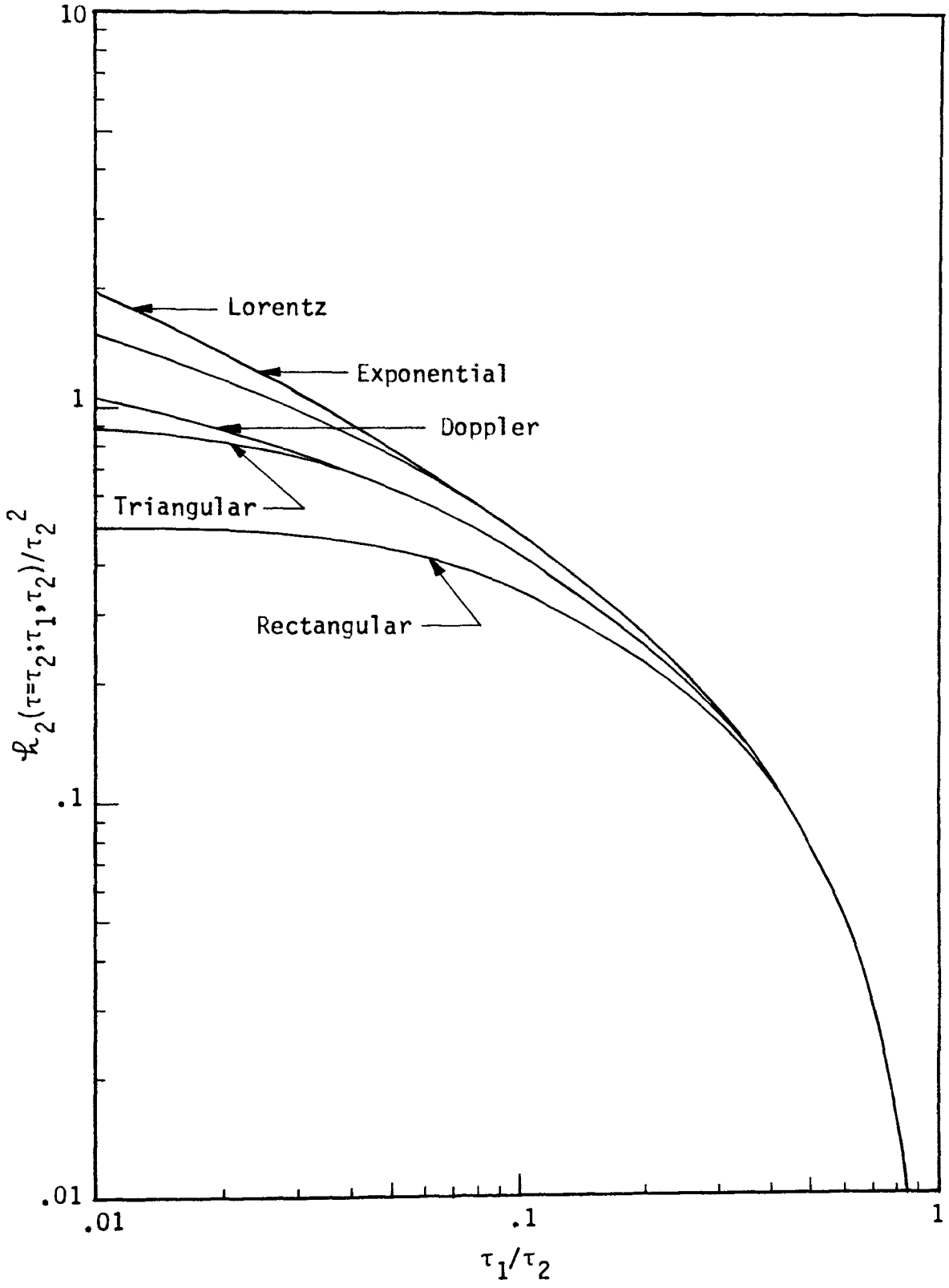

Figure 5.12 - Function $\mathcal{R}_2(\tau=\tau_2;\tau_1,\tau_2)/\tau_2^2$ versus τ_1/τ_2 for $\tau_1 = 0.1$

Table 5.13

Values of the function $\mathcal{L}_2(\tau=\tau_2;\tau_1,\tau_2)/\tau_2^2$ for $\tau_1 = 1$

τ_1/τ_2	$\mathcal{L}_2(\tau=\tau_2;\tau_1,\tau_2)/\tau_2^2$				
	Rectangular	Triangular	Exponential	Doppler	Lorentz
			(iii) τ_1=1.0		
0.1	0.492500	0.895501	1.519872	1.050884	1.949365
0.2	0.470006	0.784040	1.137507	0.792945	1.292922
0.3	0.432786	0.668740	0.888082	0.663551	0.958711
0.4	0.382284	0.552576	0.691428	0.544006	0.726009
0.5	0.321233	0.438075	0.524492	0.430070	0.541553
0.6	0.252930	0.327493	0.378519	0.321423	0.386551
0.7	0.180909	0.223256	0.250382	0.219387	0.253742
0.8	0.109252	0.128598	0.140260	0.126669	0.141349
0.9	0.043827	0.048962	0.051868	0.048409	0.052048
1.0	0	0	0	0	0

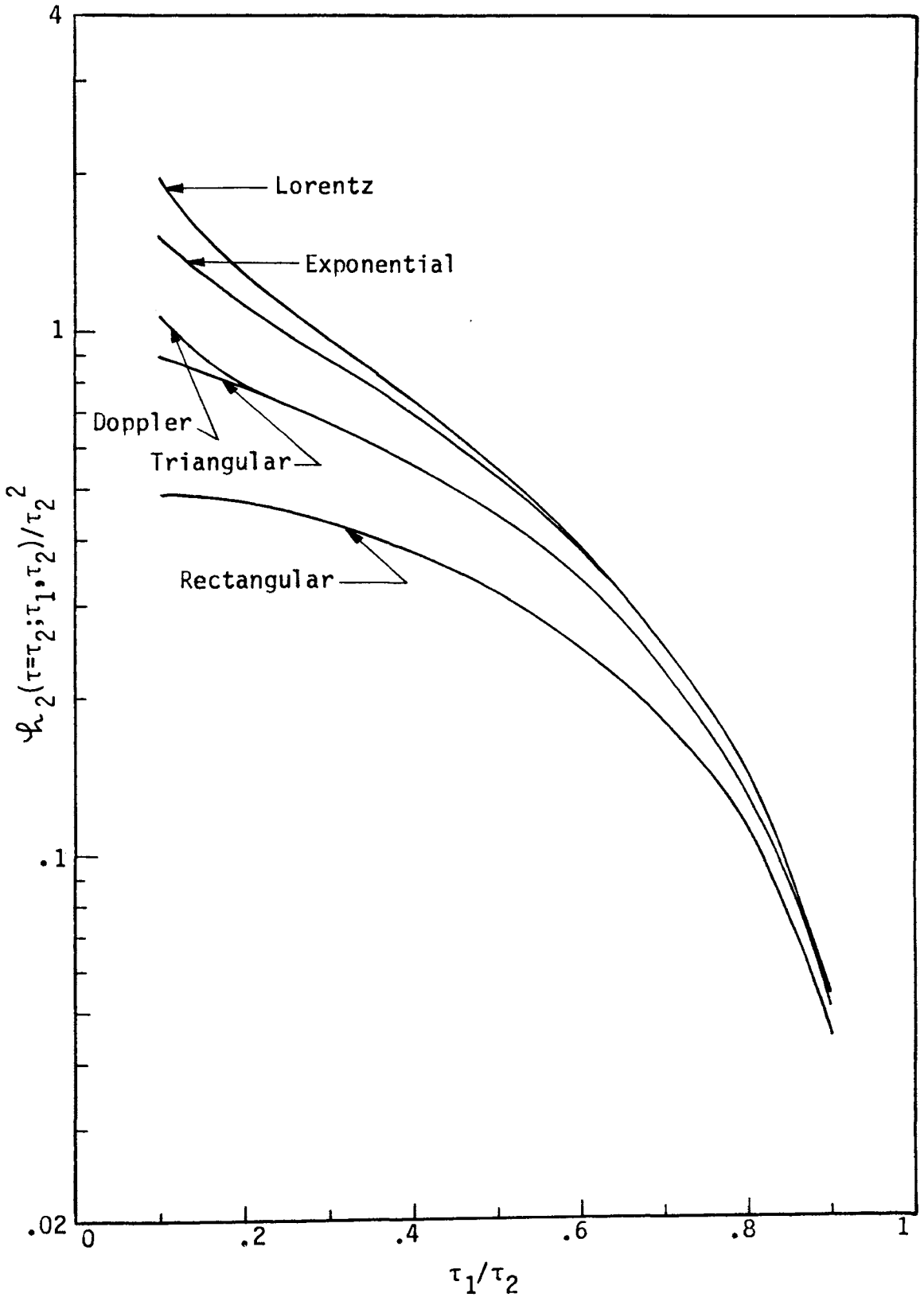

Figure 5.13 - Function $\mathcal{h}_2(\tau=\tau_2;\tau_1,\tau_2)/\tau_2^2$ versus τ_1/τ_2 for $\tau_1 = 1$

Table 5.14

Values of the function $\mathcal{L}_2(\tau=\tau_2;\tau_1,\tau_2)/\tau_2^2$ for $\tau_1 = 5$

τ_1/τ_2	$\mathcal{L}_2(\tau=\tau_2;\tau_1,\tau_2)/\tau_2^2$				
	Rectangular	Triangular	Exponential	Doppler	Lorentz
			(iv) τ_1=5.0		
0.1					
0.2					
0.3	0.454098	0.854565	1.609612		2.284717
0.4	0.418400	0.769879	1.348544	2.853524	1.780291
0.5	0.372500	0.668397	1.099665	0.705034	1.372898
0.6	0.316400	0.551200	0.855395	0.568301	1.019321
0.7	0.250102	0.419820	0.614400	0.425559	0.702343
0.8	0.173630	0.276793	0.379778	0.276323	0.417264
0.9	0.087273	0.127612	0.161200	0.125752	0.169947
1.0	0	0	0	0	0

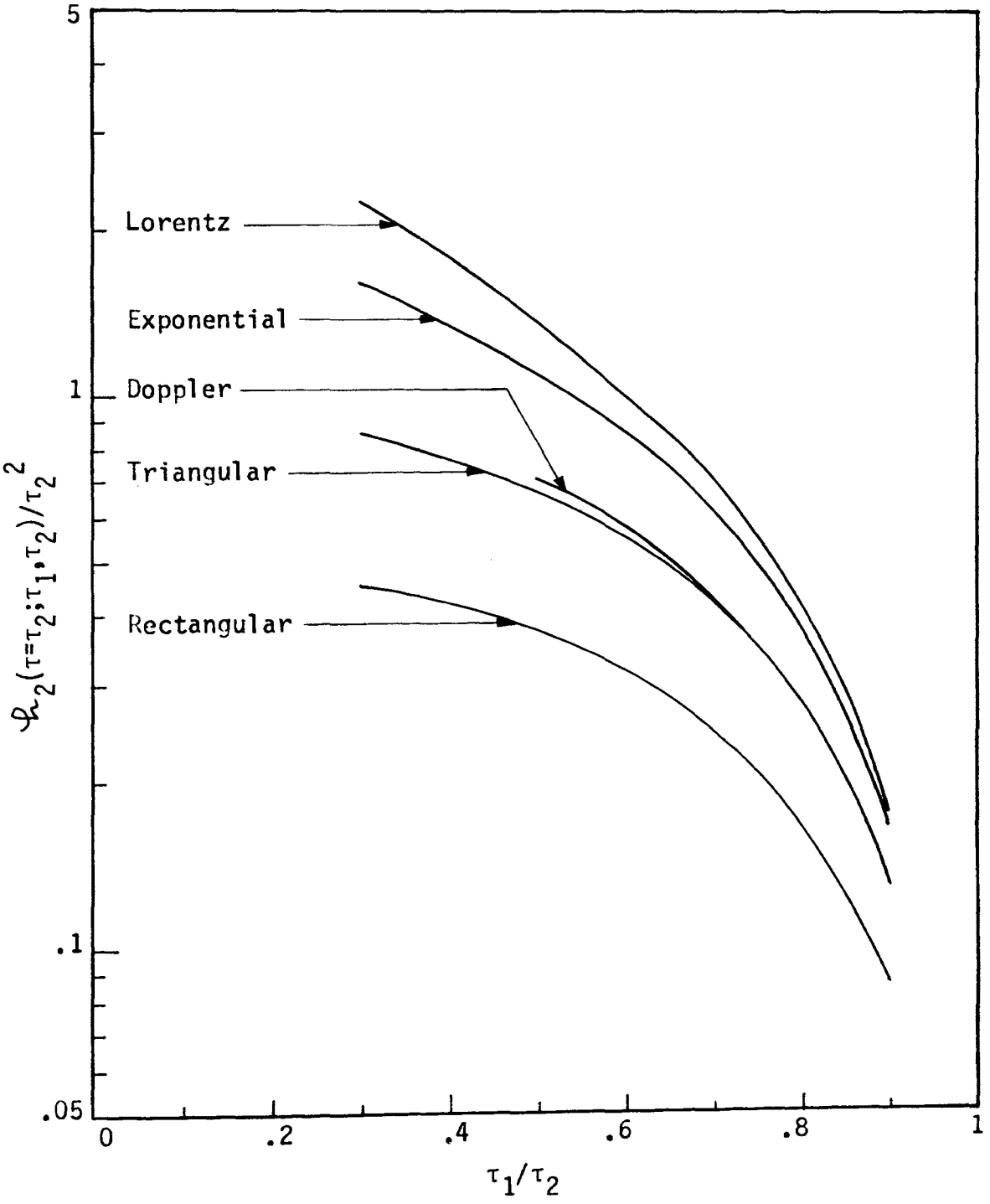

Figure 5.14 - Function $\mathcal{h}_2(\tau=\tau_2;\tau_1,\tau_2)/\tau_2^2$ versus τ_1/τ_2 for $\tau_1 = 5$

$$\frac{d}{d\tau}\int_{\tau_1}^{\tau_2} \mathcal{H}(\tau,t;\tau_1)\psi(t)\,dt = 2\,\tau^2\psi(\tau) - \tau\int_{\tau_1}^{\tau_2} \mathcal{K}(\tau,t;\tau_1)\psi(t)\,dt \qquad (5.40)$$

we obtain,

$$\psi(\tau) = \frac{1}{2\tau}\left[F_1 \mathcal{g}_1(\tau;\tau_1) + F_2 \mathcal{g}_2(\tau;\tau_1,\tau_2) + \int_{\tau_1}^{\tau_2} \mathcal{K}(\tau,t;\tau_1)\psi(t)dt\right] \qquad (5.41)$$

where

$$\mathcal{g}_1(\tau;\tau_1) = \tau_1 K_2(\tau-\tau_1) - K_3(\tau-\tau_1) + K_3[(\tau^2-\tau_1^2)^{\frac{1}{2}}] \qquad (5.42)$$

$$\mathcal{g}_2(\tau;\tau_1,\tau_2) = \tau_2 K_2(\tau_2-\tau) + K_3(\tau_2-\tau) - (\tau_2^2-\tau_1^2)^{\frac{1}{2}} K_2[(\tau_2^2-\tau_1^2)^{\frac{1}{2}} + (\tau^2-\tau_1^2)^{\frac{1}{2}}]$$

$$- K_3[(\tau_2^2-\tau_1^2)^{\frac{1}{2}} + (\tau^2-\tau_1^2)^{\frac{1}{2}}] \qquad (5.43)$$

$$\mathcal{K}(\tau,t;\tau_1) = t\,\{\,K_1(|\tau-t|) - K_1[(\tau^2-\tau_1^2)^{\frac{1}{2}} + (t^2-\tau_1^2)^{\frac{1}{2}}]\,\} \qquad (5.44)$$

The functions $\mathcal{g}_1(\tau;\tau_1)$, $\mathcal{g}_2(\tau;\tau_1,\tau_2)$ and $\mathcal{K}(\tau,t;\tau_1)$ are similar to the functions $g_1(\tau;\tau_1)$, $g_2(\tau;\tau_1,\tau_2)$ and $K(\tau,t;\tau_1)$ discussed in chapter four. These functions [(5.42) through (5.44)] contain the $K_n(\tau)$ functions instead of the $E_n(\tau)$ functions.

The transformation

$$\psi(\tau) = F_2 + (F_1-F_2)\phi(\tau) \qquad (5.45)$$

permits one to express the solution of the integral equation (5.41) in terms of an independent singular Fredholm integral equation of the second kind:

$$\phi(\tau) = \frac{1}{2\tau}\left[\mathcal{g}_1(\tau;\tau_1) + \int_{\tau_1}^{\tau_2} \mathcal{K}(\tau,t;\tau_1)\phi(t)dt\right] \qquad (5.46)$$

Equation (5.46) represents the dimensionless energy equation. Function $\phi(\tau)$ is a universal function of optical radial distance τ and the optical radii τ_1 and τ_2. Once $\phi(\tau)$ is known, the temperature distribution in the medium can be obtained by solving the transcendental equation (5.45). Substitution of the transformation (5.45) into equation (5.15) yields:

$$\tau^2 \mathcal{G}(\tau) = \tau_1^2(F_1'-F_2') + \gamma(F_1-F_2)Q(\tau) \tag{5.47}$$

where

$$Q(\tau) = 2[\mathcal{L}_1(\tau;\tau_1) + \int_{\tau_1}^{\tau_2} \mathcal{H}(\tau,t;\tau_1)\phi(t)dt] \tag{5.48}$$

In case of planar geometry, under the conditions of radiative equilibrium we know from equation (4.44) that

$$\frac{d[\mathcal{G}_p(\tau)]}{d\tau} = 0$$

Differentiation of equation (5.22) gives

$$\psi(\tau) = \frac{1}{2}[F_1K_2(\tau-\tau_1) + F_2K_2(\tau_2-\tau) + \int_{\tau_1}^{\tau_2} K_1(|\tau-t|)\psi(t)dt\ ] \tag{5.49}$$

The above integral equation defines the temperature distribution and therefore the radiative flux.

The transformation [113]

$$\psi(\tau) = F_2 + (F_1-F_2)\phi_p(\tau) \tag{5.50}$$

permits to reduce equation (5.49) in terms of a simpler singular Fredholm integral equation of the second kind:

$$\phi_p(\tau) = \frac{1}{2}\left[K_2(\tau-\tau_1) + \int_{\tau_1}^{\tau_2} K_1(|\tau-t|)\phi_p(t)\, dt \right] \tag{5.51}$$

Equation (5.51) represents the dimensionless energy equation for the radiative equilibrium case. Function $\phi(\tau)$ is a universal function of optical depth, optical thickness and the shape of the absorption coefficient. Once $\phi(\tau)$ is known, the temperature distribution in the medium can be obtained by solving equation (5.50).

Substitution of the transformation (5.50) into equation (5.22) yields

$$\mathcal{G}_p(\tau) = F_1'-F_2' + \gamma(F_1-F_2)Q_p(\tau) \tag{5.52}$$

where

$$Q_p(\tau) = 2\left[K_3(\tau-\tau_1) + \int_{\tau_1}^{\tau_2} \text{sign}(\tau-t)K_2(|\tau-t|)\phi_p(t)\, dt \right] \tag{5.53}$$

2. Function $\mathcal{G}_1(\tau;\tau_1)$

In order to get some idea about the universal function $\phi(\tau)$, a separate study of the function $\mathcal{G}_1(\tau;\tau_1)$ is undertaken in this subsection. The following cases are considered:

a. Exact Results

Numerical results obtained for expression (5.42) are shown in Tables 5.15 through 5.18 and presented graphically in Figures 5.15 through 5.18. Inspection of the results for different cases of τ_1 reveals that when $\tau_1 = 0.01$, the results for different profiles are

same graphically for values of $\tau_1/\tau \geq 0.1$. The effect of the different profiles is profound for $\tau_1 = 1$ and $\tau_1 = 5$ as seen from Figures 5.17 and 5.18. Once again it is to be noted that the values for the rectangular profile are less than those of the other four profiles. The difference in the values for the triangular and Doppler profiles become significant when $\tau-\tau_1 \geq 3$.

b. Optically Thin

With the aid of asymptotic expansions for $K_2(\tau)$ and $K_3(\tau)$ as $\tau \to 0$, the expression (5.42) for the function $\mathcal{g}_1(\tau;\tau_1)$ in the optically thin limit becomes

$$\mathcal{g}_1(\tau;\tau_1) = \tau - (\tau^2-\tau_1^2)^{\frac{1}{2}} \tag{5.53}$$

Examination of expression (5.53) shows that in the optically thin limit, the function $\mathcal{g}_1(\tau;\tau_1)$ like functions $\mathcal{h}_1(\tau;\tau_1)$ and $\mathcal{h}_2(\tau;\tau_1, \tau_2)$ become independent of the shape of the absorption coefficient.

3. Optically Thin Limit

Exact closed form solution for equation (5.46) can be obtained for the optically thin limit. With the aid of asymptotic expansions for $K_2(\tau)$ and $K_3(\tau)$ as $\tau \to 0$, the solution of equation (5.46) in the optically thin limit becomes

$$\tau\phi(\tau) = \frac{1}{2}\left[\, \tau - (\tau^2-\tau_1^2)^{\frac{1}{2}} \,\right] \tag{5.54}$$

It is worth noting that the dimensionless energy equation in the optically thin limit becomes independent of the shape of $\alpha(\nu)$. This is in keeping with the general trend observed previously for functions $\mathcal{h}_1(\tau;\tau_1)$, $\mathcal{h}_2(\tau;\tau_1,\tau_2)$ and $\mathcal{g}_1(\tau;\tau_1)$.

Table 5.15

Values of the function $g_1(\tau;\tau_1)/\tau$ for $\tau_1 = 0.01$

τ_1/τ	$g_1(\tau;\tau_1)/\tau$				
	Rectangular	Triangular	Exponential	Doppler	Lorentz
			(i) τ_1=0.01		
0.10	4.5670D-3	4.7121D-3	4.7863D-3	4.6948D-3	4.7872D-3
0.20	1.9357D-2	1.9636D-2	1.9777D-2	1.9603D-2	1.9778D-2
0.30	4.4882D-2	4.5272D-2	4.5469D-2	4.5225D-2	4.5469D-2
0.40	8.2049D-2	8.2526D-2	8.2765D-2	8.2468D-2	8.2765D-2
0.50	1.3236D-1	1.3290D-1	1.3317D-1	1.3283D-1	1.3317D-1
0.60	1.9831D-1	1.9887D-1	1.9915D-1	1.9880D-1	1.9915D-1
0.70	2.8420D-1	2.8475D-1	2.8503D-1	2.8469D-1	2.8503D-1
0.80	3.9853D-1	3.9902D-1	3.9927D-1	3.9896D-1	3.9927D-1
0.90	5.6306D-1	5.6341D-1	5.6358D-1	5.6337D-1	5.6358D-1
1.00	1.0000D+0	1.0000D+0	1.0000D+0	1.0000D+0	1.0000D+0

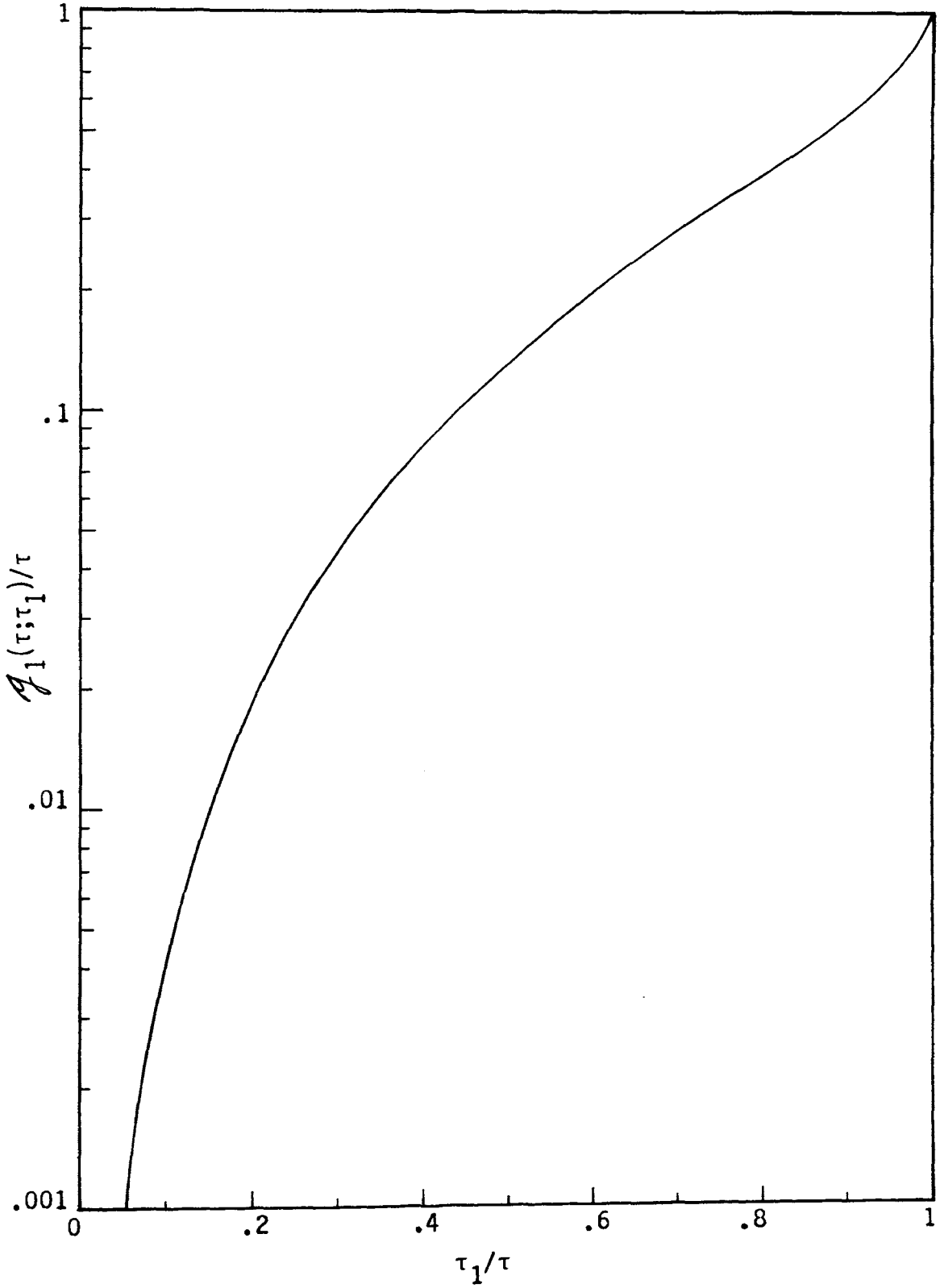

Figure 5.15 - Function $g_1(\tau;\tau_1)/\tau$ versus τ_1/τ for $\tau_1 = 0.01$

Table 5.16

Values of the function $g_1(\tau;\tau_1)/\tau$ for $\tau_1 = 0.1$

τ_1/τ	$g_1(\tau;\tau_1)/\tau$				
	Rectangular	Triangular	Exponential	Doppler	Lorentz
			(ii) τ_1=0.10		
0.10	1.9765D-3	2.7634D-3	3.2623D-3	2.6902D-3	3.3202D-3
0.20	1.3167D-2	1.5265D-2	1.6434D-2	1.5035D-2	1.6497D-2
0.30	3.5547D-2	3.8825D-2	4.0576D-2	3.8450D-2	4.0633D-2
0.40	7.0199D-2	7.4435D-2	7.6648D-2	7.3941D-2	7.6697D-2
0.50	1.1873D-1	1.2366D-1	1.2620D-1	1.2308D-1	1.2624D-1
0.60	1.8375D-1	1.8905D-1	1.9176D-1	1.8842D-1	1.9179D-1
0.70	2.6976D-1	2.7504D-1	2.7773D-1	2.7441D-1	2.7775D-1
0.80	3.8557D-1	3.9033D-1	3.9274D-1	3.8976D-1	3.9275D-1
0.90	5.5368D-1	5.5714D-1	5.5888D-1	5.5672D-1	5.5888D-1
1.00	1.0000D+0	1.0000D+0	1.0000D+0	1.0000D+0	1.0000D+0

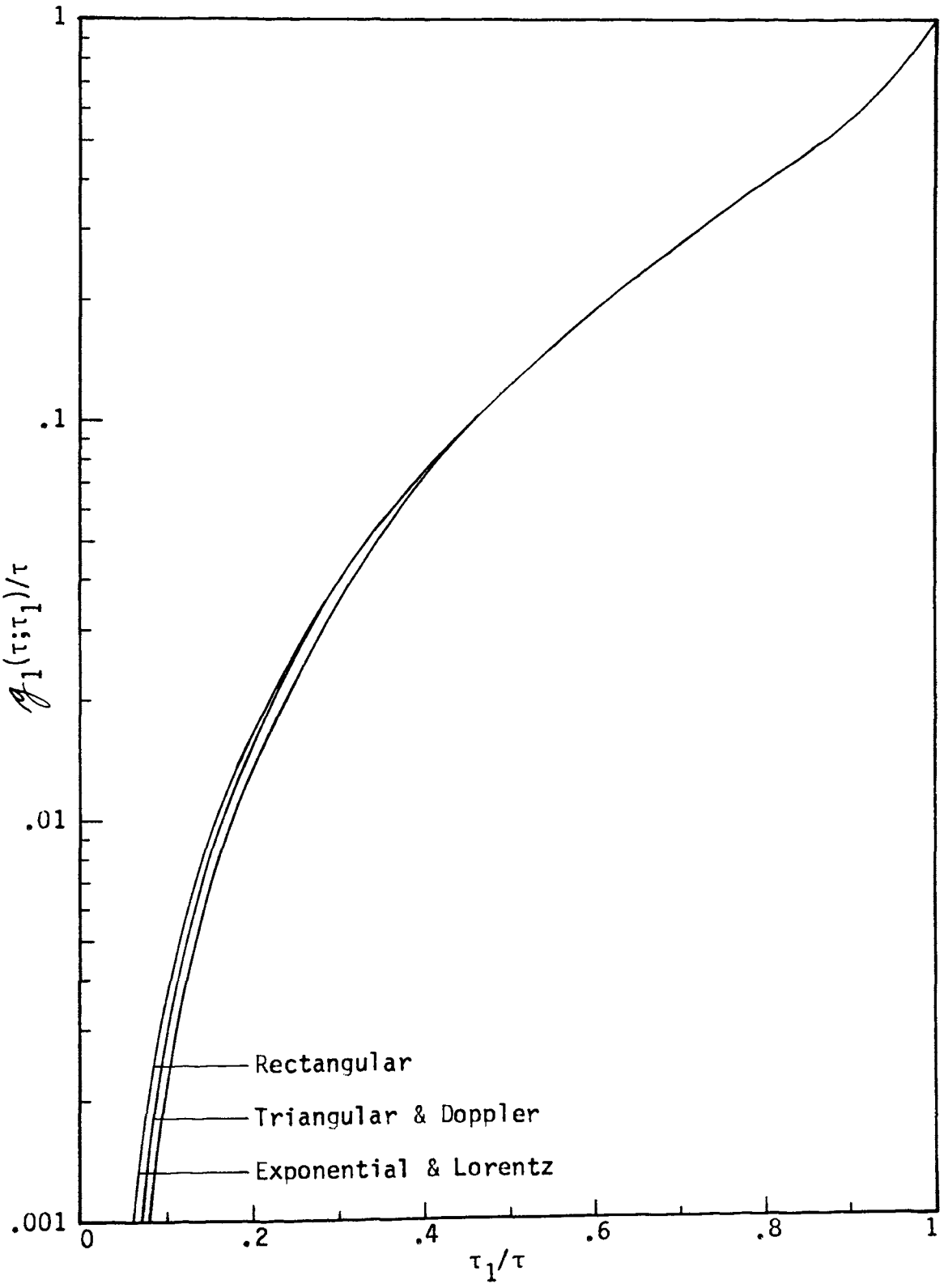

Figure 5.16 - Function $\mathcal{G}_1(\tau;\tau_1)/\tau$ versus τ_1/τ for $\tau_1 = 0.1$

Table 5.17

Values of the function $g_1(\tau;\tau_1)/\tau$ for $\tau_1 = 1$

τ_1/τ	$g_1(\tau;\tau_1)/\tau$				
	Rectangular	Triangular	Exponential	Doppler	Lorentz
			(iii) τ_1=1.0		
0.1	4.6511D-7	1.1578D-4	5.3874D-4	1.9666D-4	9.5618D-4
0.2	2.8429D-4	2.0506D-3	4.6596D-3	2.2511D-3	5.9877D-3
0.3	3.5067D-3	1.0077D-2	1.6481D-2	9.9881D-3	1.8515D-2
0.4	1.4954D-2	2.8877D-2	3.9757D-2	2.8046D-2	4.2100D-2
0.5	4.0495D-2	6.2772D-2	7.7973D-2	6.0938D-2	8.0277D-2
0.6	8.6485D-2	1.1650D-1	1.3518D-1	1.1363D-1	1.3719D-1
0.7	1.6118D-1	1.9668D-1	2.1733D-1	1.9297D-1	2.1888D-1
0.8	2.7825D-1	3.1494D-1	3.3518D-1	3.1088D-1	3.3616D-1
0.9	4.6912D-1	4.9913D-1	5.1495D-1	4.9566D-1	5.1537D-1
1.0	1.0000D+0	1.0000D+0	1.0000D+0	1.0000D+0	1.0000D+0

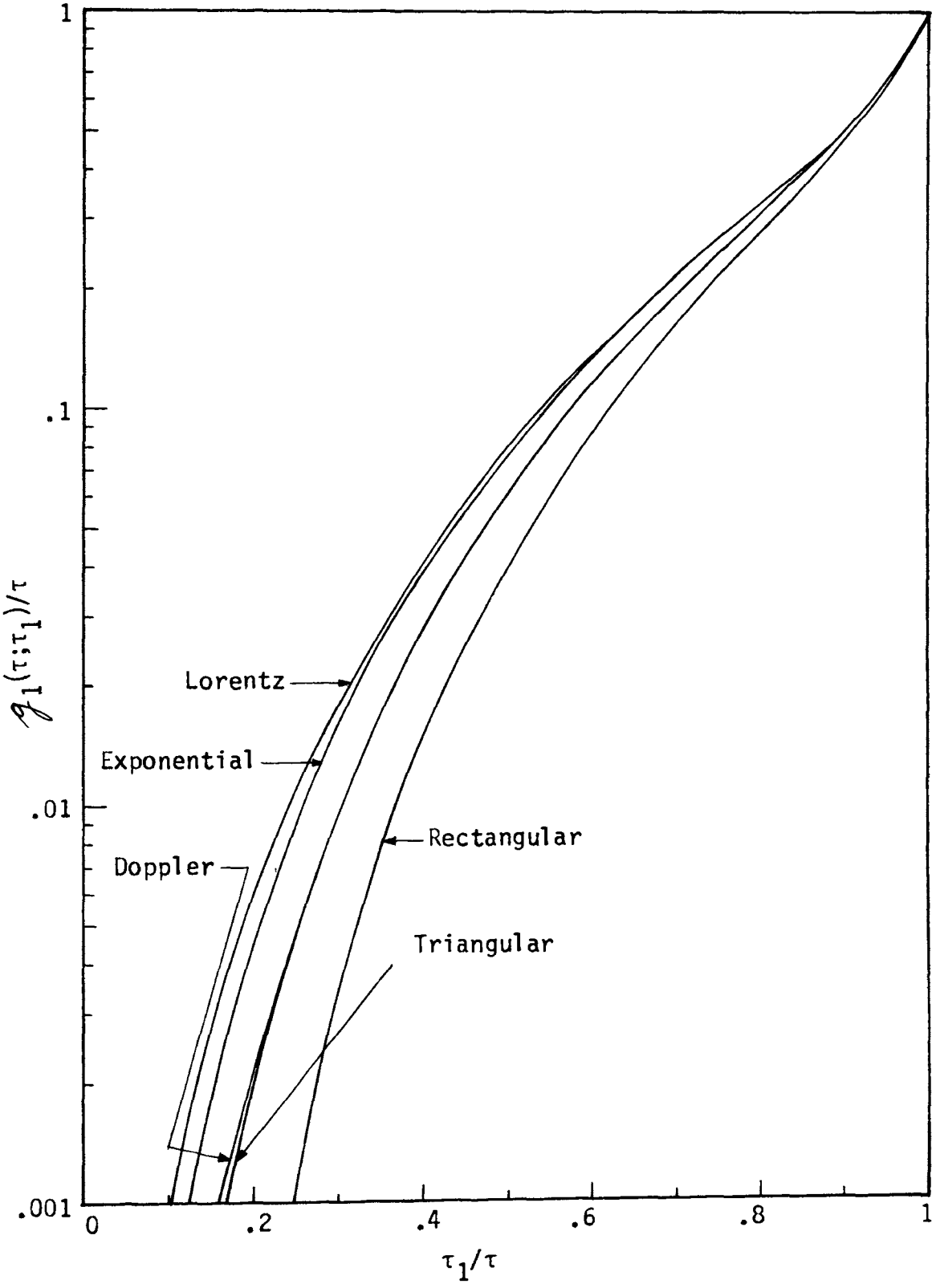

Figure 5.17 - Function $\mathcal{G}_1(\tau;\tau_1)/\tau$ versus τ_1/τ for $\tau_1 = 1$

Table 5.18

Values of the function $g_1(\tau;\tau_1)/\tau$ for $\tau_1 = 5$

τ_1/τ	$g_1(\tau;\tau_1)/\tau$				
	Rectangular	Triangular	Exponential	Doppler	Lorentz
			(iv) τ_1=5.0		
0.1					
0.2	1.0088D-9	8.8662D-5	9.4535D-4		2.4956D-3
0.3	1.5492D-7	5.5667D-4	3.5715D-3	1.2075D-3	7.3873D-3
0.4	1.9483D-5	2.2795D-3	9.7183D-3	3.6344D-3	1.6612D-2
0.5	4.1197D-4	7.5221D-3	2.2460D-2	9.5031D-3	3.2687D-2
0.6	3.5498D-3	2.1642D-2	4.7480D-2	2.3475D-2	6.0378D-2
0.7	1.8411D-2	5.6171D-2	9.5408D-2	5.6273D-2	1.0921D-1
0.8	7.0810D-2	1.3539D-1	1.8714D-1	1.3186D-1	1.9905D-1
0.9	2.3404D-1	3.1808D-1	3.7208D-1	3.1043D-1	3.7880D-1
1.0	1.0000D+0	1.0000D+0	1.0000D+0	1.0000D+0	1.0000D+0

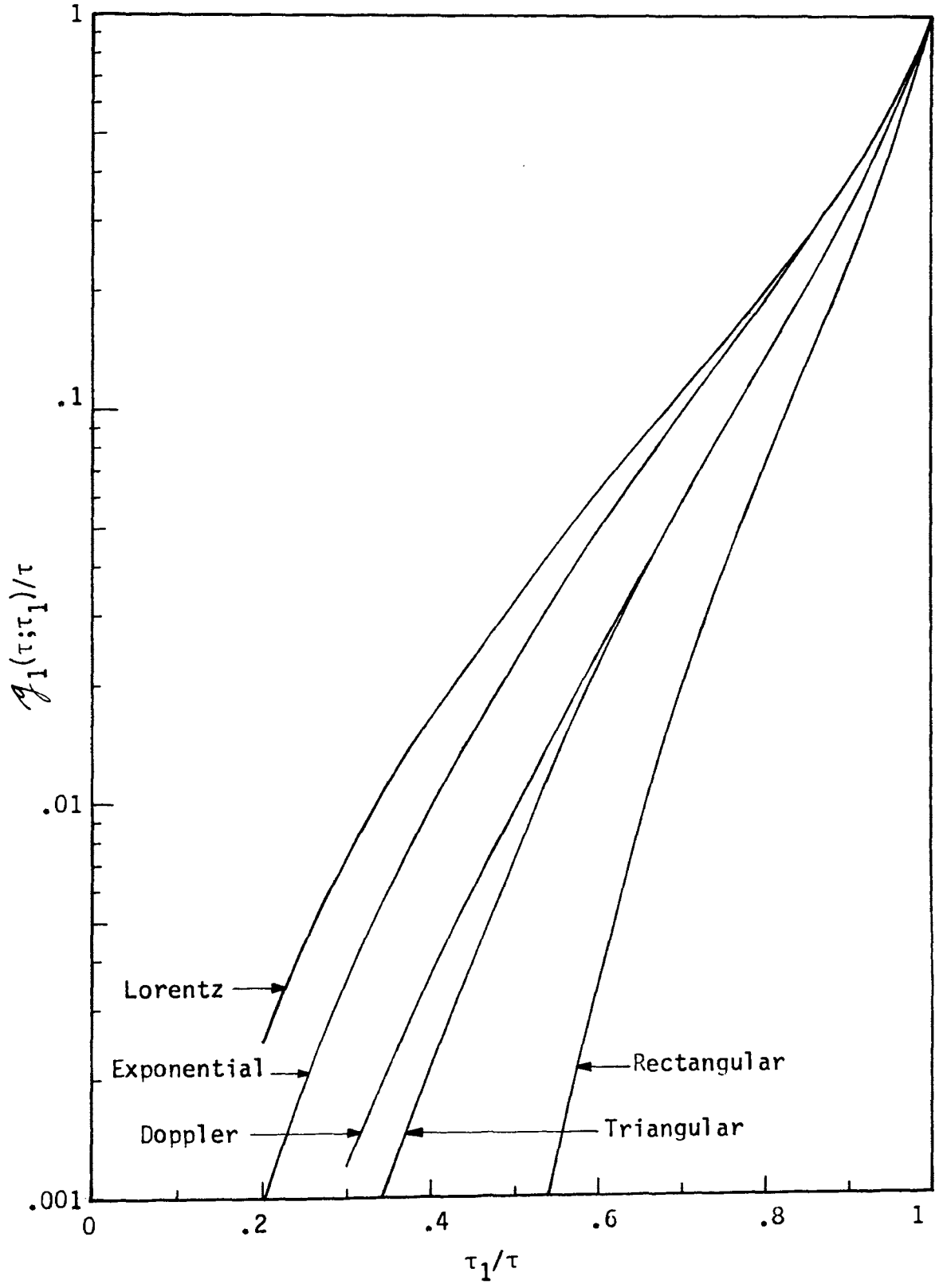

Figure 5.18 - Function $\mathcal{G}_1(\tau;\tau_1)/\tau$ versus τ_1/τ for $\tau_1 = 5$

E. Conclusions

The expression obtained for the local radiative flux is very similar to the one obtained for the rectangular model in chapter four, the only difference being that $E_n(\tau)$ functions are replaced by $K_n(\tau)$ functions. The mathematics involved in the isothermal analysis are not complex. By undertaking a separate study of functions $\mathcal{H}_1(\tau;\tau_1)$, $\mathcal{H}_2(\tau;\tau_1,\tau_2)$ and $\mathcal{G}_1(\tau;\tau_1)$, the behavior of these functions is examined. It is found that in the optically thin limit, the functions $\mathcal{H}_1(\tau;\tau_1)$, $\mathcal{H}_2(\tau;\tau_1,\tau_2)$ and $\mathcal{G}_1(\tau;\tau_1)$ become independent of the shape of the absorption coefficient. The numerical results reveals that the rectangular profile has the smallest numerical value of all the profiles. The results for the Doppler and triangular profiles are approximately the same except for large optical thicknesses. For large values of τ, the effect of the "wings" of the Doppler, exponential and Lorentz profiles is evident. This trend will manifest itself in the results for the radiative fluxes.

VI. CONCLUSIONS AND RECOMMENDATIONS

Summarizing the systematic investigation of radiative heat transfer from an absorbing-emitting media in spherical and planar geometry presented in this study, one may conclude:

(1) The study of the isothermal analysis is simple because there is no complexity in the mathematics involved.

(2) Numerical results obtained in the study of the shock layer example (chapter three) reveals that there is considerable difference between the results for the two geometries. The effect of curvature on the dimensionless radiative fluxes is appreciable even when the inner optical radius is close to the outer optical radius.

(3) The results of the limiting cases for the functions $h_1(\tau;\tau_1)$ and $h_2(\tau;\tau_1,\tau_2)$ show that the validity of the optically thin approximation is very limited, while the optically thick approximation is useful for large optical thickness.

(4) Numerical results obtained for a particular nonisothermal case in the study of the gray analysis reveals that the temperature variations are important and cannot be neglected.

(5) The expression for the local radiative flux in case of the nongray rectangular model depends on the same functions which are discussed in the gray medium problem. With a small amount of additional computational work, one can obtain results in a manner similar to that used in the gray analysis.

(6) The results of the carbon monoxide example indicate that the gray analysis is of limited utility and should be used with extreme caution.

(7) The effect of band or line shape on local radiative flux is accounted for by the functions $\mathcal{h}_1$, $\mathcal{h}_2$ and $\mathcal{H}$ which are very similar to the functions h_1, h_2 and H, respectively.

(8) The results of the functions $\mathcal{h}_1(\tau;\tau_1)$, $\mathcal{h}_2(\tau;\tau_1,\tau_2)$ and $\mathcal{g}_1(\tau;\tau_1)$ reveals that the rectangular profile has the smallest numerical value of all the profiles, while the results for the Doppler and triangular profiles are essentially the same upto an optical thickness of 2. The influence of the "wings" of the profiles on the functions $\mathcal{h}_1(\tau;\tau_1)$, $\mathcal{h}_2(\tau=\tau_2;\tau_1,\tau_2)$ and $\mathcal{g}_1(\tau;\tau_1)$ increases with the optical thickness.

A number of assumptions have been introduced in the formulation of the problem and it is recognized that some of them may be unrealistic under certain conditions. Except in certain idealized geometries, nongray calculations are so prohibitively complicated that some simplification is necessary.

The following recommendations are made:

(1) The nonisothermal case when the medium is nongray should be considered.

(2) A method to solve the dimensionless energy equation of chapter five should be developed.

(3) Experimental work in this field of study should be performed.

(4) An interchange of information between the fields of thermal radiation, neutron transport and astrophysics should be initiated.

BIBLIOGRAPHY

1. E.S. Kuznetsov, Radiant Equilibrium in a Gaseous Shell Surrounding a Perfectly Black Sphere, Izv. Akad. Nauk SSSR, Seriya Geofizicheskaya 15, 69-93 (1951) (in Russian).

2. H. Kennet and S.L. Strack, Stagnation Point Radiative Transfer, ARS Jl. 31, 370-372 (1961).

3. E.M. Sparrow, C.M. Usiskin and H.A. Hubbard, Radiation Heat Transfer in a Spherical Enclosure Containing a Participating Heat-Generating Gas, J. Heat Transfer 83, 199-206 (1961).

4. S.L. Strack, Radiant Heat Transfer Around Re-Entry Bodies, ARS Jl. 32, 744-748 (1962).

5. J.C.Y. Koh, Radiation from Nonisothermal Gases to the Stagnation Point of a Hypersonic Blunt Body, ARS Jl. 32, 1374-1377 (1962).

6. E.S. Kuznetsov, Temperature Distribution in an Infinite Cylinder and in a Sphere in a State of Non-Monochromatic Radiation Equilibrium, USSR Comp. Math and Mech. Phys. 2, 230-254 (1963).

7. S. Cuperman, F. Engelmann and J. Oxenius, Nonthermal Impurity Radiation From a Spherical Plasma, Physics Fluids 7, 108-115 (1963).

8. S. Cuperman, F. Engelmann and J. Oxenius, Nonthermal Impurity Radiation From a Spherical Plasma II, Physics Fluids 7, 428-438 (1964).

9. S. Giuffre and F. Engelmann, Nonequilibrium Line Radiation for Generalized Lorentz Profiles in a Spherical Plasma of Large Optical Thickness, Private Communication (1964).

10. M.A. Heaslet and R.F. Warming, Application of Invariance Principles to a Radiative Transfer Problem in a Homogeneous Spherical Medium, J. Quant. Spectrosc. Radiat. Transfer 5, 669-682 (1965).

11. J.C.Y. Koh, Radiation of Spherically-Shaped Gases, Int. J. Heat Mass Transfer 8, 373-374 (1965).

12. R. Viskanta and P.S. Lall, Transient Cooling of a Spherical Mass of High-Temperature Gas by Thermal Radiation, J. Appl. Mech. 32, 740-746 (1965).

13. M.A. Heaslet and R.F. Warming, Radiation Flux From a Slab or Sphere, J. Math. Analysis Applic. 14, 359-369 (1966).

14. I.L. Ryhming, Radiative Transfer Between Two Concentric Spheres Separated by an Absorbing and Emitting Gas, Int. J. Heat Mass Transfer 9, 315-324 (1966).

15. R. Viskanta and P.S. Lall, Transient Heating and Cooling of a Spherical Mass of Gray Gas by Thermal Radiation, Proceedings of the 1966 Heat Transfer and Fluid Mechanics Institute (M.A. Saad and J.A. Miller, Editors) pp. 181-197, Stanford University Press, Stanford, Calif. (1966).

16. P.S. Lall and R. Viskanta, Transient Energy Transfer in a Gray Radiating Gas During Expansion, Physics Fluids 10, 98-107 (1967).

17. R. Viskanta and A.L. Crosbie, Radiative Transfer Through a Spherical Shell of an Absorbing-Emitting Gray Medium, J. Quant. Spectrosc. Radiat. Transfer 7, 871-889 (1967).

18. R.F. Chisnell, Radiant Heat Transfer in a Spherically Symmetric Medium, AIAA Jl 6, 1389-1391 (1968).

19. Y.S. Chou and C.L. Tien, A Modified Moment Method for Radiative Transfer in Non-Planar Systems, J. Quant. Spectrosc. Radiat. Transfer 8, 919-933 (1968).

20. G. Emanuel, Application of Matched Asymptotic Expansions to Radiative Transfer in an Optically Thick Gas, Aerospace Report No. TR-0158 (3240-20) - 14, Aerospace Corporation, El Segundo, Calif. (1968).

21. B.L. Hunt, An Examination of the Method of Regional Averaging for Radiative Transfer Between Concentric Spheres, Int. J. Heat Mass Transfer 11, 1071-1076 (1968).

22. D.B. Olfe, Application of a Modified Differential Approximation to Radiative Transfer in a Gray Medium Between Concentric Spheres and Cylinders, J. Quant. Spectrosc. Radiat. Transfer 8, 899-907 (1968).

23. R. Viskanta and R.L. Merriam, Heat Transfer by Combined Conduction and Radiation Between Concentric Spheres Separated by Radiating Medium, J. Heat Transfer 90, 248-256 (1968).

24. O.V. Voinov, A.M. Golovin and A.G. Petrov, Energy Transfer From a Radiating Sphere into a Medium with Molecular Heat Conduction, PMM 32, 882-893 (1968).

25. O.V. Voinov, A.M. Golovin and A.G. Petrov, Unsteady Energy Transfer From a Radiating Sphere in a Medium with Molecular Heat Conduction, PMM 33, 364-367 (1969).

26. E.A. Dennar and M. Sibulkin, An Evaluation of the Differential Approximation for Spherically Symmetric Radiative Transfer, J. Heat Transfer 91, 73-76 (1969).

27. G. Emanuel, Radiative Energy Transfer From a Small Sphere, Int. J. Heat Mass Transfer 12, 1327-1331 (1969).

28. R.L. Lee and D.B. Olfe, An Iterative Method for Non-Planar Radiative Transfer Problems, J. Quant. Spectrosc. Radiat. Transfer 9, 297-308 (1969).

29. F. Shahrokhi and P. Wolf, An Investigation of Radiative Heat Transfer in Participating Media, AIAA Jl 7, 791-793 (1969).

30. F. Shahrokhi and P. Wolf, An Investigation of Radiative Heat Transfer in Absorbing, Emitting, and Scattering Media, AIAA 4th Thermophysics Conference, AIAA Paper No. 69-626 (1969).

31. S.C. Traugott, An Improved Differential Approximation for Radiative Transfer with Spherical Symmetry, AIAA Jl 7, 1825-1832 (1969).

32. G. Emanuel, Doppler Line Super-Radiant Emission from a Sphere, Aerospace Report No. TR-0059 (6240-20) - 4, Aerospace Corporation, El Segundo, Calif. (1970).

33. E.C. Gritton and A. Leonard, Exact Solutions to the Radiation Heat Transport Equation in Gaseous Media Using Singular Integral Equation Theory, J. Quant. Spectrosc. Radiat. Transfer 10, 1095-1118 (1970).

34. S.K. Loyalka, Application of a Variational Technique to Radiative Transfer in a Gray Medium Between Concentric Spheres, J. Quant. Spectrosc. Radiat. Transfer 10, 523-528 (1970).

35. K.Y. Chien, Application of the S_n Method to Spherically Symmetric Radiative Transfer Problems, AIAA 6th Thermophysics Conference, AIAA Paper No. 71-466, (1971).

36. D. Finkleman, Generalized Differential Approximation in One-Dimensional Radiative Transfer, J. Quant. Spectrosc. Radiat. Transfer 11, 175-196 (1971).

37. A.N. Saad, Heat Transfer Through a Spherical Gas Shell, M.S. Thesis, Department of Mechanical Engineering, University of Missouri, Rolla (1971).

38. W.H. McCrea, A Note on Dr. P.A. Taylor's Paper, "The Equilibrium of the Calcium Chromosphere." Mon. Not. R. Astr. Soc. 88, 729-740 (1928).

39. S. Chandrasekhar, The Radiative Equilibrium of Extended Stellar Atmospheres, Mon. Not. R. Astr. Soc. 94, 444-458 (1934)

40. N.A. Kosirev, Radiative Equilibrium of the Extended Photosphere, Mon. Not. R. Astr. Soc. 94, 430-443 (1934)

41. S. Chandrasekhar, On the Effective Temperatures of Extended Photospheres, Proc. Camb. Phil. Soc. 31, 390-393 (1935).

42. S. Chandrasekhar, On the Radiative Equilibrium of a Stellar Atmosphere V, Astrophys. J. 101, 95-107 (1945).

43. A.B. Underhill, The Schuster Problem for an Extended Atmosphere, Astrophs. J. 107, 247-264 (1948).

44. H.K. Sen, The Radiative Equilibrium of a Spherical Planetary Nebula, Astrophys. J. 110, 276-287 (1949).

45. M.H. Wrubel, The Transfer of Radiation in a Spherical Atmosphere of Electrons, Astrophys. J. 110, 288-303 (1949).

46. S. Chandrasekhar, Radiative Transfer, Dover Publications, New York (1950) pp. 364-372.

47. R. Bellman and R. Kalaba, On the Principle of Invariant Imbedding and Diffuse Reflection From Cylindrical Regions, Proc. Natn. Acad. Sci., U.S.A. 43, 514-517 (1957).

48. V.V. Sobolev, The Brightness of a Spherical Nebula, Soviet Astronomy 4, 1-6 (1960).

49. V.V. Sobolev, Selected Problems in the Theory of Radiation Diffusion, Soviet Physics - Doklady 4, 1235-1238 (1960).

50. J. Lenoble and Z. Sekera, Equation of Radiative Transfer in a Planetary Spherical Atmosphere, Proc. Natn. Acad. Sci. U.S.A. 47, 372-378 (1961).

51. V.I. Barkov, Radiation Transfer in a Homogeneous Sphere with a Central Point Source, Optics Spectrosc. 14, 285-288 (1963).

52. I.N. Minin and V.V. Sobolev, The Scattering of Light in a Spherical Atmosphere II, Cosmic Research 1, 190-195 (1963).

53. I.N. Minin and V.V. Sobolev, The Theory of Radiation Scattering in Planetary Atmospheres, Soviet Astronomy 7, 379-383 (1963).

54. M.G. Smith, An Approximate Solution of the Spherically Symmetric Transport Equation, Q. Jl. Mech. Appl. Math. XVI Pt.2, 239-252 (1963).

55. V.V. Sobolev and I.N. Minin, Light Scattering in a Spherical Atmosphere - I, Planet. Space Sci. 11, 657-662 (1963)

56. I.N. Minin and V.V. Sobolev, Light Scattering in a Spherical Atmosphere - III, Cosmic Research 2, 529-537 (1964).

57. M.G. Smith, The Isotropic Scattering of a Concentrated Ray Pencil from a Point Source, Proc. Camb. Phil. Soc. 60, 105-114 (1964).

58. S.J. Wilson and K.K. Sen, Modified Spherical Harmonic Method and Spherical Geometry, Annls. Astrophys. 28, 348-352 (1965).

59. S.J. Wilson and K.K. Sen, Modified Spherical Harmonic Method and Spherical Geometry, Annls. Astrophys. 28, 855-859 (1965).

60. M.G. Smith, The Isotropic Scattering of Radiation from a Point Source in a Finite Spherical Atmosphere, Proc. Camb. Phil. Soc. 61, 923-937 (1965).

61. R. Bellman, H. Kagiwada and R. Kalaba, Invariant Imbedding and Radiative Transfer in Spherical Shells, J. Comput. Phys. 1, 245-256 (1966).

62. R.D. Chapman, Radiative Transfer in Extended Stellar Atmospheres, Astrophys. J. 143, 61-74 (1966).

63. L. Auer, Improved Boundary Conditions for the Fourier Method, Astrophys. J. 150, L53-L55 (1967).

64. O.I. Smoktii, Multiple Scattering of Light in a Homogeneous Spherically Symmetrical Planetary Atmosphere, Izv., Atmospheric and Oceanic Physics 3, 140-146 (1967).

65. O.I. Smoktii, Determining the Brightness of an Inhomogeneous Spherically Symmetrical Planetary Atmosphere, Izv., Atmospheric and Oceanic Physics 3, 221-226 (1967).

66. O.I. Smoktii, Multiple Scattering of Light in an Inhomogeneous Spherically Symmetrical Planetary Atmosphere, Izv., Atmospheric and Oceanic Physics 3, 281-286 (1967).

67. R.E. Bellman, H.H. Kagiwada, R.E. Kalaba and S. Ueno, Diffuse Transmission of Light from a Central Source Through an Inhomogeneous Spherical Shell with Isotropic Scattering, J. Math. Phys. 9, 909-912 (1968).

68. J.S. Cassell, Note on the Isotropic Scattering of Radiation from a Point Source in a Finite Spherical Atmosphere, Proc. Camb. Phil. Soc. 64, 711-719 (1968).

69. T.K. Leong and K.K. Sen, Probabilistic Model for Transfer Problem in an Externally Illuminated Spherical Shell Atmosphere with a Perfectly Absorbing Core, Annls. Astrophys. 31, 467-474 (1968).

70. R. Bellman, H.H. Kagiwada, R.E. Kalaba and S. Ueno, Diffuse Reflection of Solar Rays by a Spherical Shell Atmosphere, Icarus 11, 417-423 (1969).

71. S. Huang, Transfer of Radiation in Circumstellar Dust Envelopes II, Intermediate Case, Astrophys. J. 157, 843-855 (1969).

72. G.C. Pomraning, An Extension of the Eddington Approximation, J. Quant. Spectrosc. Radiat. Transfer 9, 407-422 (1969).

73. G.B. Rybicki, A Note on the Computation of Diffuse Reflection Functions for Spherical Shells, J. Comput. Phys. 6, 131-135 (1970).

74. C.G. Davis, Jr., Radiative Transfer Effects in Cepheid Atmospheres, J. Quant. Spectrosc. Radiat. Transfer 11, 647-653 (1971).

75. J. Gruschinske and S. Ueno, Bellman's New Approach to the Numerical Solution of Fredholm Integral Equations with Positive Kernals, J. Quant. Spectrosc. Radiat. Transfer 11, 641-646 (1971).

76. S. Huang, Transfer of Radiation in Circumstellar Dust Envelopes III, The Case of Distant Envelopes, Astrophys. J. 164, 91-96 (1971).

77. D.G. Hummer and G.B. Rybicki, Radiative Transfer in Spherically Symmetric Systems, Joint Institute for Laboratory Astrophysics Publication No. 721 (1971).

78. G. Placzek, Notes on Diffusion of Neutrons Without Change in Energy, MT-4 Atomic Energy Projects, Division of Research, National Research Council of Canada, Chalk River, Ontario (1943).

79. E.P. Wigner, Solution of Boltzmann's Equation for Monoenergetic Neutrons in an Infinite Homogeneous Medium, Unclassified Report No. CP-1120 A-1603, Metallurgical Laboratory, University of Chicago, Chicago, Illinois (1943).

80. B. Davison, Angular Distribution Due to An Isotropic Point Source and Spherically Symmetric Eigensolutions of the Transport Equation, MT-112 Atomic Energy Projects, Division of Research, National Research Council of Canada, Chalf River, Ontario (1945).

81. R.E. Marshak, Note on the Spherical Harmonic Method as Applied to the Milne Problem for a Sphere, Phys. Rev. 71, 443-446 (1947).

82. G. Placzek and G. Volkoff, A Theorem on Neutron Multiplication, Can. J. Res. A. 25, 276-292 (1947).

83. A.H. Wilson, The General Properties of the Transport Equation and Its Uses in Determining the Multiplication in Bodies Having Spherical Symmetry, A.E.R.E. Harwell Report, M.S. 105 A, Dec. 1950.

84. B. Davison, Influence of a Black Sphere and of a Black Cylinder Upon the Neutron Density in an Infinite Non-Capturing Medium, Proc. Phys. Soc. 64 A, 881-902 (1951).

85. K.M. Case, F. Hoffmann and G. Placzek, Introduction to the Theory of Neutron Diffusion Volume I, Los Alamos Scientific Laboratory, Los Alamos, New Mexico (1953).

86. B.G. Carlson and G.I. Bell, Solution of the Transport Equation by the S_n Method, Proceedings of the Second United Nations International Conference on the Peaceful Uses of Atomic Energy Volume 16, pp. 578-585, Nuclear Data and Reactor Theory, Geneva (1958).

87. C.C. Grosjean, Multiple Isotropic Scattering in Convex Homogeneous Media Bounded by Vacuum, Proceedings of the Second United Nations International Conference on the Peaceful Uses of Atomic Energy Volume 16, pp. 413-430, Nuclear Data and Reactor Theory, Geneva (1958).

88. C.C. Grosjean, Multiple Isotropic Scattering in Convex Homogeneous Media Bounded by Vacuum, Part II: Some Practical Applications, Proceedings of the Second United Nations International Conference on the Peaceful Uses of Atomic Energy Volume 16, pp. 431-446, Nuclear Data and Reactor Theory, Geneva (1958).

89. J.R. Triplett, Generalized Diffusion Theory Methods for Reactor Survey Applications, Proceedings of the Second United Nations International Conference on the Peaceful Uses of Atomic Energy Volume 16, pp. 578-585, Nuclear Data and Reactor Theory, Geneva (1958).

90. D.W. Drawbaugh and L.C. Noderer, The Double Spherical Harmonic Method for Cylinders and Spheres, Nucl. Sci. Engng. 6, 79-81 (1959).

91. W. Kofink, New Solutions of the Boltzmann Equations for Monoenergetic Neutron Transport in Spherical Geometry, ORNL -3216, Oak Ridge National Laboratory, Oak Ridge, Tennessee (1961).

92. A. Leonard and T.W. Mullikin, Solutions to the Criticality Problems for Spheres and Slabs, RM-3256-PR, The Rand Corporation, Santa Monica, Calif. (1962).

93. T.W. Mullikin, Estimate of Critical Dimensions of Spherical and Slab Reactors, J. Math. Analysis Applic. 5, 184-199 (1962).

94. G.J. Mitsis, Transport Solutions to the Monoenergetic Critical Problems, ANL-6787, Applied Mathematics Division, Argonne National Laboratory, Argonne, Illinois, Office of Technical Services, United States Government Printing Office, Washington, D.C. (1963).

95. A. Leonard and T.W. Mullikin, Green's Functions for One-Velocity Neutron Transport in a One-Dimensional Slab and Sphere, Proc. Natn. Acad. Sci., U.S.A. 52, 683-688 (1964).

96. P.B. Bailey, A Rigorous Derivation of Some Invariant Imbedding Equations of Transport Theory, J. Math. Analysis Applic. 8, 144-169 (1964).

97. P.B. Bailey and G.M. Wing, A Correction to Some Invariant Imbedding Equations of Transport Theory Obtained by "Particle Counting", J. Math. Analysis Applic. 8, 170-174 (1964).

98. S.J. Wilson and K.K. Sen, Modified Spherical Harmonic Method and Neutron Transport Problem with Finite Spherical Core, Can. J. Phys. 43, 432-437 (1965).

99. D.C. Sahni, The Effect of a Black Sphere on the Flux Distribution in an Infinite Moderator, J. Nucl. Energy 20, 915-920 (1966).

100. E. Schmidt and E.M. Gelbard, A Double-P_N Method for Spheres and Cylinders, Amer. Nucl. Soc. Trans. 9, 432-433 (1966).

101. R.C. Erdmann and C.E. Siewert, Green's Functions for the One-Speed Transport Equation in Spherical Geometry, J. Math. Phys. 9, 81-89 (1968).

102. A.A. Shkurpelov, The Spectrum of the Monoenergetic Neutron Transport Operator in Spherical Geometry, USSR Comp. Math. and Mech. Phys. 8, 309-321 (1968).

103. V.E. Troshchiev, V.F. Yudintsev and V.I. Fedyanin, Acceleration of the Convergence of Iterations in Solving the Kinetic Equation, USSR Comp. Math. and Mech. Phys. 8, 298-308 (1968).

104. E.H. Bareiss and I.K. Abu-Shumays, On the Structure of Isotropic Transport Operators in Space, SIAM - AMS Proceedings Volume 1: Transport Theory (R. Bellman, G. Birkhoff and I. Abu-Shumays, editors), pp. 37-38, American Mathematical Society, Providence, Rhode Island (1969).

105. E.M. Gelbard, J.A. Davis and L.A. Hageman, Solution of the Discrete Ordinate Equations in One and Two Dimensions, SIAM-AMS Proceedings Volume 1: Transport Theory (R. Bellman, G. Birkhoff, and I. Abu-Shumays, editors), pp. 129-158, American Mathematical Society, Providence, Rhode Island (1969).

106. O.J. Smith, Radiation Transport in Plane and Spherical Media, Ph.D. Thesis, Department of Nuclear Engineering, North Carolina State University, Raleigh (1969).

107. K.M. Case, R. Zelazny and M. Kanal, Spherically Symmetric Boundary - Value Problems in One-Speed Transport Theory, J. Math. Phys. 11, 223-239 (1970).

108. T.W. Schnatz and C.E. Siewert, Two-Group Neutron Transport Theory in Spherical Geometry, J. Math. Phys. 11, 766-771 (1970).

109. E.M. Sparrow and R.D. Cess, Radiation Heat Transfer, Brooks/Cole Publishing Company, Belmont, Calif. (1966).

110. S.I. Pai, Radiation Gas Dynamics, Springer-Verlag New York Inc. (1966).

111. A.L. Crosbie and R. Viskanta, The Exact Solution to a Simple Nongray Radiative Transfer Problem, J. Quant. Spectrosc. Radiat. Transfer 9, 553-568 (1969).

112. R.D. Cess, P. Mighdoll and S.N. Tiwari, Infrared Radiative Heat Transfer in Nongray Gases, Int. J. Heat Mass Transfer 10, 1521-1531 (1967).

113. A.L. Crosbie and R. Viskanta, Effect of Band or Line Shape on the Radiative Transfer in a Nongray Planar Medium, J. Quant. Spectrosc. Radiat. Transfer 10, 487-509 (1970).

114. A.L. Crosbie and R. Viskanta, Nongray Radiative Transfer in a Planar Medium Exposed to a Collimated Flux, J. Quant. Spectrosc. Radiat. Transfer 10, 465-485 (1970).

115. A.L. Crosbie and R. Viskanta, On the Validity of the Narrow Band Approximation, J. Quant. Spectrosc. Radiat. Transfer 11, 135-139 (1971).

116. V. Kourganoff, Basic Methods in Transfer Problems, Oxford University Press, London (1952).

117. M. Abramowitz and I.A. Stegun, Handbook of Mathematical Functions, N.B.S. Applied Mathematics Series (1964).

VITA

Hakimuddin Kalimuddin Khalil was born on October 11, 1945, in Bombay, India. He received his Bachelor of Engineering degree in Mechanical Engineering from the University of Poona, Poona, India, in December 1968.

He has been enrolled in the Graduate School of the University of Missouri-Rolla since January 1970.

APPENDIX A

THE EXPONENTIAL INTEGRALS

The nth exponential integral is defined for positive real arguments by

$$E_n(\tau) = \int_0^1 \mu^{n-2}\, e^{-\tau/\mu}\, d\mu \tag{A.1}$$

Integrating equation (A.1) by parts, one obtains the recurrence relation

$$nE_{n+1}(\tau) = e^{-\tau} - \tau E_n(\tau) \tag{A.2}$$

The initial values are found from equation (A.1) to be

$$E_n(0) = \frac{1}{n-1} \qquad n = 2, 3, 4, \ldots \tag{A.3}$$

while differentiation of equation (A.4) yields

$$\frac{dE_n(\tau)}{d\tau} = - E_{n-1}(\tau) \tag{A.4}$$

$$\frac{dE_1(\tau)}{d\tau} = - \frac{1}{\tau} e^{-\tau} \tag{A.5}$$

Conversely,

$$\int E_n(\tau)dt = - E_{n+1}(\tau) \tag{A.6}$$

Series expansions of $E_1(\tau)$, $E_2(\tau)$, $E_3(\tau)$, $E_4(\tau)$ and $E_5(\tau)$ are of the form

$$E_1(\tau) = -\gamma - \ln\tau + \sum_{n=1}^{\infty} \frac{(-1)^{n-1}\tau^n}{nn!} \tag{A.7}$$

$$E_2(\tau) = 1 + \tau(\gamma - 1 + \ln \tau) + \sum_{n=1}^{\infty} \frac{(-1)^n \tau^{n+1}}{n(n+1)!} \tag{A.8}$$

$$E_3(\tau) = \frac{1}{2} - \tau + \frac{\tau^2}{2}\left(-\gamma + \frac{3}{2} - \ln \tau\right) + \sum_{n=1}^{\infty} \frac{(-1)^{n+1} \tau^{n+2}}{n(n+2)!} \tag{A.9}$$

$$E_4(\tau) = \frac{1}{3} - \frac{\tau}{2} + \frac{\tau^2}{2} + \frac{\tau^3}{6}\left(\gamma - \frac{11}{6} + \ln \tau\right) + \sum_{n=1}^{\infty} \frac{(-1)^{n+2} \tau^{n+3}}{n(n+3)!} \tag{A.10}$$

$$E_5(\tau) = \frac{1}{4} - \frac{\tau}{3} + \frac{\tau^2}{4} - \frac{\tau^3}{6} + \frac{\tau^4}{24}\left(-\gamma + \frac{50}{24} - \ln \tau\right) + \sum_{n=1}^{\infty} \frac{(-1)^{n+3} \tau^{n+4}}{n(n+4)!} \tag{A.11}$$

where $\gamma = 0.5772156$. From equation (A.7) it is seen that $E_1(\tau)$ has a logarithmic singularity at the origin.

According to Reference [116], $\tau E_1(\tau) \to 0$ as $\tau \to 0$ and the functions $E_2(\tau)$, $E_3(\tau)$, $E_4(\tau)$ and $E_5(\tau)$ have the following asymptotic expansions as $\tau \to 0$:

$$E_2(\tau) = 1 + O(\tau) \tag{A.12}$$

$$E_3(\tau) = \frac{1}{2} - \tau + O(\tau^2) \tag{A.13}$$

$$E_4(\tau) = \frac{1}{3} - \frac{\tau}{2} + \frac{\tau^2}{2} + O(\tau^3) \tag{A.14}$$

$$E_5(\tau) = \frac{1}{4} - \frac{\tau}{3} + \frac{\tau^2}{4} - \frac{\tau^3}{6} + O(\tau^4) \tag{A.15}$$

For large τ [117],

$$E_n(\tau) \simeq \frac{e^{-\tau}}{\tau+n} \tag{A.16}$$

APPENDIX B

MATHEMATICAL PROPERTIES OF THE FUNCTIONS $K_n(\tau)$

The functions $K_1(\tau)$, $K_2(\tau)$, $K_3(\tau)$, $K_4(\tau)$ and $K_5(\tau)$ are defined as follows

$$K_1(\tau) = \int_R \alpha^2(\nu)\, E_1[\alpha(\nu)\tau]\, d\nu \,/\, \gamma \tag{B.1}$$

$$K_2(\tau) = \int_R \alpha(\nu)\, E_2[\alpha(\nu)\tau]\, d\nu \,/\, \gamma \tag{B.2}$$

$$K_3(\tau) = \int_R \{E_3[\alpha(\nu)\tau] - \tfrac{1}{2}\}\, d\nu \,/\, \gamma \tag{B.3}$$

$$K_4(\tau) = \int_R \{(E_4[\alpha(\nu)\tau] - \tfrac{1}{3} + \frac{\alpha(\nu)\tau}{2}) \,/\, \alpha(\nu)\}\, d\nu \,/\, \gamma \tag{B.4}$$

$$K_5(\tau) = \int_R \{(E_5[\alpha(\nu)\tau] - \tfrac{1}{4} + \frac{\alpha(\nu)\tau}{3} - \frac{\alpha^2(\nu)\tau^2}{4}) / \alpha^2(\nu)\}\, d\nu \,/\, \gamma \tag{B.5}$$

In the above equations the quantity γ is defined as follows

$$\gamma = \int_R \alpha(\nu)\, d\nu \tag{B.6}$$

R refers to the region of the spectrum over which the absorption coefficient does not vanish.

Since the functions $K_n(\tau)$ and $E_n(\tau)$ are related, many of the mathematical properties of the two functions are similar. The derivative of the function $K_n(\tau)$ with respect to τ yields

$$\frac{dK_n(\tau)}{d\tau} = - K_{n-1}(\tau) \qquad n > 1$$

with

$$K_1(0) = \infty$$

$$K_2(0) = 1$$

$$K_n(0) = 0 \qquad n > 2$$

By utilizing the definitions for functions $K_n(\tau)$ (expressions (B.1) through (B.5)) and the recurrence relation (A.2), one obtains the following relations:

$$K_2(\tau) + \tau K_1(\tau) = \int_R \alpha(\nu)\, e^{-\alpha(\nu)\tau}\, d\nu / \gamma \tag{B.7}$$

$$2K_3(\tau) + \tau K_2(\tau) = \int_R [e^{-\alpha(\nu)\tau} - 1]\, d\nu / \gamma \tag{B.8}$$

$$3K_4(\tau) + \tau K_3(\tau) = \int_R \{[e^{-\alpha(\nu)\tau} - 1 + \alpha(\nu)\tau] / \alpha(\nu)\}\, d\nu / \gamma \tag{B.9}$$

$$4K_5(\tau) + \tau K_4(\tau) = \int_R \{[e^{-\alpha(\nu)\tau} - 1 + \alpha(\nu)\tau - \frac{\alpha^2(\nu)\tau^2}{2}] / \alpha^2(\nu)\, d\nu / \gamma \tag{B.10}$$

Substituting the standard series expansions for $E_n(\tau)$ into the definitions for $K_n(\tau)$ yields the expansions

$$K_1(\tau) = A_2(-\gamma_e - \ln \tau) + B_0 - \sum_{n=1}^{\infty} \frac{A_{n+2}(-\tau)^n}{nn!} \tag{B.11}$$

$$K_2(\tau) = 1 + A_2(\gamma_e - 1 + \ln \tau) - B_0\tau - \sum_{n=1}^{\infty} \frac{A_{n+2}(-\tau)^{n+1}}{n(n+1)!} \tag{B.12}$$

$$K_3(\tau) = -\tau + \frac{1}{2} A_2(-\gamma_e + \frac{3}{2} - \ln \tau)\, \tau^2 + \frac{1}{2} B_0\tau^2 - \sum_{n=1}^{\infty} \frac{A_{n+2}(-\tau)^{n+2}}{n(n+2)!} \tag{B.13}$$

$$K_4(\tau) = \frac{\tau^2}{2} + \frac{1}{6} A_2(\gamma_e - \frac{11}{6} + \ln \tau)\, \tau^3 - \frac{1}{6} B_0 \tau^3 - \sum_{n=1}^{\infty} \frac{A_{n+2}(-\tau)^{n+3}}{n(n+3)!} \qquad (B.14)$$

$$K_5(\tau) = \frac{-\tau^3}{6} + \frac{1}{24} A_2(-\gamma_e + \frac{50}{24} - \ln \tau)\, \tau^4 + \frac{1}{24} B_0 \tau^4 - \sum_{n=1}^{\infty} \frac{A_{n+2}(-\tau)^{n+4}}{n(n+4)!} \qquad (B.15)$$

where $\gamma_e = 0.5772156$ and

$$B_0 = \int_R \alpha^2(\nu)[-\ln \alpha(\nu)]\, d\nu \,/\, \gamma \qquad (B.16)$$

$$A_k = \int_R \alpha^k(\nu)\, d\nu \,/\, \gamma \qquad (B.17)$$

The constants A_k, B_0 and γ for the various profiles are summarized in Table B.1.

TABLE B.1

Constants A_k, B_0 and γ for the various profiles

Profile	A_k	B_0	γ
Rectangular	1	0	$\Delta\nu$
Triangular	$\frac{2}{k+1}$	$\frac{2}{9}$	$\frac{\Delta\nu}{2}$
Exponential	$\frac{1}{k}$	$\frac{1}{4}$	$\frac{2}{d}$
Doppler	$\frac{1}{\sqrt{k}}$	$\frac{1}{4\sqrt{2}}$	$\frac{\Pi}{d}$
Lorentz	$A_1 = 1$	$\ln 2 - \frac{1}{2}$	$\frac{\Pi}{\sqrt{d}}$

$$A_{k+1} = \frac{2k-1}{2k} A_k$$

From expressions (B.11) through (B.15) one observes that $\tau K_1(\tau) \to 0$ as $\tau \to 0$ and the functions $K_2(\tau)$, $K_3(\tau)$, $K_4(\tau)$ and $K_5(\tau)$ have the following asymptotic expansions as $\tau \to 0$:

$$K_2(\tau) = 1 + O(\tau) \tag{B.18}$$

$$K_3(\tau) = -\tau + O(\tau^2) \tag{B.19}$$

$$K_4(\tau) = \frac{\tau^2}{2} + O(\tau^3) \tag{B.20}$$

$$K_5(\tau) = \frac{-\tau^3}{6} + O(\tau^4) \tag{B.21}$$

Substitution of the definition of $E_1(\tau)$ into expression for $K_1(\tau)$ with the assumption that the absorption coefficient is symmetric about $\nu = \nu_c$ yields

$$K_1(\tau) = \frac{2}{\gamma} \int_0^a \int_0^1 \alpha^2(y) \exp\left[-\alpha(y)\tau / \mu\right] \frac{d\mu}{\mu} dy \tag{B.22}$$

where $\gamma = 2 \int_0^a \alpha(y)\, dy$ with $y = (\nu - \nu_c) / D$.

The constants a and D for the various profiles are defined in Table B.2. Letting $x = \mu / \alpha(y)$, the function $K_1(\tau)$ can be expressed as follows

$$K_1(\tau) = \frac{2}{\gamma} \int_0^a \int_0^{\frac{1}{\alpha(y)}} \alpha^2(y) \exp\left(-\frac{\tau}{x}\right) \frac{dx}{x} dy \tag{B.23}$$

Changing the order of integration requires that the integral be broken into two parts

$$K_1(\tau) = \frac{2}{\gamma} \left\{ \int_0^1 \left[\int_0^a \alpha^2(y)dy \right] \exp\left(-\frac{\tau}{x}\right) \frac{dx}{x} \right.$$

$$\left. + \int_1^\infty \left[\int_{f(x)}^a \alpha^2(y)dy \right] \exp\left(-\frac{\tau}{x}\right) \frac{dx}{x} \right. \qquad (B.24)$$

Rewriting equation (B.24) in a more compact form yields

$$K_1(\tau) = \int_0^\infty \exp\left(-\frac{\tau}{x}\right) G(x) \frac{dx}{x} \qquad (B.25)$$

where

$$G(x) = G_1 = \frac{2}{\gamma} \int_0^a \alpha^2(y)dy \qquad 0 < x < 1 \qquad (B.25a)$$

$$G(x) = G_2 = \frac{2}{\gamma} \int_{f(x)}^a \alpha^2(y)dy \qquad x > 1 \qquad (B.25b)$$

The functions G(x) and f(x) for the various profiles are summarized in Table B.2. Similarly, the functions $K_2(\tau)$, $K_3(\tau)$, $K_4(\tau)$ and $K_5(\tau)$ can be expressed as

$$K_2(\tau) = \int_0^\infty \exp\left(-\frac{\tau}{x}\right) G(x)\, dx \qquad (B.26)$$

$$K_3(\tau) = \int_0^\infty \left[\exp\left(-\frac{\tau}{x}\right) - 1\right] \times G(x)\, dx \qquad (B.27)$$

$$K_4(\tau) = \int_0^\infty \left[\exp\left(-\frac{\tau}{x}\right) - 1 + \frac{\tau}{x}\right] x^2\, G(x)\, dx \qquad (B.28)$$

Table B.2

Functions G(x) and f(x) for the various profiles

Profile	$\alpha(y)(0 \leq y \leq a)$	a	D	γ	G_1	G_2	f(x)
Rectangular	1	1	$\frac{\Delta\nu}{2}$	2	1	0	--
Triangular	1-y	1	$\frac{\Delta\nu}{2}$	1	$\frac{2}{3}$	$\frac{2}{3}\frac{1}{x}3$	(x-1)/x
Exponential	exp(-y)	∞	$\frac{1}{d}$	2	$\frac{1}{2}$	$\frac{1}{2}\frac{1}{x}2$	ln x
Doppler	$\exp(-y^2)$	∞	$\frac{1}{\sqrt{d}}$	$\sqrt{\pi}$	$\frac{1}{\sqrt{2}}$	$\mathrm{erfc}[\sqrt{(2 \ln x)}]/\sqrt{2}$	$\sqrt{(\ln x)}$
Lorentz	$1/(1+y^2)$	∞	$\frac{1}{\sqrt{d}}$	π	$\frac{1}{2}$	$\frac{1}{2} - \frac{1}{\pi}\tan^{-1}\sqrt{x-1} - \frac{1}{\pi}\frac{\sqrt{(x-1)}}{x}$	x-1

$$K_5(\tau) = \int_0^\infty [\exp(-\frac{\tau}{x}) - 1 + \frac{\tau}{x} - \frac{\tau^2}{2x^2}]\, x^3\, G(x)\, dx \qquad (B.29)$$

Substituting the functions G(x) and f(x) for the rectangular, triangular and exponential profiles into expressions (B.25) through (B.29) and then evaluating the corresponding integrals, we arrive at the following expressions for the $K_n(\tau)$ functions.

Rectangular profile:

$$K_1(\tau) = E_1(\tau) \qquad (B.30a)$$

$$K_2(\tau) = E_2(\tau) \qquad (B.30b)$$

$$K_3(\tau) = E_3(\tau) - \frac{1}{2} \qquad (B.30c)$$

$$K_4(\tau) = E_4(\tau) - \frac{1}{3} + \frac{\tau}{2} \qquad (B.30d)$$

$$K_5(\tau) = E_5(\tau) - \frac{1}{4} + \frac{\tau}{3} - \frac{\tau^2}{4} \qquad (B.30e)$$

Triangular profile:

$$K_1(\tau) = \frac{2}{3}[E_1(\tau) - \frac{e^{-\tau}}{\tau^3}(\tau^2 + 2\tau + 2) + \frac{2}{3\tau^3}] \qquad (B.31a)$$

$$K_2(\tau) = \frac{2}{3}[E_2(\tau) - \frac{e^{-\tau}}{\tau^2}(\tau + 1) + \frac{1}{\tau^2}] \qquad (B.31b)$$

$$K_3(\tau) = \frac{2}{3}[E_3(\tau) - \frac{e^{-\tau}}{\tau} + \frac{1}{\tau} - \frac{3}{2}] \qquad (B.31c)$$

$$K_4(\tau) = \frac{2}{3}[E_4(\tau) - E_1(\tau) - \ln\tau + \frac{3\tau}{2} - \gamma - \frac{1}{3}] \qquad (B.31d)$$

$$K_5(\tau) = \frac{2}{3}[E_5(\tau) + \tau E_1(\tau) + \tau \ln\tau - e^{-\tau} - \frac{3\tau^2}{4} - \frac{2\tau}{3} + \gamma\tau + \frac{3}{4}] \qquad (B.31e)$$

Exponential profile:

$$K_1(\tau) = \frac{1}{2}\left[E_1(\tau) - \frac{e^{-\tau}}{\tau^2}(\tau + 1) + \frac{1}{\tau^2}\right] \tag{B.32a}$$

$$K_2(\tau) = \frac{1}{2}\left[E_2(\tau) - \frac{e^{-\tau}}{\tau} + \frac{1}{\tau}\right] \tag{B.32b}$$

$$K_3(\tau) = \frac{1}{2}\left[E_3(\tau) - E_1(\tau) - \ln \tau - \gamma - \frac{1}{2}\right] \tag{B.32c}$$

$$K_4(\tau) = \frac{1}{2}\left[E_4(\tau) + \tau E_1(\tau) + \tau \ln \tau - e^{-\tau} + \tau\left(\gamma - \frac{1}{2}\right) + \frac{2}{3}\right] \tag{B.32d}$$

$$K_5(\tau) = \frac{1}{2}\left[E_5(\tau) - \frac{\tau^2}{2} E_1(\tau) - \frac{\tau^2}{2} \ln \tau + e^{-\tau}\left(\frac{\tau}{2} - \frac{1}{2}\right)\right.$$

$$\left. - \tau^2\left(\frac{\gamma}{2} - \frac{1}{2}\right) - \frac{2\tau}{3} + \frac{1}{4}\right] \tag{B.32e}$$

Using the relation for large τ as given by equation (A.16), the following approximate expressions of $K_n(\tau)$ functions for the rectangular, triangular and exponential profiles are obtained

Rectangular profile:

$$K_1(\tau) = \frac{e^{-\tau}}{\tau + 1} \tag{B.33a}$$

$$K_2(\tau) = \frac{e^{-\tau}}{\tau + 2} \tag{B.33b}$$

$$K_3(\tau) = \frac{e^{-\tau}}{\tau + 3} - \frac{1}{2} \tag{B.33c}$$

$$K_4(\tau) = \frac{e^{-\tau}}{\tau + 4} - \frac{1}{3} + \frac{\tau}{2} \tag{B.33d}$$

$$K_5(\tau) = \frac{e^{-\tau}}{\tau + 5} - \frac{1}{4} + \frac{\tau}{3} - \frac{\tau^2}{4} \tag{B.33e}$$

Triangular profile:

$$K_1(\tau) = \frac{2e^{-\tau}(-3\tau^2 - 4\tau - 2)}{3\tau^3(\tau + 1)} + \frac{4}{3\tau^3} \tag{B.34a}$$

$$K_2(\tau) = \frac{2e^{-\tau}(-3\tau - 2)}{3\tau^2(\tau + 2)} + \frac{2}{3\tau^2} \tag{B.34b}$$

$$K_3(\tau) = \frac{-2e^{-\tau}}{\tau(\tau + 3)} + \frac{2}{3\tau} - 1 \tag{B.34c}$$

$$K_4(\tau) = \frac{-2e^{-\tau}}{(\tau + 4)(\tau + 1)} - \frac{2}{3}\left[\ln \tau + \gamma + \frac{1}{3}\right] + \tau \tag{B.34d}$$

$$K_5(\tau) = \frac{-8e^{-\tau}}{3(\tau + 5)(\tau + 1)} + \frac{2}{3}\left[\tau \ln \tau - \frac{3}{4}\tau^2 - \left(\frac{2}{3} - \gamma\right)\tau + \frac{3}{4}\right] \tag{B.34e}$$

Exponential profile:

$$K_1(\tau) = \frac{e^{-\tau}(-2\tau - 1)}{2\tau^2(\tau + 1)} + \frac{1}{2\tau^2} \tag{B.35a}$$

$$K_2(\tau) = \frac{-e^{-\tau}}{\tau(\tau + 2)} + \frac{1}{2\tau} \tag{B.35b}$$

$$K_3(\tau) = \frac{-e^{-\tau}}{(\tau + 3)(\tau + 1)} - \frac{1}{2}\left[\ln \tau + \gamma + \frac{1}{2}\right] \tag{B.35c}$$

$$K_4(\tau) = \frac{-3e^{-\tau}}{2(\tau + 4)(\tau + 1)} + \frac{1}{2}\left[\tau \ln \tau + \left(\gamma - \frac{1}{2}\right)\tau + \frac{2}{3}\right] \tag{B.35d}$$

$$K_5(\tau) = \frac{e^{-\tau}(\tau - 3)}{4(\tau + 5)(\tau + 1)} - \frac{1}{4}\left[\tau^2 \ln \tau - (1 - \gamma)\tau^2 + \frac{4}{3}\tau - \frac{1}{2}\right] \tag{B.35e}$$

The functions $K_1(\tau)$, $K_2(\tau)$ and $K_3(\tau)$ are presented in graphical and tabular form in Reference [113]. In this Appendix, the functions $K_4(\tau)$ and $K_5(\tau)$ are presented in graphical and tabular form. The series representation is used to evaluate the $K_n(\tau)$ functions. While the series given by equations (B.11) through (B.15) converge for all values of τ, there is a practical limitation. For large values of τ,

the evaluation involves summing of positive and negative numbers which result in a small number. To help overcome this difficulty the series were evaluated using double precision.

The behavior of the $K_4(\tau)$ and $K_5(\tau)$ functions for the various profiles is illustrated in Figures B.1 and B.2 respectively. The actual numerical values are given in Tables B.3 and B.4. Except for the fact that $K_4(\tau)$ and $-K_5(\tau)$ are increasing functions, Figures B.1 and B.2 do not illustrate any general trends. $K_4(\tau)$ and $-K_5(\tau)$ for the rectangular profile has the smallest numerical value of all the profiles. For large values of τ, the effect of the "wings" of the Doppler, exponential and Lorentz profiles is evident. As for the other $K_n(\tau)$ functions, the results for the Doppler and triangular profiles are approximately the same except for large τ. Unlike $K_4(\tau)$, the function $K_5(\tau)$ is always negative.

The results obtained by using the approximate expressions (B.33) through (B.35) of $K_n(\tau)$ functions for the rectangular, triangular and exponential profiles are tabulated in Tables B.5 and B.6. The first term of the approximate expression for $K_n(\tau)$ functions is omitted. The results of $K_1(\tau)$ function show fairly good agreement for all the three profiles for all values of $\tau > 10$, while the results of $K_5(\tau)$ function agree for all values of $\tau > 5$.

Table B.3

Function $K_4(\tau)$ for the various profiles

τ	$K_4(\tau)$				
	Rectangular	Triangular	Exponential	Doppler	Lorentz
0.01	4.9023D-5	4.9312D-5	4.9470D-5	4.9280D-5	4.9479D-5
0.02	1.9310D-4	1.9511D-4	1.9622D-4	1.9489D-4	1.9629D-4
0.03	4.2853D-4	4.3470D-4	4.3815D-4	4.3403D-4	4.3840D-4
0.04	7.5216D-4	7.6575D-4	7.7343D-4	7.6430D-4	7.7403D-4
0.05	1.1612D-3	1.1862D-3	1.2004D-3	1.1835D-3	1.2016D-3
0.06	1.6530D-3	1.6941D-3	1.7176D-3	1.6897D-3	1.7196D-3
0.07	2.2252D-3	2.2876D-3	2.3235D-3	2.2810D-3	2.3267D-3
0.08	2.8756D-3	2.9650D-3	3.0167D-3	2.9557D-3	3.0215D-3
0.09	3.6021D-3	3.7249D-3	3.7961D-3	3.7122D-3	3.8029D-3
0.10	4.4028D-3	4.5655D-3	4.6604D-3	4.5488D-3	4.6697D-3
0.20	1.6114D-2	1.7124D-2	1.7734D-2	1.7025D-2	1.7808D-2
0.30	3.3602D-2	3.6455D-2	3.8230D-2	3.6187D-2	3.8472D-2
0.40	5.5802D-2	6.1665D-2	6.5402D-2	6.1134D-2	6.5966D-2
0.50	8.1909D-2	9.2045D-2	9.8650D-2	9.1160D-2	9.9733D-2
0.60	1.1129D-1	1.2702D-1	1.3747D-1	1.2569D-1	1.3931D-1
0.70	1.4345D-1	1.6609D-1	1.8144D-1	1.6425D-1	1.8431D-1
0.80	1.7796D-1	2.0886D-1	2.3018D-1	2.0644D-1	2.3440D-1
0.90	2.1448D-1	2.5496D-1	2.8337D-1	2.5190D-1	2.8928D-1
1.00	2.5273D-1	3.0409D-1	3.4072D-1	3.0034D-1	3.4869D-1
2.00	6.9169D-1	9.1495D-1	1.0974D+0	9.0422D-1	1.1520D+0
3.00	1.1743D+0	1.6570D+0	2.0956D+0	1.6446D+0	2.2558D+0
4.00	1.6691D+0	2.4679D+0	3.2600D+0	2.4641D+0	3.5945D+0
5.00	2.1674D+0	3.3198D+0	4.5499D+0	3.3365D+0	5.1318D+0
6.00	2.6669D+0	4.1984D+0	5.9402D+0	4.2482D+0	6.8442D+0
7.00	3.1668D+0	5.0957D+0	7.4143D+0	5.1908D+0	8.7150D+0
8.00	3.6667D+0	6.0067D+0	8.9600D+0	6.1587D+0	1.0732D+1
9.00	4.1667D+0	6.9281D+0	1.0568D+1	7.1481D+0	1.2885D+1
10.00	4.6667D+0	7.8579D+0	1.2232D+1	8.1561D+0	1.5165D+1
20.00	9.6667D+0	1.7396D+1	3.1063D+1	1.8824D+1	4.3860D+1
30.00	1.4667D+1	2.7126D+1	5.2510D+1		8.1180D+1
40.00	1.9691D+1	3.6936D+1	7.5655D+1		1.2545D+2

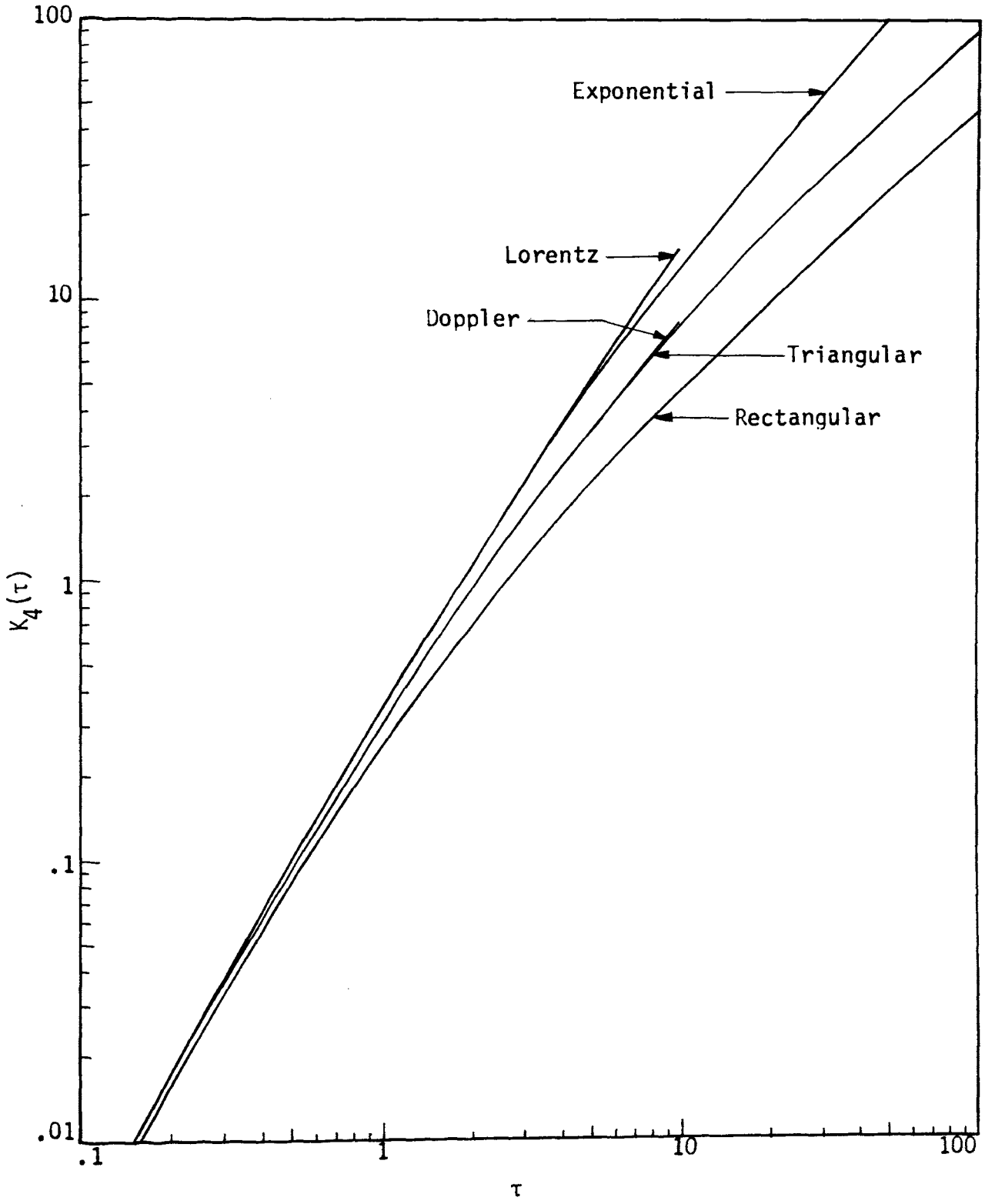

Figure B.1 - Comparison of function $K_4(\tau)$ for the various profiles

Table B.4

Function $K_5(\tau)$ for the various profiles

τ	$-K_5(\tau)$				
	Rectangular	Triangular	Exponential	Doppler	Lorentz
0.01	1.6412D-7	1.6488D-7	1.6529D-7	1.6479D-7	1.6531D-7
0.02	1.2972D-6	1.3078D-6	1.3136D-6	1.3066D-6	1.3140D-6
0.03	4.3306D-6	4.3796D-6	4.4069D-6	4.3743D-6	4.4088D-6
0.04	1.0162D-5	1.0307D-5	1.0388D-5	1.0291D-5	1.0394D-5
0.05	1.9658D-5	1.9993D-5	2.0181D-5	1.9957D-5	2.0196D-5
0.06	3.3661D-5	3.4322D-5	3.4697D-5	3.4251D-5	3.4727D-5
0.07	5.2986D-5	5.4159D-5	5.4828D-5	5.4035D-5	5.4885D-5
0.08	7.8425D-5	8.0353D-5	8.1457D-5	8.0150D-5	8.1553D-5
0.09	1.1075D-4	1.1373D-4	1.1545D-4	1.1342D-4	1.1560D-4
0.10	1.5071D-4	1.5512D-4	1.5766D-4	1.5466D-4	1.5790D-4
0.20	1.1230D-3	1.1787D-3	1.2119D-3	1.1732D-3	1.2156D-3
0.30	3.5656D-3	3.8053D-3	3.9517D-3	3.7821D-3	3.9700D-3
0.40	8.0002D-3	8.6655D-3	9.0803D-3	8.6031D-3	9.1376D-3
0.50	1.4856D-2	1.6310D-2	1.7234D-2	1.6178D-2	1.7372D-2
0.60	2.4491D-2	2.7227D-2	2.8996D-2	2.6985D-2	2.9278D-2
0.70	3.7207D-2	4.1850D-2	4.4900D-2	4.1451D-2	4.5415D-2
0.80	5.3259D-2	6.0569D-2	6.5443D-2	5.9956D-2	6.6310D-2
0.90	7.2865D-2	8.3733D-2	9.1085D-2	8.2847D-2	9.2455D-2
1.00	9.6212D-2	1.1166D-1	1.2226D-1	1.1044D-1	1.2432D-1
2.00	5.6201D-1	7.0588D-1	8.1644D-1	6.9728D-1	8.4549D-1
3.00	1.4933D+0	1.9843D+0	2.3967D+0	1.9635D+0	2.5278D+0
4.00	2.9145D+0	4.0424D+0	5.0627D+0	4.0126D+0	5.4352D+0
5.00	4.8326D+0	6.9336D+0	8.9583D+0	6.9092D+0	9.7829D+0
6.00	7.2498D+0	1.0691D+1	1.4196D+1	1.0699D+1	1.5757D+1
7.00	1.0167D+1	1.5337D+1	2.0867D+1	1.5416D+1	2.3524D+1
8.00	1.3583D+1	2.0887D+1	2.9048D+1	2.1089D+1	3.3236D+1
9.00	1.7500D+1	2.7353D+1	3.8807D+1	2.7740D+1	4.5033D+1
10.00	2.1917D+1	3.4746D+1	5.0203D+1	3.5391D+1	5.9047D+1
20.00	9.3583D+1	1.6075D+2	2.6384D+2	1.6986D+2	3.4592D+2
30.00	2.1525D+2	3.8327D+2	6.8002D+2		9.6480D+2
40.00	3.8690D+2	7.0352D+2	1.3196D+3		1.9926D+3
50.00	7.3840D+2	1.1154D+3	2.2128D+3		3.4981D+3

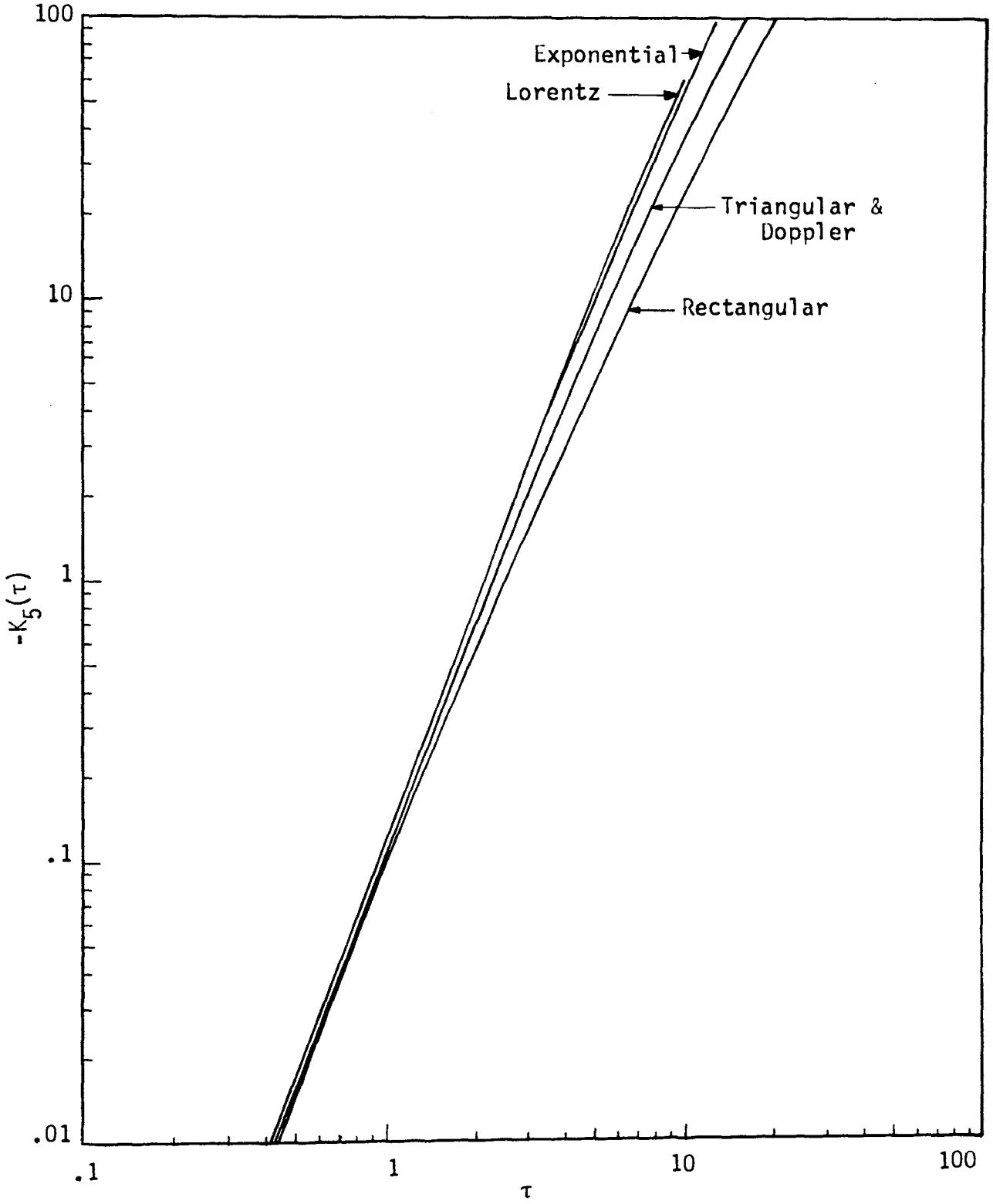

Figure B.2 - Comparison of function $K_5(\tau)$ for the various profiles

Table B.5

Comparison of the exact and approximate values of the function $K_1(\tau)$

τ	$K_1(\tau)$					
	Rectangular		Triangular		Exponential	
	Exact	Approximate	Exact	Approximate	Exact	Approximate
1	2.1938D-01	1.8394D-01	2.5332D-01	1.3333D+0	2.4181D-1	5.0000D-1
2	4.8901D-02	4.5112D-02	8.6488D-02	1.6667D-1	9.8700D-2	1.2500D-1
3	1.3048D-02	1.2447D-02	3.7183D-02	4.9383D-2	5.1016D-2	5.5556D-2
4	3.7794D-03	3.6631D-03	1.8392D-02	2.0833D-2	3.0278D-2	3.1250D-2
5	1.1483D-03	1.1230D-03	1.0103D-02	1.0667D-2	1.9766D-2	2.0000D-2
6	3.6008D-04	3.5411D-04	6.0304D-03	6.1728D-3	1.3828D-2	1.3889D-2
7	1.1548D-04	1.1399D-04	3.8491D-03	3.8873D-3	1.0187D-2	1.0204D-2
8	3.7666D-05	3.7274D-05	2.5935D-03	2.6042D-3	7.8077D-3	7.8125D-3
9	1.2447D-05	1.2341D-05	1.8259D-03	1.8290D-3	6.1714D-3	6.1728D-3
10	4.1570D-06	4.1273D-06	1.3324D-03	1.3333D-3	4.9996D-3	5.0000D-3
15	1.9186D-08	1.9119D-08	3.9506D-04	3.9506D-4	2.2222D-3	2.2222D-3
20	9.8355D-11	9.8150D-11	1.6667D-04	1.6667D-4	1.2500D-3	1.2500D-3
25	5.3489D-13	5.3415D-13	8.5333D-05	8.5333D-5	8.0000D-4	8.0000D-4
30		3.0186D-15	4.9383D-05	4.9383D-5	5.5556D-4	5.5556D-4
35		1.7514D-17	3.1098D-05	3.1098D-5	4.0816D-4	4.0816D-4
40		1.0362D-19	2.0833D-05	2.0833D-5	3.1250D-4	3.1250D-4
45		6.2229D-22	1.4632D-05	1.4632D-5	2.4691D-4	2.4691D-4
50		3.7819D-24	1.0667D-05	1.0667D-5	2.0000D-4	2.0000D-4

Table B.6

Comparison of the exact and approximate values of the function $K_5(\tau)$

τ	$-K_5(\tau)$					
	Rectangular		Triangular		Exponential	
	Exact	Approximate	Exact	Approximate	Exact	Approximate
1	9.6212D-2	1.0535D-1	1.1166D-1	5.9634D-2	1.2226D-1	1.0264D-1
2	5.6201D-1	5.6400D-1	7.0588D-1	6.9507D-1	8.1644D-1	8.1203D-1
3	1.4933D+0	1.4938D+0	1.9843D+0	1.9817D+0	2.3967D+0	2.3956D+0
4	2.9145D+0	2.9146D+0	4.0424D+0	4.0418D+0	5.0627D+0	5.0624D+0
5	4.8326D+0	4.8327D+0	6.9336D+0	6.9334D+0	8.9583D+0	8.9583D+0
6	7.2498D+0	7.2498D+0	1.0691D+1	1.0691D+1	1.4196D+1	1.4196D+1
7	1.0167D+1	1.0167D+1	1.5337D+1	1.5337D+1	2.0867D+1	2.0867D+1
8	1.3583D+1	1.3583D+1	2.0887D+1	2.0887D+1	2.9048D+1	2.9048D+1
9	1.7500D+1	1.7500D+1	2.7353D+1	2.7353D+1	3.8807D+1	3.8807D+1
10	2.1917D+1	2.1917D+1	3.4746D+1	3.4746D+1	5.0203D+1	5.0203D+1
15	5.1500D+1	5.1500D+1	8.5814D+1	8.5814D+1	1.3342D+2	1.3342D+2
20	9.3583D+1	9.3583D+1	1.6075D+2	1.6075D+2	2.6384D+2	2.6384D+2
25	1.4817D+2	1.4817D+2	2.5984D+2	2.5984D+2	4.4510D+2	4.4510D+2
30	2.1525D+2	2.1525D+2	3.8327D+2	3.8327D+2	6.8002D+2	6.8002D+2
35	2.9483D+2	2.9483D+2	5.3113D+2	5.3113D+2	9.7089D+2	9.7089D+2
40	3.8690D+2	3.8692D+2	7.0352D+2	7.0352D+2	1.3196D+3	1.3196D+3
45	4.9146D+2	4.9150D+2	9.0043D+2	9.0048D+2	1.7278D+3	1.7280D+3
50	7.3840D+2	6.0858D+2	1.1154D+3	1.1221D+3	2.2128D+3	2.1973D+3